uOttawa

L'Université canadienne
Canada's university

FACULTÉ DES ÉTUDES SUPÉRIEURES ET POSTOCTORALES

uOttawa

L'Université canadienne
Canada's university

FACULTY OF GRADUATE AND POSDOCTORAL STUDIES

Marie Laferrière
AUTEUR DE LA THÈSE / AUTHOR OF THESIS

Ph.D. (Chemistry)
GRADE / DEGREE

Department of Chemistry
FACULTÉ, ÉCOLE, DÉPARTEMENT / FACULTY, SCHOOL, DEPARTMENT

Applications of Photochemical Techniques to Imaging of Surfaces and Nanoparticles

TITRE DE LA THÈSE / TITLE OF THESIS

Juan C. Scaiano
DIRECTEUR (DIRECTRICE) DE LA THÈSE / THESIS SUPERVISOR

CO-DIRECTEUR (CO-DIRECTRICE) DE LA THÈSE / THESIS CO-SUPERVISOR

EXAMINATEURS (EXAMINATRICES) DE LA THÈSE / THESIS EXAMINERS

André Beauchemin

Bruce Lennox

Maria de Rosa

Javier Giorgi

Gary W. Slater
Le Doyen de la Faculté des études supérieures et postdoctorales / Dean of the Faculty of Graduate and Postdoctoral Studies

Applications of Photochemical Techniques to Imaging of Surfaces and Nanoparticles

Marie Laferrière

Thesis submitted to the
Faculty of Graduate and Postdoctoral Studies
University of Ottawa
In partial fulfillment of the requirements for the
PhD degree in the
Ottawa-Carleton Chemistry Institute

Thèse soumise à la
Faculté des études supérieures et postdoctorales
Université d'Ottawa
En vue de l'obtention du doctorat es sciences à
L'institut de chimie d'Ottawa-Carleton

Your file Votre référence
ISBN: 978-0-494-25880-4
Our file Notre référence
ISBN: 978-0-494-25880-4

Abstract

Highly energetic 157 nm laser irradiation was explored for possible use in the nanolithographic process; 157 nm irradiation of photoresists containing photoacid generators (PAG) was shown to generate acid as it does at longer wavelengths. Irradiation of polymers films that did not contain a PAG was also shown to generate acid but required a higher exposure dose. These polymer films were also shown to generate HF upon 157 nm irradiation. Experiments in solution have shown that 1,1,1,3,3,3-hexafluoro-2-propanol could trap electrons with a rate constant of 6.6×10^{10} $M^{-1}s^{-1}$. Electrons would be generated by the non-fluorinated moieties of the polymer film upon 157 nm irradiation and subsequently trapped by the fluorinated moieties leading to the release of fluoride, deprotonation at the ionization site would lead to HF formation.

Laser flash photolysis of films with 157 nm as the excitation wavelength was attempted, this experiment was technically very challenging because of the high absorbance of most organic compounds, water and oxygen at 157 nm. However, a triplet absorbance for xanthone in perfluorononane was detected.

TEMPO and 4-amino-TEMPO were shown to quench the fluorescence of CdSe quantum dots covered with tri-octylphosphine oxide (TOPO). The quenching is size-dependent, being more efficient for the smaller than for the larger quantum dots. Furthermore, 4-amino-TEMPO is more efficient at quenching the fluorescence of quantum dots than TEMPO. Stern-Volmer plots for the quenching of quantum dots by TEMPO are upward curving, indicating distance dependent

quenching. The Perrin model was used to analyse the results. 4-Amino-TEMPO was shown to form complexes with quantum dots by electron spin resonance spectroscopy. Downward curving Stern-Volmer plots for fluorescence quenching by 4-amino-TEMPO (4AT) indicate that 4AT may first bind in openings in the TOPO ligand shell and subsequently bind by displacing the TOPO ligands.

Prefluorescent probes were developed. The fluorescence of the 4AT-quantum dot complex was restored in the presence of photogenerated radicals from azobisisobutyronitrile (AIBN).

UV irradiation of polymer films containing quantum dots was shown to enhance the fluorescence of quantum dots.

Quenching by TEMPO and 4AT of quantum dots and subsequent quantum dot fluorescence recovery in channels of photonic crystal fibres was recorded by fluorescence imaging. It is explained by the non-linear quenching observed in solution and by the diffusion of the quantum dot and the quencher in the channels of the photonic crystal fibres.

Acknowledgements

I would like to thank my supervisor Professor J. C. Scaiano for allowing me this great opportunity to work in his group. I would like to thank him for believing in me and giving me the chance to be involved in many different and interesting projects. I was very fortunate to be part of such a rich scientific environment. I will always remember the great scientist that he is but also the strong family values that are dear to him.

I would like to acknowledge my coworkers past and present for all their support and encouragement. Their help during the preparation of seminars, talks and posters was invaluable. I would like to thank Gino Cuglietta for his help with everything related to lasers and Betty Yakimenko for her great help with everything administrative.

J'aimerais remercier le CRSNG ainsi que NATEQ et l'Université d'Ottawa pour leur soutien financier tout au long de mes études.

J'aimerais remercier mon mari Sylvain ainsi que mes enfants, Alexandre, Antoine et Frédéric pour leur soutien. Merci également à ma mère et ma soeur qui m'ont toujours encouragé à persévérer.

Table of Contents

List of Schemes

List of Tables

List of Figures

List of Abbreviations

1,4-DMB	1,4-dimethoxybenzene
4AT	4-amino-TEMPO
AFM	Atomic Force Microscope
AIBN	Azobisisobutyronitrile
BA	Benzyl acetate
C4TIPS	4-Methyl-7-(triisopropyl-silanyloxy)-coumarin
C6	Coumarin 6
CHA	Cyclohexylamine
DFBP	Decafluorobenzophenone
EC	Ethyl cellulose
ESR	Electron spin resonance
FP	Fluorinated polymer XP0921
Green 505	CdSe QD (emission 505 nm)
Green 515	CdSe QD (emission 515 nm)
Green 520	CdSe QD (emission 520 nm)
HFP	1,1,1,3,3,3-hexafluoro-2-propanol
LFP	Laser flash photolysis
LIPSS	Laser Induced periodic surface structure
OMAP	ortho-Methylacetophenone
PAG	Photoacid Generator
PCF	Photonic crystal fibre

PMMA	Polymethylmethacrylate
PMSSQ	Polymethylsilsesquioxane
PS	Polystyrene
QD	Quantum dot
TEMPO	2,2,6,6-tetramethylpiperidine-N-oxide free radical
TFE	2,2,2-Trifluoroethanol
TOPO	Trioctylphosphine oxide

Introduction

I had the opportunity to work on many different projects over the past few years while in Professor Scaiano's group. Chapter 1 will give a brief description of the instruments used in the course of this project. I will present the results I obtained with the laser at 157 nm in chapter 2 and 3. Our goal was to verify acid generation in photoresists at 157 nm. We also wanted to perform laser flash photolysis at 157 nm, since it is a technique widely used in our group that can provide important mechanistic information.

In relation to another project, I will present the results I obtained with CdSe quantum dots, which is the latest project I was involved with, in chapters 4, 5 and 6. Nanotechnology is a field of research that has been receiving a lot of attention in the past decade. Nanomaterials possess different properties than bulk materials and can play a major role in the development of new materials and in the field of biosciences.

While these two projects may seem very different, they both involve the interaction of light with matter, the application of spectroscopic techniques and fluorescence imaging. They also share the common thread of photochemical studies of films either for use at 157 nm or containing CdSe quantum dots.

Chapter 1
Instrumentation

Table of contents

Chapter 1
Instrumentation

1.1 Introduction

This chapter is intended to give a brief and general description of the various instruments that were used during the course of this research. Relevant information to specific experiments is given in the experimental section of the related chapters.

A description of the two spectrofluorimeters employed, the UV-vis absorbance spectrometer, the microscope with the different filter cubes, the spin coater, the thin film analyser, and of the techniques of AFM and laser flash photolysis will be presented.

1.2 Spectrometers

Absorption spectra were acquired with a Varian Cary-50 UV-vis spectrometer.

Light is passed through a monochromator and the selected excitation wavelength is passed through the sample. The sample is usually contained in a quartz cuvette, which lets pass all visible and most UV light. The radiant power that emerges from the cell (P) is referenced to the radiant power (P_0) obtained with

the same excitation wavelength but passed through an identical cell without the analyte.[1] Transmittance or absorbance can then be calculated from the values of power, according to Equation 1.1.[1] Absorbance can be related to the concentration of the analyte, c, the molar absorptivity, ε, and the pathlength, l according to Beer's law, see Equation 1.2.[1]

(1.1) $$T = \frac{P}{P_0} \quad A = -\log(T) = -\log\left(\frac{P}{P_0}\right)$$

(1.2) $$A = \varepsilon c l$$

Fluorescence measurements were performed with two different instruments. The Perkin Elmer Luminescence Spectrometer LS50 can be fitted with a holder to measure fluorescence of films and was used mostly for this purpose. Fluorescence spectra of solutions were recorded with a Photon Technology International (PTI) Spectrometer.

The excitation wavelength is selected with a first monochromator. The selected wavelength is absorbed by the sample and the resulting emission is detected, usually at 90°, with a second monochromator.[1] The emission intensity at low concentrations is proportional to the sample concentration and the incident radiant power.[1] An emission spectrum is obtained when the excitation wavelength remains constant and the emission wavelengths are varied and an excitation spectrum is obtained when the emission wavelength is constant and the excitation wavelengths are varied.[1]

1.3 Atomic Force Microscopy

Atomic force microscopy (AFM) measurements were performed at the National Research Council of Canada (NRC). We are grateful to Drs L. J. Johnson, M. Chakrapani, and M. Tomietto for their help. AFM topographs were obtained with a Multimode Nanoscope III atomic force microscope from Digital Instrument. The J scanner (120 mm) and 200-mm-long soft cantilevers with integrated pyramidal silicon nitride tips (spring constant of 60 mN/m) were used for all measurements. The small glass disks onto which the samples were spin coated were positioned in a sample holder suspended in a Faraday cage.

The surface is scanned with a small tip, that can be pyramidally or conically shaped with a tip curvature radius of 2-50 nm positioned at the end of a cantilever.[2] The tip is positioned at a characteristic small distance from the surface and the surface is scanned. The tip or the sample can be moved relative to the other using piezoelectric tubes.[3] The deflection of the cantilever is monitored optically, a laser beam is focused on the end of the cantilever and the deflection of the laser beam as the cantilever moves is amplified and recorded via a diode detector, see Scheme 1.1.

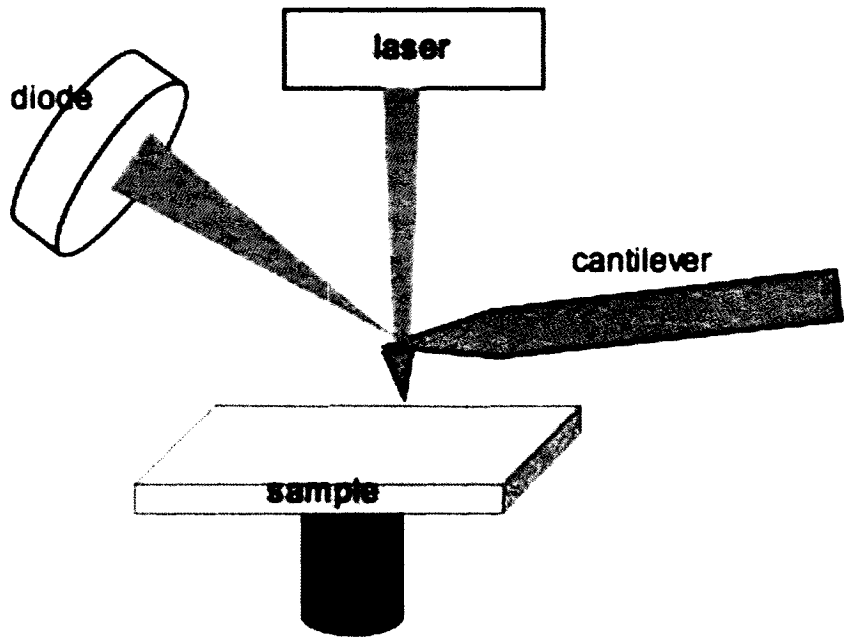

Scheme 1.1 *Atomic Force Microscope schematic principle of operation*

There are different modes of scanning; contact, non-contact and tapping. In the non-contact mode, van der Waals, electrostatic, magnetic or capillary forces produce the image and in the contact mode it is the ionic repulsion forces that help produce the image.[3] In the contact mode, deformation and wear of the surface can be generated by the tip as it drags near the surface.[2] In the non-contact mode, the cantilever and tip oscillate at resonant frequency, relatively far from the surface, more than 1 nm, and it is the interaction with the surface that perturbs the oscillating cantilever.[2,3] This mode is not recommended for topography measurements because the tip being far from the surface, spatial resolution is reduced.[2] In the tapping mode, the tip oscillates but a distance that is much closer

than in the non-contact mode. It oscillates near the repulsive limit of interaction between the tip and the surface, same as for the contact mode, but the small contact time limits the damage to the surface.[2]

1.4 Microscope

Fluorescence imaging was performed with a Leica DMLS microscope and a cooled Leica DFC300 FX camera. The microscope is equipped with a 50 W mercury lamp for fluorescence. Fluorescence images are obtained with incident light illumination whereas transmitted light is used for all other images. Filter cubes E4 and M2 were purchased from Leica. Filter cube XF02-2 was acquired from Omega optical. Scheme 1.2 is a scheme of the path of the incident fluorescence light and of the resulting fluorescence through the filter cube. Figure 1.1 shows the excitation spectra recorded for the different filters and Table 1.1 lists the different components of the filter cubes.

Table 1.1 *Filter cubes characteristics*

FILTER	EXCITER	DICHROIC	EMITTER
E4	BP 436 ± 7 nm	455 nm	LP 470 nm
M2	BP 546 ± 14 nm	580 nm	LP 590 nm
XF02-2	WB 330 ± 40 nm	400 nm	LP 400 nm

Where BP is band pass filter, LP is long pass filter and WB is wide band

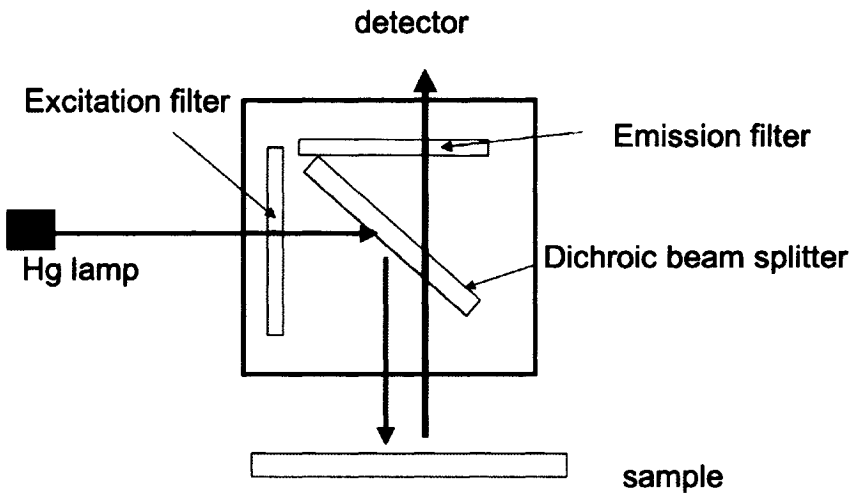

Scheme 1.2 *Filter cube schematic representation*

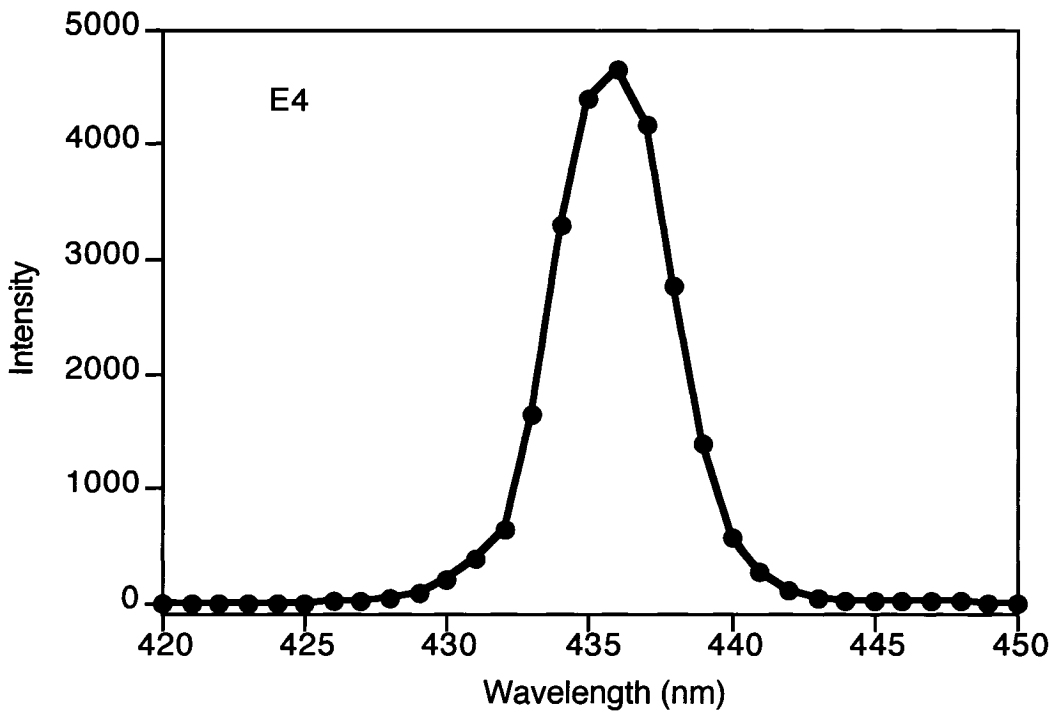

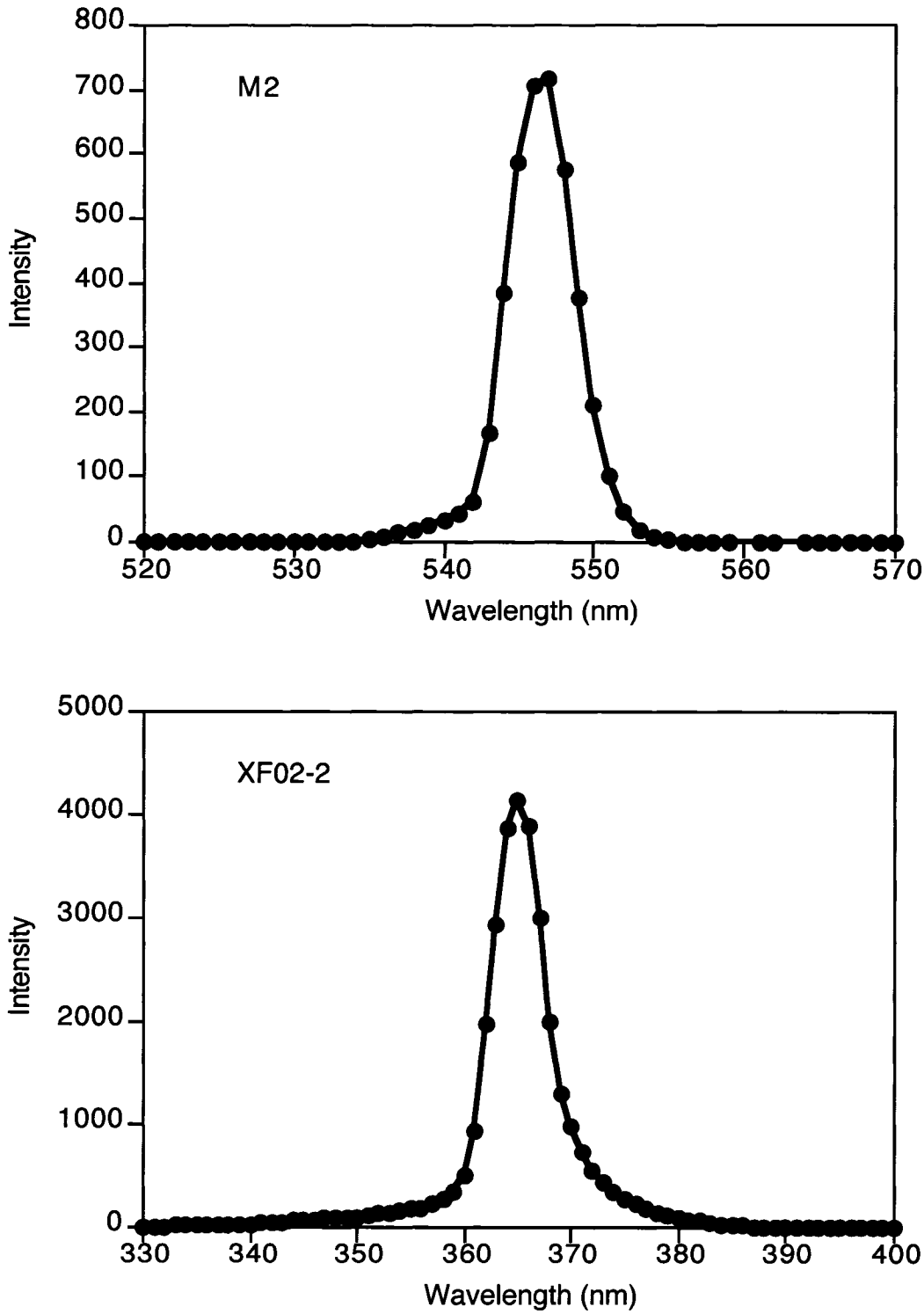

Figure 1.1 *Excitation spectra recorded for the filters E4, M2 and XF02-2.*

1.5 Spin Coater

Films are prepared by spin coating with the P-6000 spin coater from Specialty Coating Systems. The spin coater is connected to a vacuum pump. The spin coater has a spinning chuck. The sample disks are centered and maintained in position by vacuum on the chuck that is centered in a covered metallic bowl. There are different sizes of chuck to accommodate smaller or larger disks. The instrument allows selection of the acceleration, revolutions per minute (rpm) and time during which the rpm is maintained.

1.6 Thin Film Analyzer

The thicknesses of thin films were measured with a thin film analyser TFA-11 from Luzchem.

When light reaches the interface of two materials, it can be transmitted absorbed or reflected.[4] The amount of light that is reflected depends on the refractive index and the extinction coefficient differences in the two materials.[4] When a thin film is coated onto a substrate, more interfaces are created, the first one is between air and the top surface of the film, the second at the bottom of the film and the top of the substrate. Reflected light from these two interfaces can add constructively or destructively depending on their phase.[4] The phase depends on the optical path of the reflections which depends on the thickness of the film.[4] Equation 1.3 describes how the reflectance R varies inversely with the

wavelength.[4] For a very thin film, only a few oscillations can be seen over a wavelength range while for thicker films many oscillations can be seen.[4] The instrument allows the choice of models for the values of refractive index and extinction coefficient, which vary with wavelength, and the thickness is derived from a fit of a model curve to the experimental curve using the least parameters possible over the range of wavelength selected.

(1.3) $$R \approx A + B\cos\left(\frac{4\pi}{\lambda} nd\right)$$

1.7 Laser Flash Photolysis

Laser flash photolysis uses a laser to generate a transient or excited state in a sample and the change in absorption in the sample is monitored with a continuous light source. The change in absorptivity of the sample following the laser pulse changes the intensity of the monitoring beam.[5] The lifetime of the generated transient must also be longer than the length of the laser pulse in order to monitor it.

Different excitation wavelengths are provided by multiple lasers; 266 nm, 355 nm and 532 nm by two Surelite Nd-YAG laser, 308 nm by an EX 530 Lumonics laser, and 157nm, 193 and 248 nm by a GSI-Lumonics excimer laser. The monitoring beam is a 150 W Xe pulsed lamp. The monitoring lamp is pulsed in order to increase the intensity by a factor of 5-20 for a period of a few ms.[5]

Alain Berinstain was a graduate student in Professor Scaiano laboratory who participated in the development of the laser flash photolysis system. Most of the information about the system was taken from his PhD. thesis. The monitoring lamp is focused with the help of lenses onto the sample. The laser beam is directed at 90° on the sample where it is concentrated.[5] A monochromator and a photomultiplier tube (pmt) are positioned after the sample. The system is connected to an oscilloscope, a line synchronizer and a computer, see Scheme 1.3. The sequence that leads to data acquisition is coordinated with a line synchronizer.[5] The sequence is as follows; the lamp shutter is first opened and a first channel records the monitoring lamp intensity.[5] The photomultiplier (pmt) voltage decreases when the lamp is pulsed. The laser shutter opens and the laser is fired, the laser beam reaches an optic fiber that sends a signal to the digitizer to start acquiring data points in a second channel.[5] The laser beam reaches the sample where a transient is formed and the laser shutter is subsequently closed. The monitoring beam shutter is finally closed. The signal from the monitoring beam acts as a baseline and is subtracted from the signal. [5] The changes in pmt voltage are representative of the changes in absorption of the sample during and after laser irradiation.

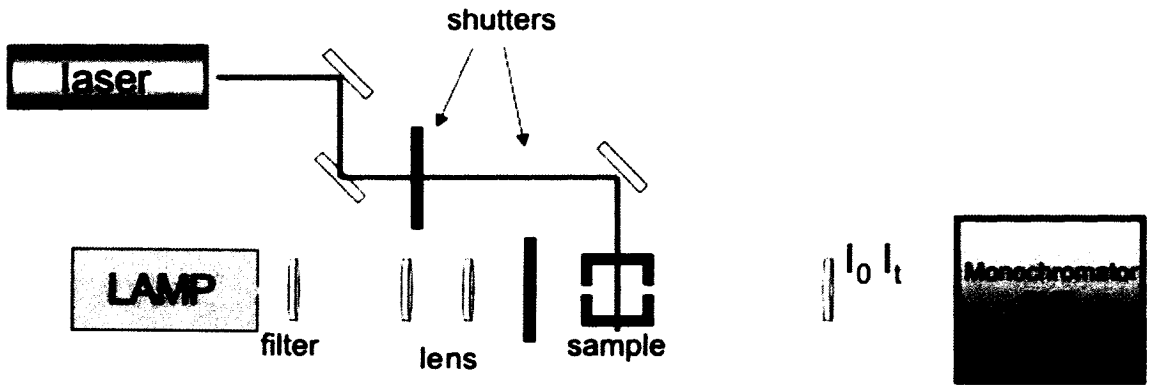

Scheme 1.3 *Schematic laser flash photolysis setup*

1.8 References

(1) Harris, D. C. *Quantitative Chemical Analysis*; 4th ed.; W. H. Freeman and Company: New York, 1996.

(2) Frétigny, C. *Les nanosciences Nanotechnologies et nanophysique*; Belin: Paris, 2004.

(3) Ebert, P.; Szot, K.; Roelofs, A. *Nanoelectronics and InformationTechnology*; WILEY-VCH: Weinheim, 2003.

(4) Taking the Mystery Out of Thin Film Measurements, Filmetrics, 2006.

(5) Berinstain, A., Ph. D. Thesis, University of Ottawa, 1997.

Chapter 2
Acid Generation with 157 nm

Table of Contents

Chapter 2
Acid Generation with 157 nm

2.1 Introduction

The ability to store more information on computer chips in order to increase the performance has led to great progress in the electronics industry. Gordon E. Moore, co-founder of Intel, had predicted in 1965 that the number of transistors on a chip would double every two years. This is now known as Moore's law.

The processing power measured by millions of instructions per second (MIP) has seen a steady increase over the years. The electronic industry has been looking to reduce the feature size on integrated circuits (ICs) through the use of shorter wavelengths or increasing the numerical aperture (NA) of the optical tools. The resolution limit for optical lithography, determined by the Raleigh equation, is proportional to the excitation wavelength and inversely proportional to the NA.[1]

A wavelength of 365 nm in use in the 1990s would allow a minimum feature size of 0.6 μm[1]. The feature size that can be written by 193 nm is now shorter than 100 nm. The microlithographic process has seen the wavelength of light employed to write the features being reduced over the last few years. The industry now mostly uses 248 nm or 193nm. Shorter wavelength means smaller features can be written on a computer chip. Over the last decade we have seen the feature size

become significantly smaller than the excitation wavelength. The use of 157 nm as the excitation wavelength could lead to feature sizes of 50 nm or smaller.

The last few years have seen an oscillating interest for 157 nm lithography. In 2001, Richard Harbison from International Sematech was predicting the use of 157 nm technology by the start of 2003 and broad development by 2005.[2] Intel at that time was still interested in 157 nm but was keeping also a good interest in pushing the limits at 193 nm.[2] There were many difficulties foreseen with the use of 157 nm as a viable wavelength for nanolithography. New photoresists and new materials for the optics had to be developed and contamination control had to be addressed.[2]

This wavelength can be generated from a fluorine excimer laser. A wavelength of 157 nm corresponds to 7.88 eV or 182 $kcalmol^{-1}$, more than enough to photoionize and or photofragment chemical bonds that are otherwise stable at longer wavelengths. There is also sufficient energy to generate "hot" intermediates in many cases.[3,4]

A major experimental problem with the use of 157 nm is the high absorbance of most materials at this wavelength. Most organic solvents, oxygen and water vapour absorb highly at that wavelength.[5,6] New photoresists were being developed for 157 nm imaging. Fluorinated moieties seemed to alleviate the absorbance problems but at the same time the first films being developed were not thick enough. These new resists had a lower absorbance but were less resistant to etching. Another experimental problem is the high absorbance of most imaging materials such as quartz. The use of CaF_2 as optical windows and of fluorinated

solvents and materials seemed to be a step in the right direction to solve these absorbance problems. There are other fluorinated material but MgF_2 could not be used because it is birefringent and BaF_2 is hydroscopic and harder than other materials.[2]

One of our goals was to verify that acid generation could be effected at 157 nm. In order to continue development of photoresists for lithography at 157 nm, it was important to make sure that the acid generation process would also happen at this wavelength. The photoresists that are developed for lithography at 157 nm contain fluorinated moieties but the photoacid generators (PAGs) are frequently the same as those for lithography at 248 or 193 nm. These PAGs had not been tested to see if they generate acid and with what efficiency at this shorter wavelength. We decided to use Coumarin 6, a dye that had already shown its efficiency at longer wavelengths, for monitoring acid formation.[7] We will show that irradiation with 157 nm light generates acid in films of photoresists but most importantly also in polymer films that do not contain a PAG. We will show that the energy dose required to induce acid generation is much higher in films that do not contain a PAG. We will also demonstrate that certain fluorinated moieties contained in the new photoresists for 157 nm can generate hydrofluoric acid (HF) upon laser exposure. The research on acid generation in polymer films and in photoresists at 157 nm was a collaboration with Marius G. Ivan, and Dr. Carlos Sanramé developed the fluoride sensor.

The future of the electronic industry now relies on the development of techniques for immersion lithography at 193 nm. Sematech reported at the

beginning of 2004, that they believe this technique could be implemented by 2009. This decision was prompted by the discovery that CaF_2 was also birefringent at 157 nm.

The lithographic process, which consists of transferring a pattern onto a substrate, is a very important industrial process used to manufacture integrated circuits. There are many techniques available such as soft lithography and photolithography. There are many different wavelengths that can be used to write the patterns as well as electron beams. Extreme ultraviolet (EUV) and electron projection lithography (EPL) are contenders in the search for the next generation lithography technology. However, photolithography in the UV region is the most important process used by the electronics industry to date.

A specific polymer blend with additives, called a photoresist, is spin coated onto a substrate, usually a silicon wafer. The photolithographic process in chemically amplified systems relies on the generation of acid to alter the chemical properties, usually solubility, of the photoresist in the exposed regions in order to create an image on a silicon wafer. As can be seen in Scheme 2.1, a photoresist is deposited onto the substrate. Upon irradiation, acid is generated in the exposed areas and this acid creates chemical change in the exposed areas. The acid can deprotect some groups in the polymer rendering it more soluble in the development step or the acid generated can induce crosslinking in the polymer coating rendering it less soluble in the development step. After development, etching, and stripping, a negative or positive image of the mask is obtained on the substrate.

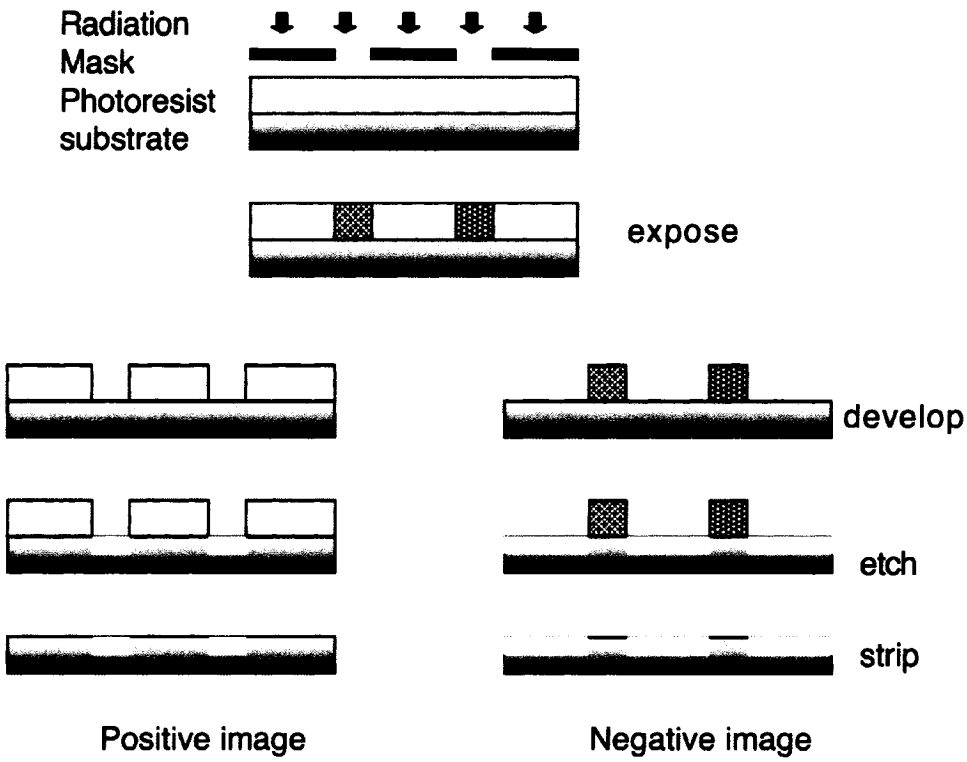

Scheme 2.1 *Description of the photolithographic process*

The photoresists that were being developed for 157 nm contain different monomers that each confers a distinct property to the photoresist. They have fluorinated moieties for transparency purposes, other moieties are included for etch resistance, adhesion and also an important acid-labile group, see Scheme 2.2.[8]

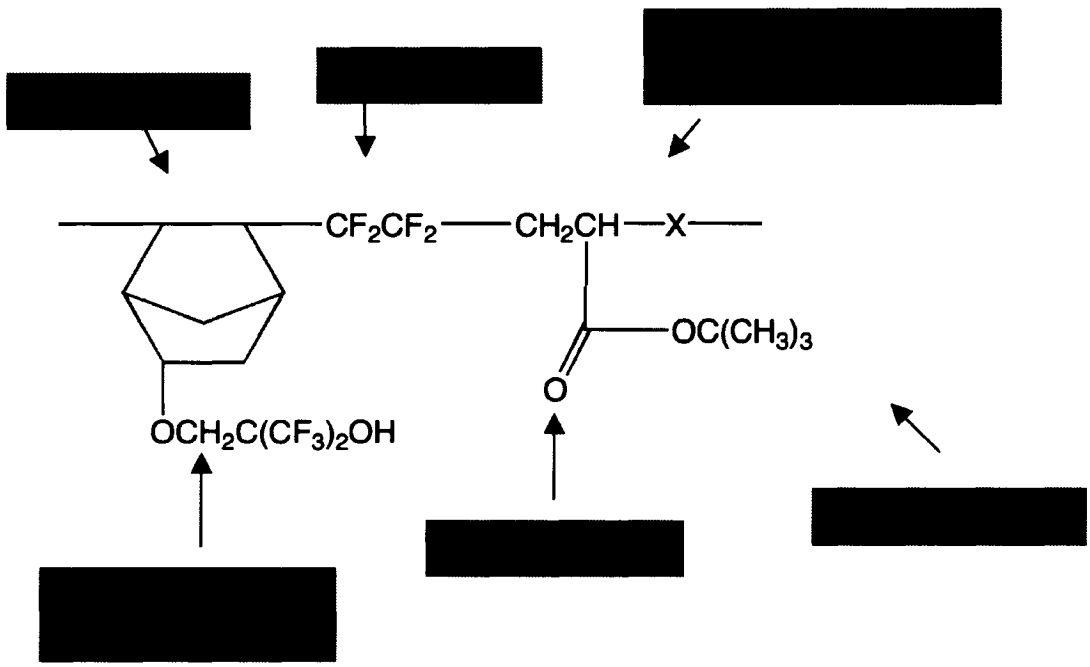

Scheme 2.2 *Typical polymer being developed for photolithography at 157 nm.*

Chemically amplified resists contain a photoacid generator (PAG). Upon exposure the PAG generates acid, as shown in Scheme 2.3. PAGs for photolithography are usually onium salts. A common PAG for photolithography at 193 nm is triphenyl sulfonium triflate.[9] The acid generated will deprotect tert-butyl ester groups in the photoresist generating isobutene, which is volatile, carboxylic acid pendant groups and regenerate the acid, see Scheme 2.4.

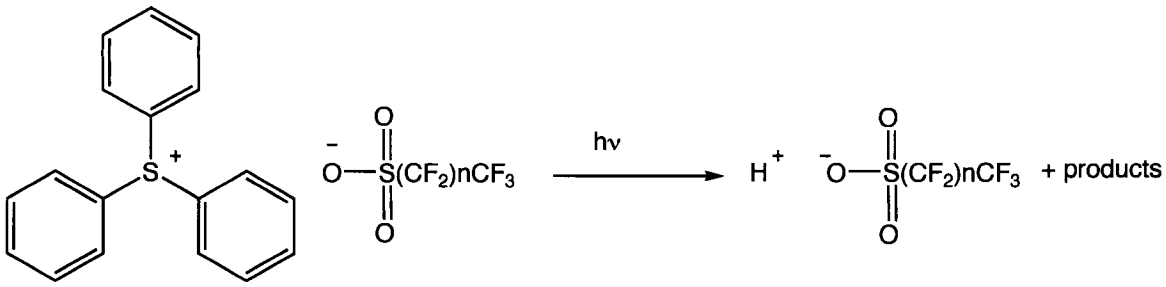

Scheme 2.3 *Triphenylsulphonium salts (PAG) contained in photoresists generate acid upon irradiation.*

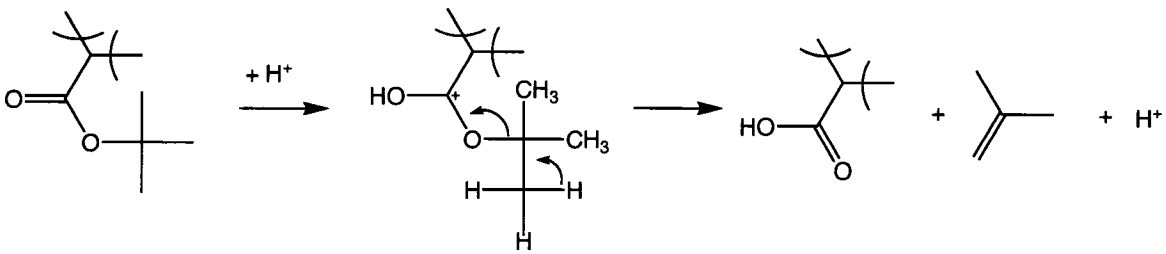

Scheme 2.4 *The acid generated by the PAG will deprotect the tert-butyl moiety and regenerate the acid.*

The exposed areas that were hydrophobic become hydrophilic upon irradiation. The process is catalytic, as the acid is regenerated. Typical turnover rates are around 800-1200.[9]

A method was previously reported by which acid formation can be monitored without going through the development, etching and stripping steps.[7,10] Pohlers, Scaiano and Sinta determined that coumarin 6 (C6) could be used to determine the quantum yield of acid formation in solution after photolysis.[10] Feke *et al.* have used C6 as a pH acid sensor in order to determine quantum yields of

acid generation with chemically amplified resists designed for use at 193 nm.[7] Coenjarts et al. reported that acid loss during post-exposure bake of polymer films could be monitored using C6.[11] The previous methods consisted of irradiating several wafers, then there was dissolution of the exposed resists and quantification of the acid generated by acid-base titrations or colorimetric analysis.

As the dye, coumarin 6, is added to the photoresist formulation it will get protonated by the acid generated upon irradiation, as seen in Scheme 2.5. This dye can be used because it possesses, as can be seen in Figures 2.1-2.3, a different absorption and fluorescence emission depending on its protonation state.

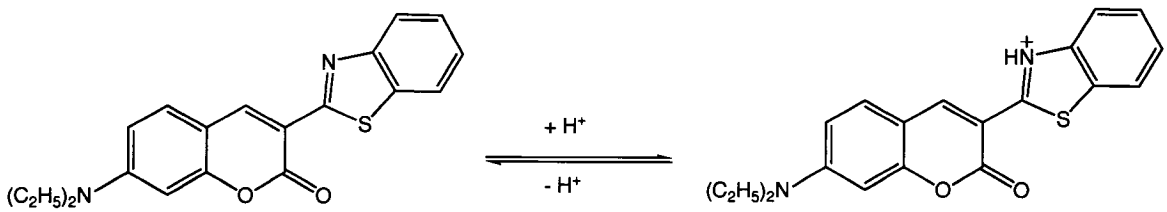

Scheme 2.5 *Coumarin 6 (C6) protonation equilibrium.*

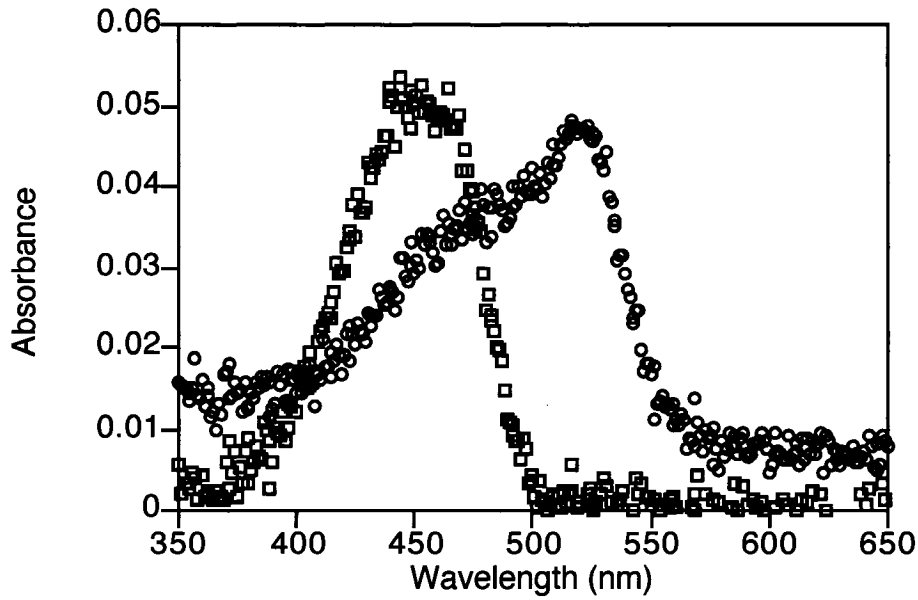

Figure 2.1 *Absorbance spectra of Coumarin 6 (C6) contained in a thin film of fluorinated polymer with PAG before and after flood exposure to 248 nm. The absorbance spectra for the neutral form of the dye (□) and the protonated form (○) show a significant shift.*

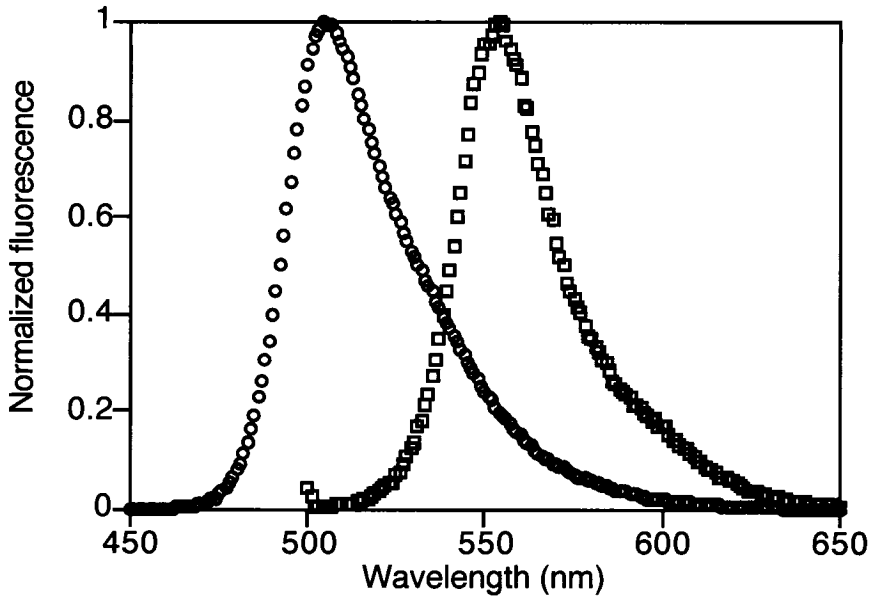

Figure 2.2 *Fluorescence spectra of Coumarin 6 (C6) in ethanol, of the neutral form(○) and of the protonated form (□). The protonated form was obtained by addition of trifluoroacetic acid to the solution.*

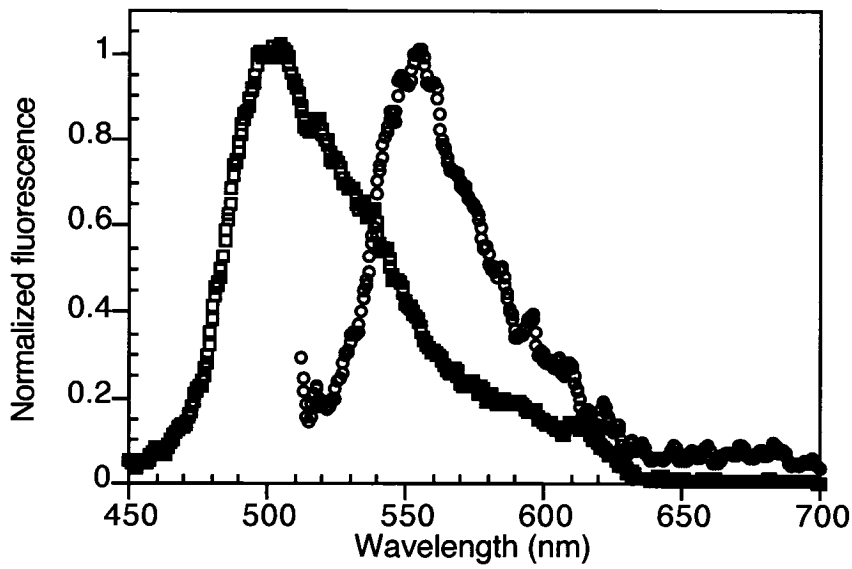

Figure 2.3 *Fluorescence spectra of Coumarin 6 (C6), neutral form (□) and of the protonated form (○). The protonated form was measured after flood exposure to 248 nm of a fluorinated photoresist containing a PAG.*

Upon irradiation through a mask with Coumarin 6 present in the film, the dye will get protonated by the acid generated in the exposed areas. Since Coumarin 6 in its protonated form has a different emission than the unprotonated form, it becomes possible to monitor where acid is generated. It creates a latent image of the pattern that is visible with fluorescence imaging. It would have been better to find a dye that was transparent at 157 nm, but that is impossible at that wavelength of excitation. The use of C6 as an acid sensor has previously been reported.[7] In spite of the higher extinction coefficient of the dye, all has been done to minimize the impact of the dye presence. The dye was added in small amounts, 0.5% of the polymer weight, in order to reduce its overall absorbance. The high sensitivity of the fluorescence technique requires minimal dye concentration.[12] The film thickness employed is usually less than 500 nm.

Fluoride electrodes can be used to detect fluoride in aqueous systems. However, in thin films, fluoride detection can be challenging as there are only trace amounts generated and conventional aqueous detection systems do not work. A fluoride sensor, C4TIPS, was developed by a postdoctoral fellow in our group, Dr. Carlos Sanramé. Coumarin 4 was protected in the 7-hydroxy position by a triisopropylsilanyl group rendering the molecules non-fluorescent. In the presence of a halide such as fluoride, the molecule is deprotected according to Scheme 2.6 and the fluorescence is restored.[13] While this sensor has not been fully characterized to be specific for fluoride detection, there is no other halide in our systems.

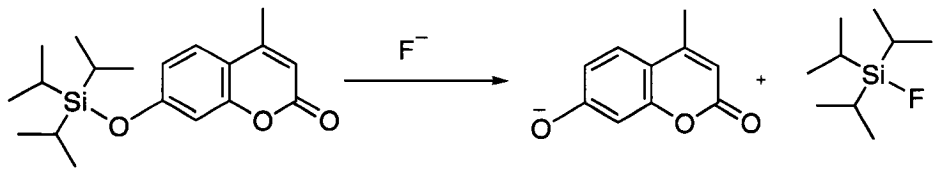

Scheme 2.6 *C4TIPS is fluorescent in its deprotected form.*

Irradiation of polymer films can generate a fine structure in the exposed areas known as Laser Induced Periodic Surface Structure or LIPSS. Figure 2.4 shows an example of LIPSS created in a polymer film after 157 nm irradiation. These LIPSS are dependent on the laser fluence and wavelength of irradiation as well as many other factors such as angle of incidence, quality of starting film, etc. Bor and Csete reported that LIPSS are generated on polyethylene-teraphtalate films with fluences of 3-5 $mJcm^{-2}$ using a excimer laser at 193 nm.[14] They show that there is a dependence of the LIPSS period with the angle of incidence. The LIPSS period increases with the angle of incidence. They conclude from SEM experiments that there is no ablation of material but only a redistribution of the material on the surface. They also conclude that the process takes place around granules already present on the surface. The incident beam creates new granules after the first 100-200 laser shots of 3-5 $mJcm^{-2}$. As the number of shots increases, elliptical structures are formed around the granules and after 1000 shots, ripples develop on the surface. They do not see these LIPSS formed at lower fluences, only additional granules are formed or at larger fluences, where they observe that the surface becomes molten. Lippert and Dickinson report that for doped polymers containing a strongly absorbing polymer, the doped regions are

responsible for the bulk of laser absorption.[15] These regions then thermalize under irradiation and lead to decomposition of the polymer. These thermal processes lead to ablation.[15] Laser ablation of polymers has been known since the early 1980s.[15-17] There is an interest in using the LIPSS or patterns produced on the surface by irradiation towards the fabrication of nanodevices. They would be an alternative to nanolithography. Hubert *et al.* show that the interaction of linearly and circularly polarised laser beams with an azo-polymer film generates sub-micrometer hexagonal patterns.[18] They also observed that irradiation time and laser beam intensity did not change the periodicity of the structures generated. They report that ripples can be formed by the interference between the incident and the scattered radiation field caused by microscopic roughness.

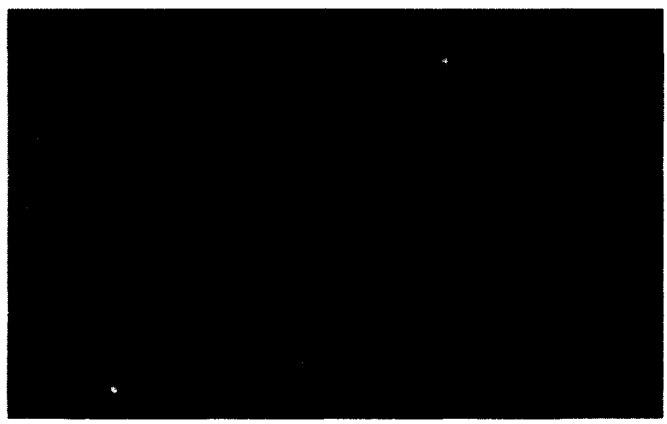

Figure 2.4 *Arrow in AFM image points at the LIPSS created by 157 nm laser irradiation of a polymer film with a mask.*

Ablation was used by Tanaka *et al.* to micropattern a glass substrate with trimethylsilyl cellulose (TMSC).[19] A thin film of TMSC was deposited by the Langmuir-Blodgett deposition method. The film was irradiated through an electron

microscope grid with a 500 W mercury arc lamp for 30 minutes. The exposed areas were completely ablated creating hydrophilic domains on the surface. Selective deposition of fluorescein-labelled bovine serum albumin in the exposed region permitted attachment of human erythrocytes only in the specific domains. This allowed templating of native biomembranes without losing the orientation and lateral density of their native state. This permits further evaluation of their function on solid substrates.

The research that is being done on ablation and patterning of thin films at longer wavelengths can be extended to 157 nm. The interest of ablation at 157 nm is that 157 nm is a very energetic wavelength and that the effect on the topography of the exposed films could be different than at longer wavelengths.

Solution experiments were also performed at wavelengths other than 157 nm. They are experiments that were relevant to understanding the photolithographic process in films. Preparative work in solution was made in order to get information on electron ejection and electron trapping from common moieties that are to be included in photoresist at 157 nm. The photoresists that are being developed for use at 157 nm contain fluorinated moieties that can be modeled by 1,1,1,3,3,3-hexafluoropropan-2-ol (HFP) and ester moieties that can be modeled by benzyl acetate. 1,4-Dimethoxybenzene was used as a photoinduced electron generator in solution. Under irradiation 1,4-DMB generates an electron according to Scheme 2.7.

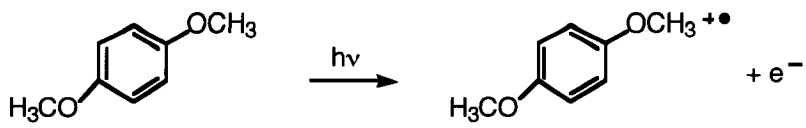

Scheme 2.7 *Irradiation of 1,4-dimethoxybenzene generates a solvated electron and the radical cation of 1,4-DMB.*

Since we do not have access to laser flash photolysis at 157 nm or to pulse radiolysis, these experiments were very useful in giving us an insight of what may be happening at 157 nm. We developed model systems using 1,4-dimethoxybenzene as an electron donor and benzyl acetate or HFP as the electron acceptors. The goal of these experiments was to monitor electron behavior following ejection. Many other substrates (not as electron rich as 1,4-DMB) may also yield electrons by exposure to 157 nm.

Polymers under investigation for development of new resists for 157 nm lithography contain ester groups. It was shown that ester radical anions trap electrons produced by pulse radiolysis.[20,21] Christensen *et al.* reported that benzyl acetate could trap an electron in water with a rate constant of 1.1×10^9 $Lmol^{-1}$ s^{-1}. We used benzyl acetate as an electron trap for a model system of the ester moieties present in photoresists, see Scheme 2.8.

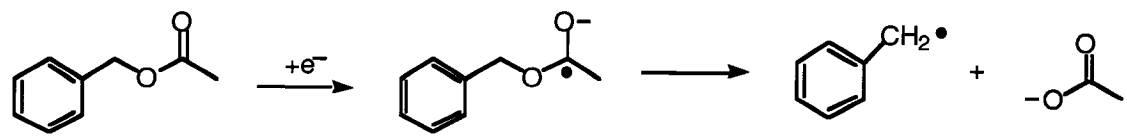

Scheme 2.8 *Benzyl acetate will trap an electron to generate a radical anion that will subsequently cleave to give acetate and a benzyl radical*

We also used 1,1,1,3,3,3-hexafluoro-2-propanol (HFP) as a model system for some of the fluorinated moieties present in the test polymers for lithography at 157 nm. HFP will trap an electron and generate the radical anion, which could lead to formation of hydrogen fluoride.

Decafluorobenzophenone (DFBP), see Scheme 2.9, was considered for experiments in solution because of its potential use at 157 nm where fluorinated molecules that have a lower absorbance are highly desirable. DFBP is known to abstract hydrogen from phenol to generate a ketyl radical.[22]

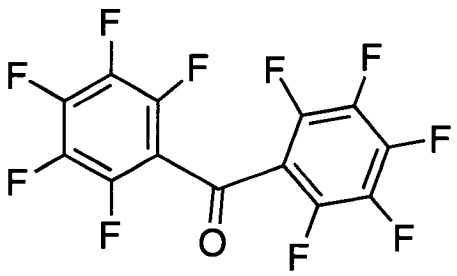

Scheme 2.9 *Decafluorobenzophenone*

Rate constants for electron trapping in solution were determined following equations for bimolecular kinetics, see Equation 2.1, where v is the rate, k the rate constant and A and e^-_{solv} are the two reactants. An apparent rate constant was first determined for each concentration of A and the slope of these apparent rates versus the concentration of A gave the desired rate constant, see Equation 2.2. The intensity of the signal obtained from laser flash photolysis at time t for the electron can be used in place of the concentration of electrons because it is proportional to it.

(2.1)
$$A + e^-_{solv} \xrightarrow{k} \text{Product}$$
$$v = k[A][e^-_{solv}]$$

(2.2)
$$k_{app} = k[A] + \text{constant}$$

The results are separated into 3 main sections.

The first section deals with experiments that were not actually performed at 157 nm. They are the solution experiments that were done as models for moieties included in test resists for 157 nm lithography.

The second section describes experiments aimed at detecting acid after exposure to 157 nm in photoresists. These resists contain photoacid generators (PAGs) that had not been tested for acid generation at 157 nm. Coumarin 6 is employed as an acid sensor.

The third section presents results of acid generation in polymer films. We looked at acid generation in a fluorinated polymer used in typical photoresists in development for use at 157 nm, polymethylsilsesquioxane (PMSSQ), polymethylmethacrylate (PMMA), and ethyl cellulose (EC) films. These films generate acid upon photolysis though in lower yield than films that contain a PAG. A fluoride sensor, C4TIPS is used to monitor fluoride formation in films of fluorinated polymers. AFM is used to detect the changes in surface topology after exposure to 157 nm.

2.2 Experimental

1,4-dimethoxybenzene, 99%, 1,1,1,3,3,3–hexafluoro-2-propanol (99.8%), benzyl acetate (99%), coumarin 6 (98%), 2-heptanone (99%), decafluorobenzophenone (98%) and ethyl cellulose (48% ethoxyl content, 100cp) were purchased from Aldrich. Methanol was purchased from EM Sciences and was Omnisolv grade. Polymethylmethacrylate (PMMA) was purchased from Polysciences Inc. The fluorinated polymer XP2332 and polymethylsilsesquioxane (PMSSQ) were a gift from Rohm & Haas Electronic Materials. Chloroform, Omnisolv grade was purchased from BDH.

Laser flash photolysis of solution was performed with a system described in Chapter 1. Quartz cells that are 7x7 mm were used for the samples. Solutions were deaerated with N_2. Solutions of non-fluorinated and fluorinated photoresists were spin coated onto quartz disks. The resist formulation contains among others, 2-heptanone as the solvent, a PAG, and a polymer. The structure of the fluorinated polymer contained in the photoresist is known but the percentage of each monomer is proprietary, see Scheme 2.2. Coumarin 6, 0.5 wt % of polymer was added to the resist formulations. We assumed a 20% weight percent of polymer in the resist solution. The resist and dye were filtered through a 0.45 μm filter. The solutions were spin coated onto quartz or CaF_2 disks or silicon wafers at 3000 rpm for 20 seconds. The films were then heated at 90 °C for 60 seconds. This allows the solvent to evaporate. The same procedure was followed for fluorinated and non-fluorinated resists.

Solutions of different polymers were prepared. Coumarin 6 was 0.5 wt % of polymer when added to the solutions. C4TIPS was 5.0 wt % of polymer when added to the solutions. The solutions were spin coated onto 1-inch quartz disks for fluorescence measurements and onto 0.5-inch glass slipcovers for AFM measurements. In order to obtain films of similar thicknesses, the films were spin coated at different rpm. PMSSQ films were prepared as 25 wt% in 2-heptanone and were spin coated 3500 rpm for 20 seconds. The FP films were prepared as 18 wt % in 2-heptanone and spin coated at 3000 rpm for 20 seconds. The ethyl cellulose (EC) solutions were prepared as follows, 1wt% EC in chloroform. The film was spin coated at 1000 rpm for 20 s. All the films were placed in the oven at 90 ° C for 1 minute in order to allow the solvent to evaporate.

All the films were then exposed under a mask, an electron microscope copper grid, to 157 nm irradiation. The electron copper grids were purchased from EM sciences and have hexagonal holes spaced at 60 μm center to center. The sample was positioned in a sample holder under an inert atmosphere. The sample chamber was deaerated with dry nitrogen for several minutes before exposure. The films containing photoresists were exposed to 157 nm with a MPB Technologies Inc. MSX-250 Excimer Laser. The repetition rate for the laser was maintained between 1 to 3 Hz during the experiments. All other films were irradiated with a GDS-Lumonics laser modified to perform at 157 nm. The repetition rate was varied between 1 and 5 Hz. The laser energy per pulse was approximately 2 $mJcm^{-2}$ for the MPB laser and could vary from 1 to 5 $mJcm^{-2}$ for the Lumonics laser.

The fluorescence images for acid generation in photoresists were taken with a Zeiss Universal microscope. Two sets of filters were used to image the latent acid images. The first filter cube has an excitation band pass filter of 485 ± 20 nm, a 510 nm long pass dichroic beam splitter and a 520 nm long pass emission filter. It was used for negative images. The second filter cube has an excitation band pass filter of 546 ± 12 nm, a 580 nm long pass dichroic and a 590 nm long pass emission filter. It was used for positive images. The black and white images were recorded with a 640 x 480 cooled CCD 8-bit monochrome camera with a 4x magnification objective. The color pictures were obtained with a Sony digital camera and a higher magnification objective.

The fluorescence images for acid generation in polymer films that do not contain a PAG were taken with a Leica DMLS microscope equipped with a DFC300 FX camera. Two filter cubes from Leica were used, E4 and M2 to obtain images of latent acid. The E4 filter cube has an excitation band pass filter of 436 ± nm, a dichroic 455 nm and an emission with a long pass filter at 470 nm. The M2 filter cube has a band pass excitation filter 546 ± 14 nm, a dichroic 580 nm and an emission with a long pass filter at 590 nm, see Chapter 1.

The film thickness was measured with a Thin Film Analyser (TFA-11) from Luzchem. The dye was omitted from the solutions and the films were prepared as usual for thickness measurements.

Imaging of the surface was done by AFM courtesy of the NRC. The instrument is a Multimode Nanoscope III atomic force microscope from digital Instruments. It was used mostly in the repulsive mode in air. The J scanner and

200-nm-long cantilevers with integrated pyramidal silicon nitride tips (spring constant of 60 mNm^{-1}) were used. Some images were also acquired in the tapping mode.

2.3 Model Systems in Solution

2.3.1 Laser Flash Photolysis of Decafluorobenzophenone

The spectrum of decafluorobenzophenone (DFBP) with HFP as a solvent show a peak around 500 nm that can be assigned to the triplet of DFBP and a shoulder that extends to 700 nm, see Figure 2.5. This shoulder cannot be assigned to solvated electrons as when the solution is degassed with N_2O, a known electron scavenger, there is no change in the spectra, see Figure 2.6.

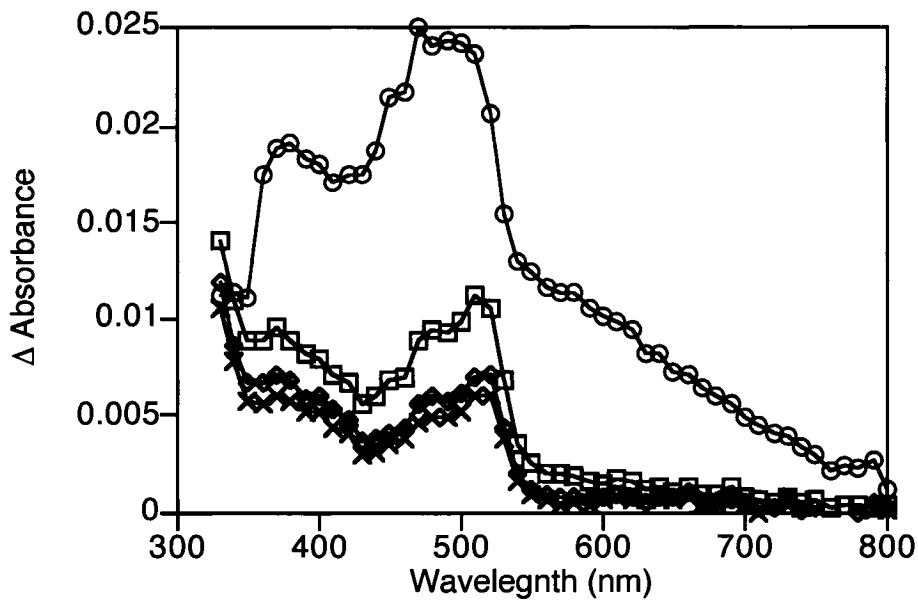

Figure 2.5 *Decafluorobenzophenone, 2.2 mM, in HFP degassed with N_2. Traces were taken, 0.48 μs (○), 2.64 μs (□), 8.64 μs (◇) and 14.9 μs (×) after the 308 nm laser pulse.*

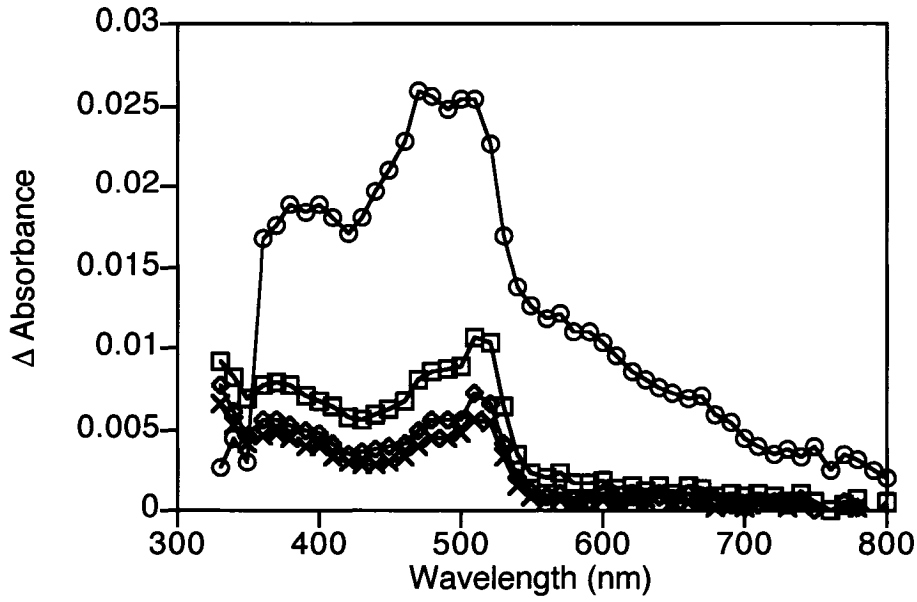

Figure 2.6 *Decafluorobenzophenone, 2.2 mM, in HFP degassed with N_2O. Traces were taken, 0.48 μs (○), 2.64 μs (□), 8.64 μs (◇) and 14.9 μs (×) after the 308 nm laser pulse.*

It would be unlikely for DFBP to photoeject an electron. Because of the high reactivity of HFP with solvated electrons, see 1,4-DMB and HFP reactivity (see Section 2.3.4), DFBP was also dissolved in methanol. The spectra acquired in methanol do not show a peak for the solvated electron. The triplet from DFBP abstracts hydrogen from methanol and generates a ketyl radical. This ketyl radical absorbs at 520 nm, as can be seen in Figure 2.7. This reaction has already been reported.[23,24] DFBP and HFP are both electron deficient molecules and there is no observable reactivity between them.

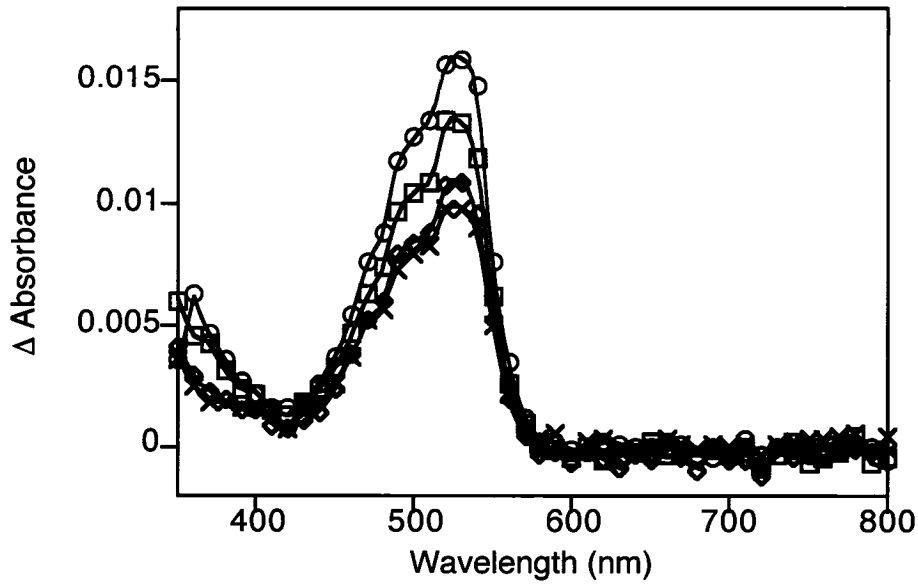

Figure 2.7 *Decafluorobenzophenone, 5.1 mM, in methanol degassed with N_2. The traces were taken 0.96 μs (○), 3.04 μs (□), 10.2 μs (◇), 21.8 μs (×) after the 266 nm laser pulse.*

2.3.2 Photogeneration of Solvated Electrons by 1,4-Dimethoxybenzene

1,4-Dimethoxybenzene (1,4-DMB) in methanol was exposed to 266 nm irradiation. As shown in Figure 2.8, a peak at 430 nm is observed and is assigned to the 1,4-DMB radical cation.[25] The second band extending beyond 650 nm is assigned to the solvated electron.

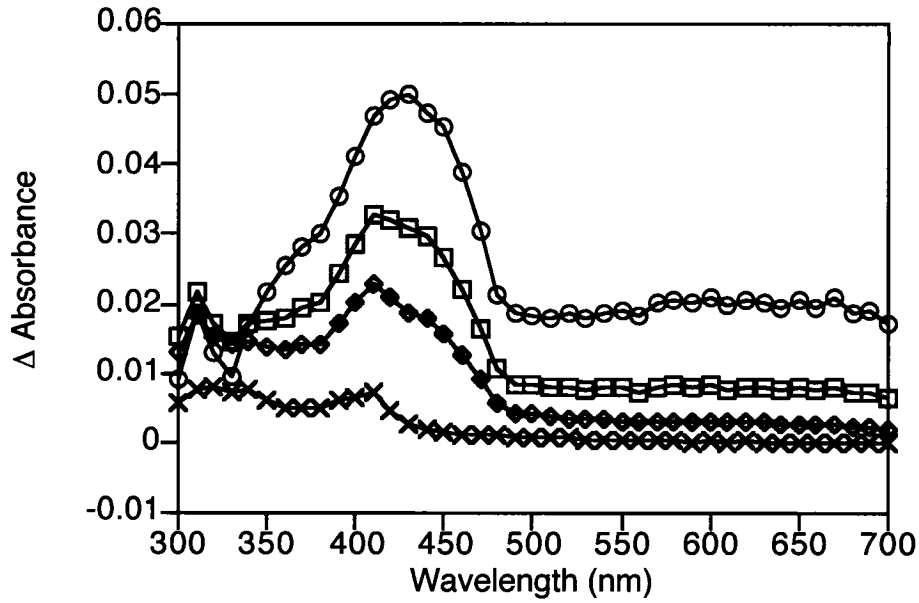

Figure 2.8 *1,4-DMB 0.65 mM in methanol deaerated with N_2. Traces shown taken 0.32 μs (○), 1.28 μs (□), 2.72 μs (◇), and 15.8 μs (×) after the 266 nm laser pulse.*

Nitrous oxide is a known electron scavenger. According to Scheme 2.10 we can see that solvated electron will be trapped by N_2O. A solution of 1,4-DMB in methanol was degassed with N_2O. As can be seen in Figure 2.9, the peak for the solvated electron is quenched by N_2O. The absorption band at 650 nm disappears.

$N_2O + e^-(aq) \rightarrow N_2 + OH\bullet + OH^-$

$N_2O + e^- (CH_3OH) \rightarrow N_2 + OH\bullet + CH_3O^-$

Scheme 2.10 *Reactivity of nitrous oxide with solvated electrons in water and in methanol*

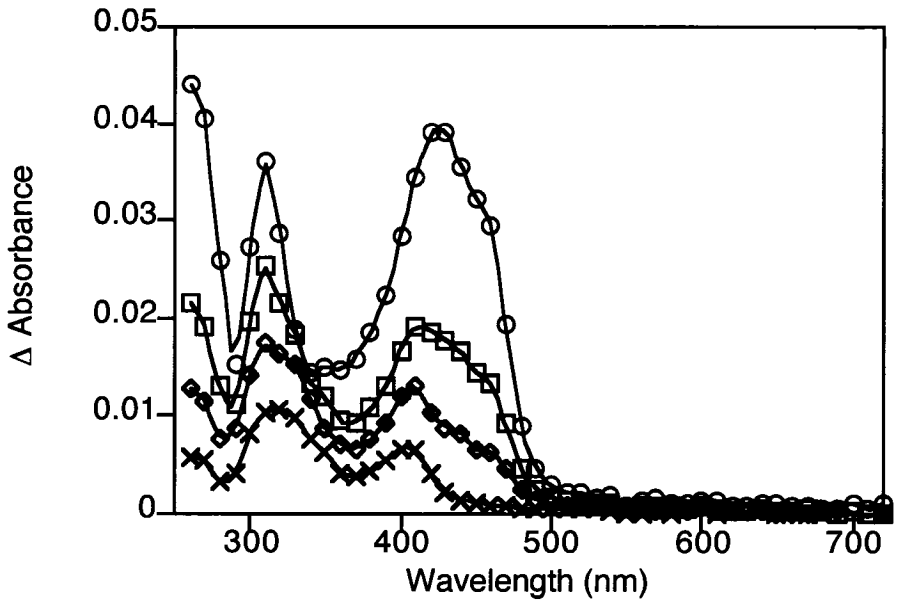

Figure 2.9 *1,4-DMB 0.66 mM in methanol deaerated with N_2 followed by degassing in N_2O. The traces shown are taken 0.24 μs (○), 2.56 μs (□), 5.52 μs (◇), and 16.4 μs (×) after the 266 nm laser pulse.*

These two experiments demonstrate that 1,4-DMB generates solvated electrons under irradiation at 266 nm using methanol as the solvent. 1,4-DMB was used as a source of electrons in solution in the following experiments designed to show the reactivity with electrons of common moieties present in photoresist designed for use at 157 nm.

2.3.3 Modeling Ester Moieties with Benzyl Acetate

Benzyl acetate (BA) in methanol was exposed to 266 nm excitation during laser flash photolysis. BA was chosen as a model for the ester moieties that are present in test photoresist for use at 157 nm. The spectra shown in Figure 2.10, shows a short-lived peak at 650 nm that can be assigned to the solvated electron.

It is important to notice that the intensity of the absorbance peak assigned to the solvated electron is much smaller for BA than for 1,4-DMB. The generation of electrons by BA is minimal. These experiments were conducted in a flow cell.

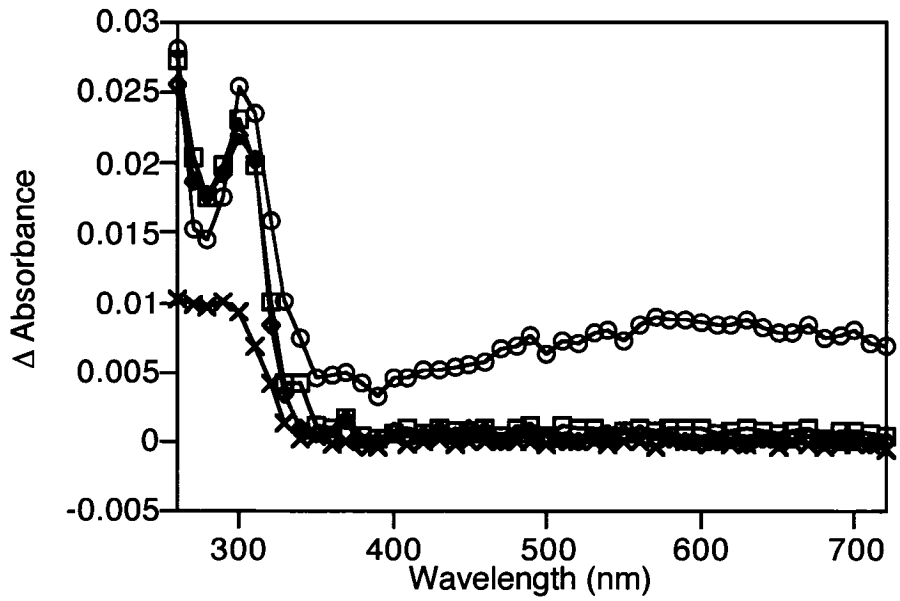

Figure 2.10 *Benzyl acetate 4.98 mM in methanol was exposed to 266 nm laser irradiation in a flow cell. The traces shown are taken 0.24 μs (○), 0.96 μs (□), 1.52 μs (◇), and 15.4 μs (×) after the laser pulse.*

Addition of benzyl acetate to 1,4-DMB in methanol traps the electron generated by 1,4-DMB upon exposure. Representative kinetic traces for different concentrations of BA are shown in Figure 2.11. The intensity of Δabsorbance immediately after the laser pulse is getting weaker with increasing BA. This decrease can probably be attributed to the competitive absorption of BA that has a low yield of electron generation. The fit of each of these kinetic traces gives an apparent rate constant for each concentration of BA present in solution.

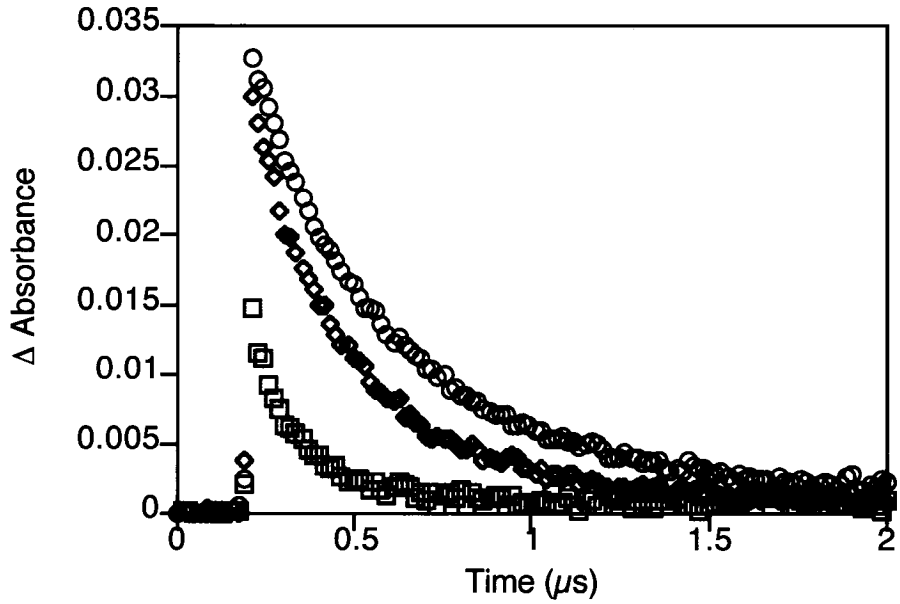

Figure 2.11 *Representative kinetic traces at 650 nm obtained during laser flash photolysis of 1,4-DMB in the presence of BA, with 266 nm laser excitation. Benzyl Acetate 0 mM (○), 3.3 mM (◇), 16.7 mM (□).*

The slope of the apparent rate constant versus concentration of BA is the rate constant for electron trapping, generated by 1,4-DMB in methanol, see Figure 2.12. We find that benzyl acetate traps electrons generated by 1,4-DMB in methanol with a rate constant of 2.9×10^{8} $M^{-1}s^{-1}$. The rate constant of a hydrated electron capture by benzyl acetate is reported to be 1.1×10^{9} $M^{-1}s^{-1}$.[21] The experimental rate constant for trapping of electrons by BA in methanol is similar to the values reported in the literature for an aqueous system.

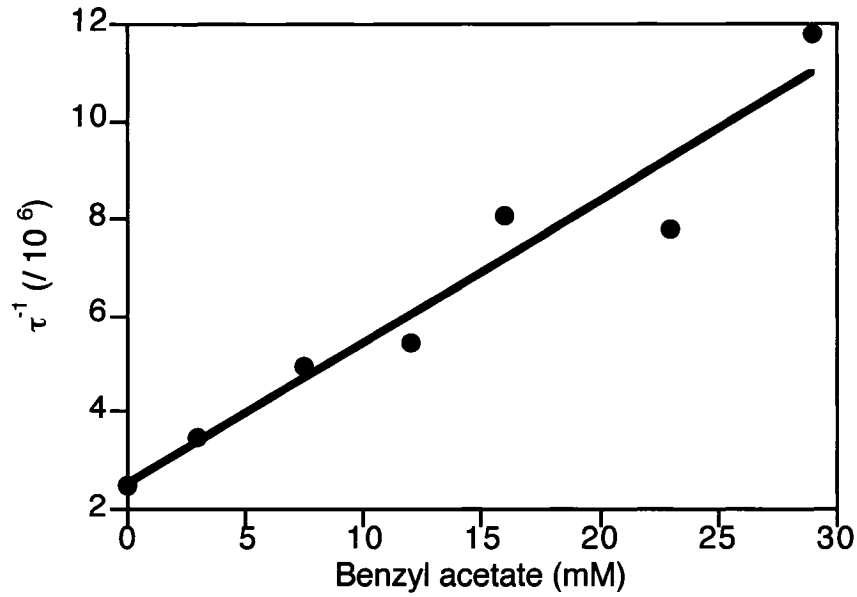

Figure 2.12 *Plot of rates versus concentration of BA for the trapping of electrons generated by 1,4-DMB at 266 nm. Concentration of 1,4-DMB constant 0.3 mM.*

2.3.4 Modeling Fluorinated Moieties with 1,1,1,3,3,3-Hexafluoropropan-2-ol

When 1,4-DMB was dissolved in HFP the peak at 650 nm for the solvated electron was not visible. Figure 2.13 shows the spectra obtained from laser flash photolysis with a 308 nm laser. A representative kinetic trace at 650 nm is shown in Figure 2.14.

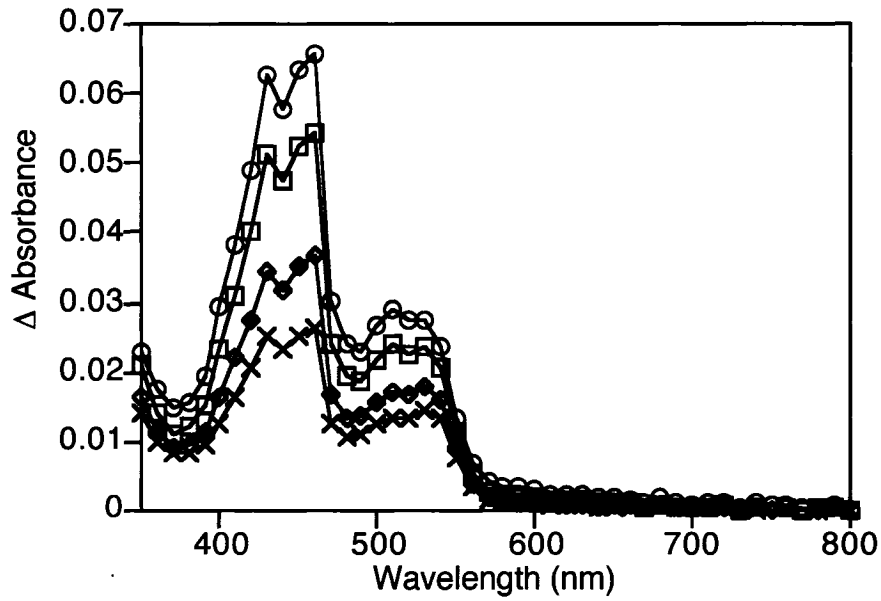

Figure 2.13 *1,4-DMB 5.1 mM in HFP. Traces were recorded, 0.48 μs (○), 2.64 μs (□), 8.64 μs (◇) and 14.9 μs (×) after the 308 nm laser pulse.*

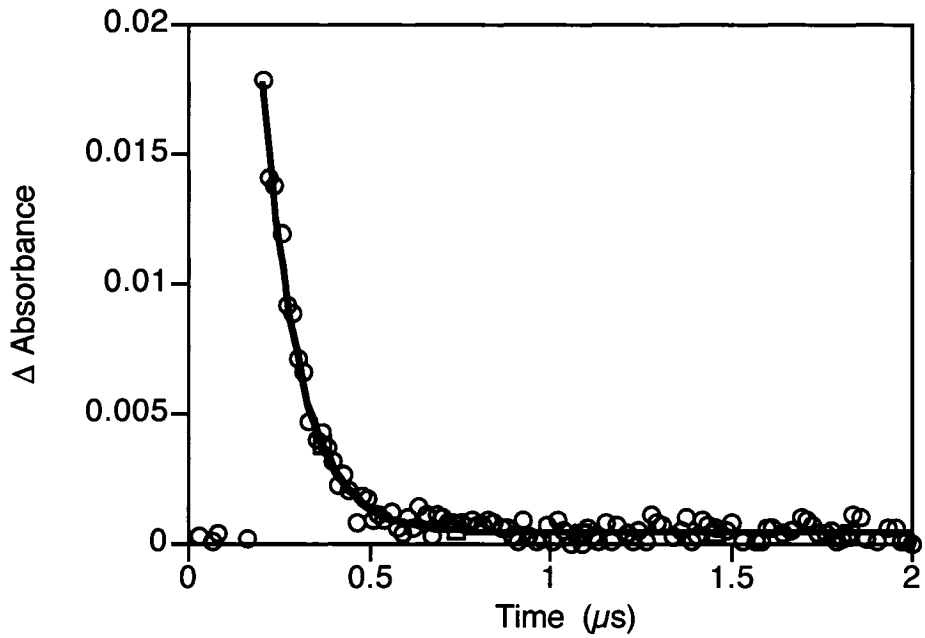

Figure 2.14 *Representative kinetic trace showing the decay of the solvated electron at 650 nm with the addition of 7.1 x 10 $^{-5}$ M HFP to 1.88 mM 1,4-DMB using 266 nm laser as the excitation source.*

Since the solvated electron generated by 1,4-DMB could not be seen in HFP, it was concluded HFP was trapping the electron generated by photoirradiation of 1,4-DMB in less than 10 ns. The rate constant of electron trapping by HFP in methanol was measured. A solution of 1,4-DMB 1.88 mM was deaerated with N_2. HFP was added by small increments. The plot of apparent rate constants versus HFP concentration, see Figure 2.15, has a slope of 6.56 x 10^{10} $M^{-1}s^{-1}$. It is the rate for electron trapping by HFP in methanol. This rate is above the diffusion limit and is consistent with the failure to detect the electron in pure HFP. The fact that HFP, a known moiety of test photoresist for 157 nm will trap electrons at a rate above the diffusion limit has great implications in the design of photoresists for use at 157 nm.

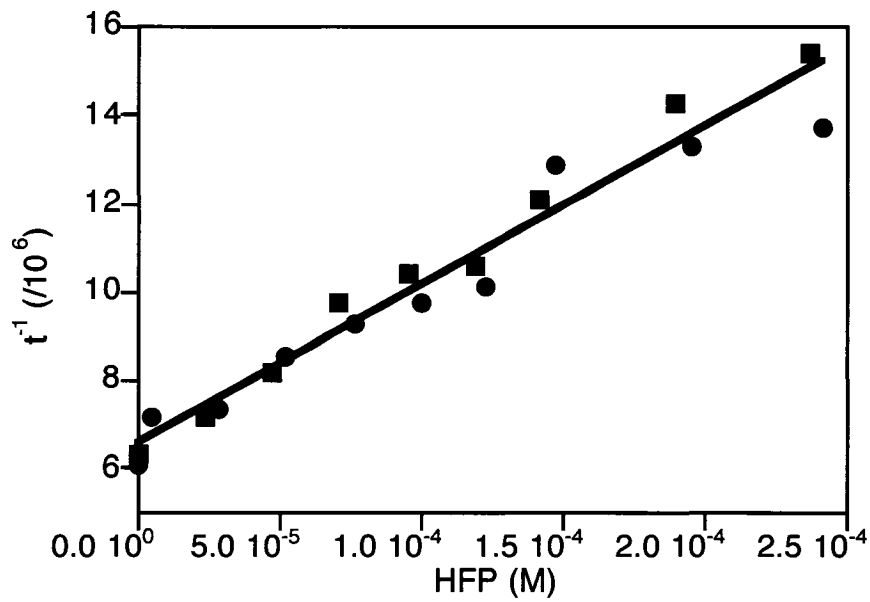

Figure 2.15 *Plot of rates vs. concentration of HFP. The slope of this plot is the rate constant for electron trapping by HFP in methanol. (■) and (●) are the values obtained on two separate trials.*

It is hypothesized that the non-fluorinated moieties present in photoresists will eject electrons upon irradiation at 157 nm. This is highly likely since the energy delivered by 157 nm is above that of most chemical bonds. The ionization sites will subsequently release a proton. Acid generation will be demonstrated in photoresists and in polymer films, see Section 2.4 and 2.5. Trapping of electrons released by the non-fluorinated moieties by the fluorinated moieties will eventually lead to fluoride release, see section 2.5.2. The proton and the fluoride will form HF, a highly undesirable side product.

2.3.5 Attempts at Showing Acid Generation in Solution

Many attempts were made to show the generation of HF in solution upon 157 nm irradiation. Coumarin 6, 0.016 g. was dissolved in 10 ml of methanol and filtered with a 0.45 μm filter. HFP was added to the green solution of C6 with no color change visible. HFP was exposed to 157 nm for more than 50 shots in the IR demountable cell. The average power of the laser varied from 1.4 to 2.3 $mJcm^{-2}$, so the total energy delivered to the sample was above 50 $mJcm^{-2}$. The IR demountable with a 0.1 mm spacer contains only a small volume of solution. The cell was demounted and the solution of coumarin 6 was added to the irradiated HFP. Since the volume was very small the C6 solution was added directly to the bottom window of the demountable cell. This prevented too much manipulation of the irradiated HFP. There was no color change visible to the naked eye. The expectation was that HF had been generated by irradiation of HFP at 157 nm. The acid would have in turn protonated the dye C6 and turned the solution's color to the characteristic red color of the protonated form of the dye. The experiment was

repeated with more than 200 shots of irradiation to the solvent HFP. Again no color change was detected. The experiment was repeated with progressively longer times of exposures, up to 20 min at a repetition rate of 5 Hz. When a solution of HCl was added to C6 in methanol an immediate color change was observed.

We could not detect acid in solution after many attempts. The volume irradiated was small and the amount of acid that could be detected is therefore small as well. The failure to detect acid is probably due to experimental difficulties. We should have had a larger volume so we could have done fluorimetry but expensive and volatile solvents limited our ability to do this. Also we did not have a large enough cell to expose large volumes. At 157 nm CaF_2 cell must be used for transparency issues and they are very expensive. We had thought of exposing the solution and then to put the exposed solution into the GC-MS but the IR demountable we were using had leakage problems. After 20 minutes of irradiation the cell was on most occasions dry. HFP is a volatile solvent and this combined with the cell not being leak proof prevented us from obtaining this information on acid formation of HF. In any event we eventually succeeded in detecting HF directly in the more relevant resist film (see next section)

2.4 Acid Generation in Photoresists

2.4.1 Acid Generation in Non- fluorinated Resists

Fluorine-free resists have a high absorbance at 157 nm of 6.8/μm (expressed here per μm of thickness of the film). This absorbance is too high for an industrial use at 157 nm. Exposure would be limited to a region near the surface and would not generate patterns with enough depth upon development. Nevertheless we did expose to 157 nm films made from this resist and containing coumarin 6 in order to monitor acid generation at this shorter wavelength. This photoresist contains a PAG.

Exposure to 1.8 $mJcm^{-2}$ with the 157 nm MPB laser of a film containing C6 through a mask generates acid in the exposed areas. The mask has hexagonal holes that measure 60 μm from center to center. As most materials have a high absorbance at 157 nm, masks that are used for exposure at longer wavelengths could not be used, as they would not have been transparent at 157 nm. As can be seen in Figure 2.16, acid was detected after exposure to only 1.8 $mJcm^{-2}$ or in this case, one laser shot. The fluorescence of the neutral form of the dye is monitored by using the appropriate filter cube, see the first column of Figure 2.16. We can observe that the fluorescence of the neutral form of the dye is visible only in the unexposed areas. We can observe fluorescence of the neutral form of C6 only under the grid of the mask and no fluorescence is visible inside the hexagonal holes, which were exposed to 157 nm irradiation

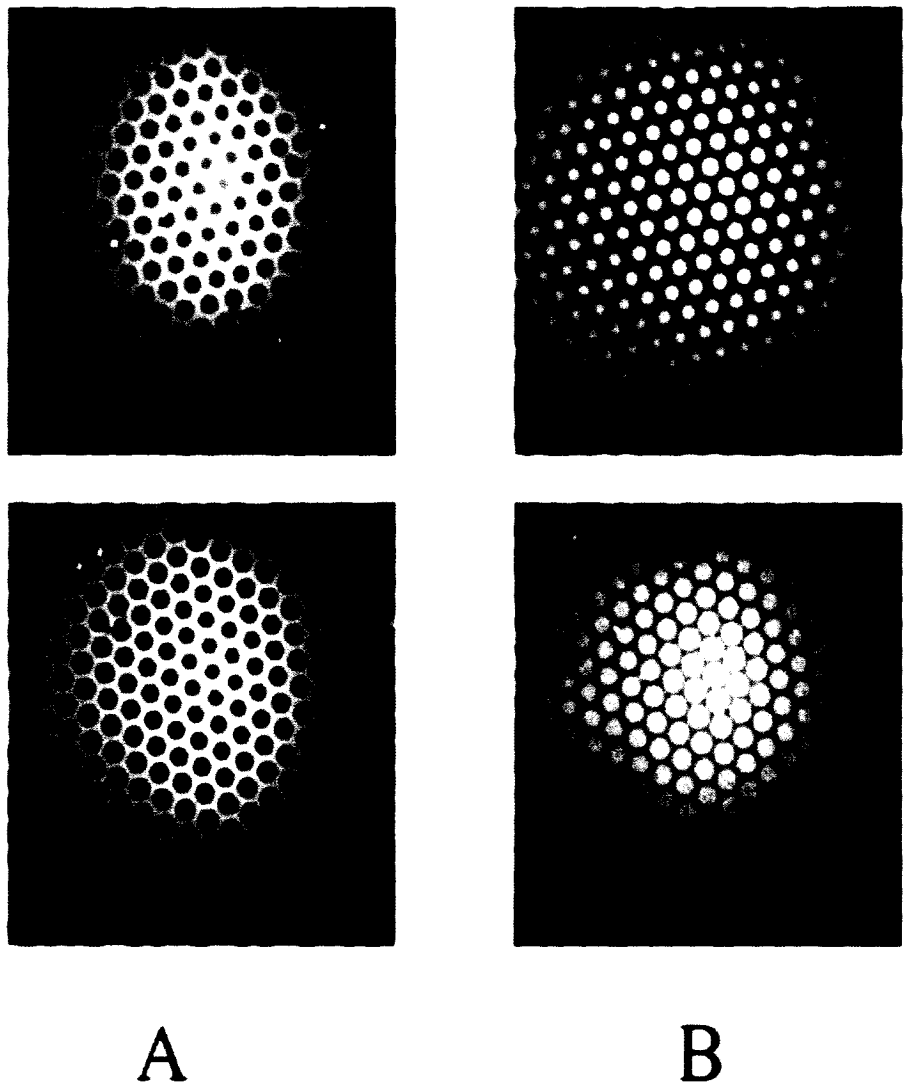

Figure 2.16 *Fluorescence images of a film containing XP2332C, a commercial non-fluorinated photoresist and coumarin 6 after exposure to 157 nm. Column A fluorescence images of the non-protonated form of coumarin; column B the protonated form of Coumarin 6. The first row shows exposure to 1.8 mJcm^{-2} or 1 shot and the second row was imaged after 20 shots or 28 mJcm^{-2}.*

By changing the filter cube on the microscope and maintaining the film in the same position, it is possible to monitor both forms of the dye in the same spot.

Acid is generated in the exposed areas, as can be seen from the fluorescence in the right column of Figure 2.16, which corresponds to the fluorescence of the protonated form of C6. In the unexposed areas there is no fluorescence of the protonated form of the dye. This clearly shows that C6 undergoes protonation upon exposure to 157 nm in this non-fluorinated photoresist; thus showing that acid is generated by irradiation at 157 nm.

2.4.2 Mapping Acid in a Fluorinated Resist

The resist that was formulated for 157 nm, XP1215AA, has a lower absorbance due to the fluorinated moieties. The polymer film contained in the resist is only partially fluorinated, see Scheme 2.2. We first verified that the resist does not absorb in the region where the dye absorbs or emits. This resist contains a PAG.

Coumarin 6 was added to the fluorinated photoresist and spin coated onto a quartz disk. Electron microscope grids with hexagonal holes were deposited on the film surface. After exposure to 1 shot at 157 nm, no acid was detected because base is usually added to these formulations. Once the added base is neutralized by the acid generated by the PAG, the excess acid is used to protonate the dye C6. After exposure to 2.3 $mJcm^{-2}$ per shot for 35 shots, acid is detected in the exposed areas as can be seen in Figure 2.17. The green fluorescence is of the neutral form of the dye and is observed in the unexposed areas only. The red fluorescence of the protonated form of the dye is observed only in the exposed areas of the film.

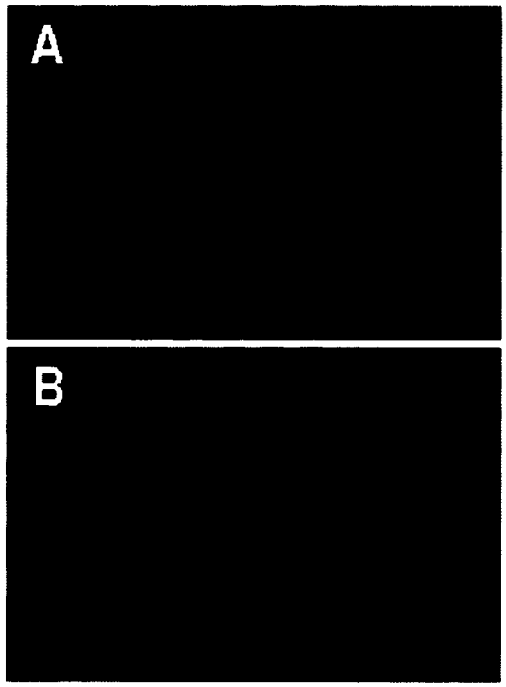

Figure 2.17 *Fluorescence images of neutral form of coumarin (A) and of the protonated form (B) after exposure to 80 mJ cm^{-2} at 157 nm of a film made with a fluorinated resist containing a PAG.*

Acid was generated upon exposure to 157 nm in a fluorinated photoresist and was monitored by the protonation of the dye C6. Protonation only occurred in the exposed areas of the mask. By using the appropriate filter cubes with the microscope, detection of the protonated form and neutral forms of the dye were performed on the same spot of the film. This demonstrates clearly that protons are generated by exposure to 157 nm in the exposed areas.

2.5 Acid Generation in PAG-free Polymer Films

2.5.1 Fluorescence Detection of Acid Formation

Films of PMMA, FP and EC with C6 were prepared according to the methods described in section 2.2. The films thicknesses were measured to be between 300 to 500 nm. The films were then exposed to the same number of shots of 157 nm irradiation under a copper electron microscope grid as a mask. Using the filters E4 and M2 to detect selectively the neutral and the protonated form of C6, fluorescence images were obtained. Figures 2.18-2.20 were obtained after exposure to 20 shots with an energy of 5 $mJcm^{-2}$ per shot. The inside of the hexagons are the exposed areas. The negative images show fluorescence from the neutral form of C6 in the unexposed areas of the films. The positive images show that protonated C6 is present in the exposed areas of the films. These images were taken on the same spot of the films, using different filter cubes. In comparison with films that contained a photoacid generator (PAG), the energy required to generate acid is much higher for films of comparable thicknesses that do not contain a PAG. PMMA films have a higher absorbance at 157 nm than the FP film and thus generate more acid than the FP films. Ionization followed by deprotonation will provide the proton necessary to generate the protonated C6.

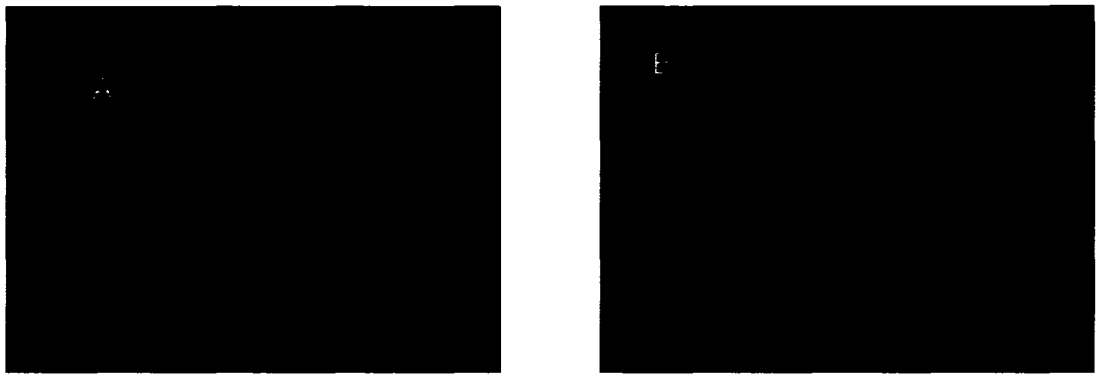

Figure 2.18 *Fluorescence images of ethyl cellulose film with C6 exposed to 157 nm. (A)The negative image is obtained with the E4 filter and show the neutral dye C6, (B) the positive image, obtained with the M2 filter, shows the fluorescence of the protonated C6 and was contrast enhanced for printing.*

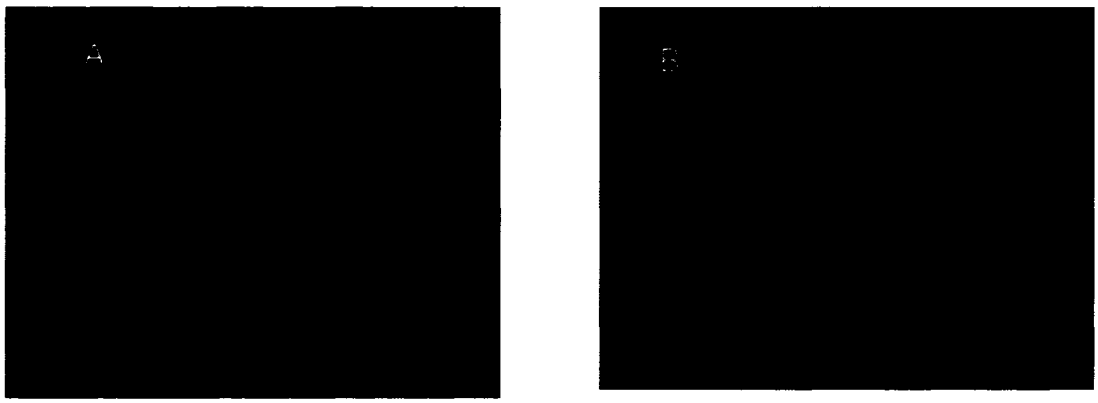

Figure 2.19 *Fluorescence images of a PMMA film with C6 exposed to 157 nm. (A)The negative image is obtained with the E4 filter and shows the neutral dye C6, contrast enhanced for printing (B) the positive image, obtained with the M2 filter, shows the fluorescence of the protonated C6.*

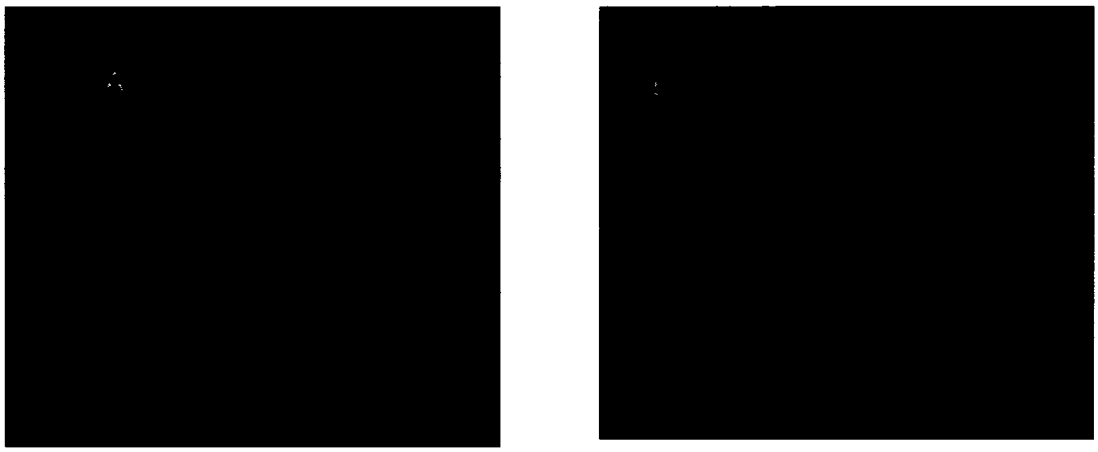

Figure 2.20 *Fluorescence images of a FP film with C6 exposed to 157 nm. (A) The negative image was obtained with the E4 filter and shows the neutral dye C6, (B) the positive image, obtained with the M2 filter, shows the fluorescence of the protonated C6. Both images were contrast enhanced for printing.*

2.5.2 Fluoride Detection

C4TIPS is a fluorescence sensor being developed by Dr. C. Sanramé, a postdoctoral fellow in our group. Films containing C4TIPS were prepared following the method described in section 2.2. Electron microscope grids were used as masks. Exposure to 157 nm irradiation of PMSSQ, and EC films do not show fluoride formation. Fluorescence imaging using the XF02-2 filter showed only minimal fluorescence in the exposed regions for these polymers. Exposure of a FP film containing C4TIPS reveals fluoride formation in the exposed regions, see Figure 2.21. All the films were exposed to 50 shots with a repetition rate of 3 shots per second for a total energy delivered to the films of 60 $mJcm^{-2}$. The blue fluorescence observed in the exposed areas is due to the deprotected form of the sensor C4TIPS. Fluorescence in the unexposed areas is minimal and can be

attributed to the residual fluorescence of C4TIPS in its protected form. The sensor has not been tested for its specificity to fluoride, however no other halide is present in the FP film. The fact that only minimal fluorescence was observed for EC and PMSSQ films after exposure strengthens the conviction that C4TIPS is sensitive to fluoride, since fluoride can only be formed in the FP films.

Figure 2.21 *Fluorescence of a FP film containing C4TIPS after exposure through a mask at 157 nm of 50 shots of 1.2 mJ* cm^{-2}.

2.5.3 AFM Imaging

AFM was used to examine the surface of the films after laser exposure. Differences in heights were observed on the surface. The exposed areas were recessed relative to the unexposed areas of the films. The degree of ablation varies with the amount of exposure as well as the nature of the polymer. Figure 2.22 shows a typical AFM topograph taken of a film of ethyl cellulose after exposure to 157 nm irradiation of approximately 250 $mJcm^{-2}$.

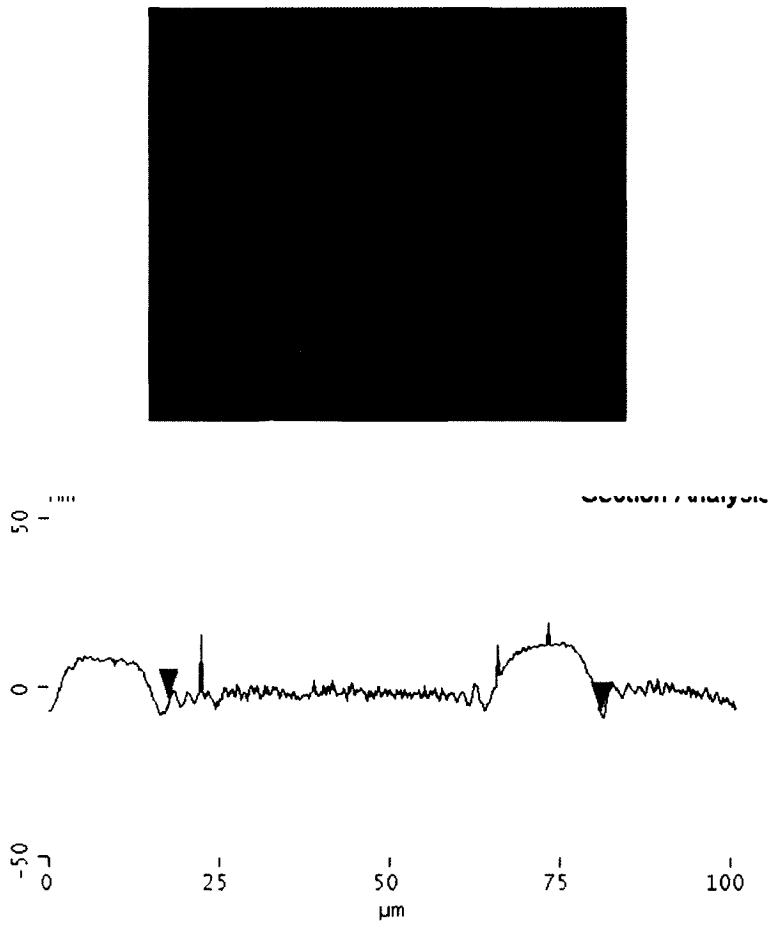

Figure 2.22 *AFM image obtained after irradiation with 250 mJcm^{-2} at 157 nm of a cellulose film containing C6. The film was exposed to 100 laser pulses with a repetition rate of 2 Hz.*

The AFM scan revealed that the film had depressions in the exposed areas. The average depth of the features on this film is 12 nm. A fluorescence image of the same film reveals that the dye C6 was not as fluorescent in the exposed areas and that the protonated form of the dye was present in the exposed areas.

The depth recorded in the exposed areas relative to the unexposed regions for different polymer films of approximately the same thickness after exposure to the same number of shots at 157 nm was recorded on different spots of the films. The depth was measured as the difference between the unexposed areas and the center of the exposed areas, in the middle of the hexagonal pattern of the electron microscope grid we used as a mask. The average depth is ~ 17 nm for the PMSSQ film, ~ 66 nm for the EC film and ~ 33 nm for the FP film after exposure to 200 laser pulses for a total energy of 460 $mJcm^{-2}$. The ablated depth is related to the energy delivered to the film as well as the absorbance of the films.

The AFM images also reveal formation of laser induced periodic surface structures. Figure 2.23 clearly shows patterns near the edges of the mask. We can only hypothesize as to what causes these LIPSS. Thermalization is quite plausible at a very energetic wavelength such as 157 nm. This would lead to decomposition of the polymer and ejection of material from the film. The film surface was cleaned with a stream of air before imaging that would have removed any debris from the surface. Therefore we did not observe any debris on the surface with AFM.

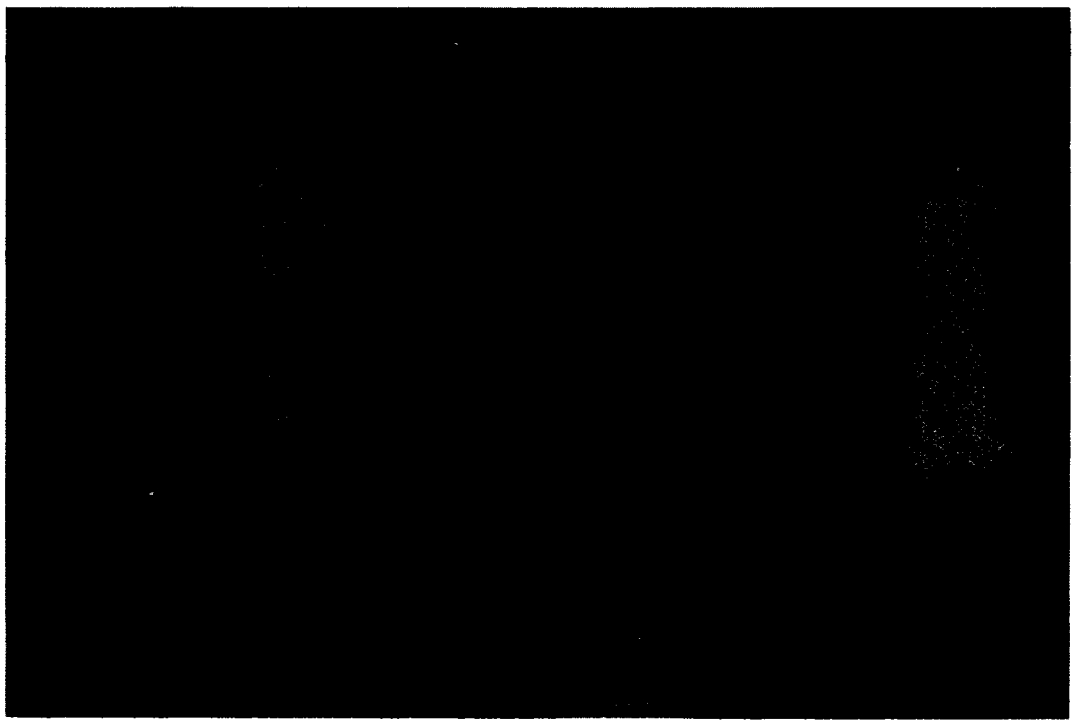

Figure 2.23 *AFM image shows LIPSS formation on an EC film containing C6 after exposure to 500 mJcm^{-2}.*

The mask is only loosely deposited on the film surface and there is not a complete adhesion of the mask to the film. Therefore, as the film is being irradiated, there can be a gap between the edge of the mask and the film surface. The laser beam is oriented as perpendicular to the film surface as possible within a few degrees but this can lead to the laser beam hitting the edge of the mask at an angle deviating slightly from the normal. These two factors combined could lead to interference patterns at the edge of the mask. These patterns could then be propagated to the rest of the film. In certain films that were more extensively exposed, LIPSS could also be observed in the unexposed areas. This is indicative of an imperfect adhesion of the mask to the film or imperfect alignment of the laser

beam relative to the mask or film. Light being diffracted at the edges of the mask could reach under the mask to regions that otherwise would be unexposed.

2.6 Discussion

The ability to map acid generated in films is an important tool. Once the wafer has been developed, etched, and stripped, it becomes more complicated to retrace the step at which something could have influenced the image quality. Recording a latent image of where the acid is formed gives additional insight into the early steps of the photolithographic process. The generation of acid and its spatial distribution in the film are crucial steps in the fabrication of computer chips. Coumarin 6 is an ideally suited dye for these experiments. Once protonated, its fluorescence is sufficiently shifted to easily distinguish the neutral and protonated forms of this dye with fluorescence microscopy using the appropriate filters.

The important conclusion we can make from irradiating films containing a PAG, is that acid formation can readily be detected at 157 nm, the same as with longer wavelengths. The fact that we can see disappearance of the unprotonated form as well as appearance of the protonated form of C6 in the irradiated areas, using the different filter cubes for the microscope, is further proof that acid is generated in the exposed areas. By looking at the negative image, it could be argued that irradiation at 157 nm could have merely destroyed the dye Coumarin 6. By having positive and negative images of the same area we have further proof that acid is generated in the exposed areas. We also note that for the fluorinated

photoresist formulation that was devised for 157 nm more than one shot is required to monitor acid formation. We assign this to the fact that many photoresist formulations have added base to minimize diffusion in the non-irradiated areas and to enhance contrast. After a single shot, insufficient acid was generated to neutralize the base present in the photoresist formulation. Acid was detected after 3 shots or 5.3 $mJcm^{-2}$ of 157 nm irradiation. This adds to the proof that the positive images that we see are due to acid formation.

We also noticed that the images were essentially the same after the onset of fluorescence whatever the energy delivered to the films. This indicates that once acid is generated the catalytic process takes over acid formation quickly. The concentration of C6 in the films is the limiting factor for our observation of the fluorescence intensity of the protonated form of the dye.

Exposure of polymers that do not contain a PAG also showed the formation of acid. The fluorinated polymer XP0921, ethyl cellulose, PMMA as well as PMSSQ films all show protonation of the dye Coumarin 6. Addition of C4TIPS, a fluoride sensor has shown that irradiation of the fluorinated polymer (FP) at 157 nm generates fluoride. The sensor has not yet been fully characterized for its selectivity to fluoride but the only halide present in our films is fluoride. The other polymer films, PMSSQ and EC do not reveal the presence of halides after exposure when C4TIPS is added in the films, as expected.

AFM demonstrates that 157 nm is a very energetic wavelength inducing variable degree of etching in the films upon exposure. The films that show the highest absorbance show the most damage. Ablation of films is also of great

concern to companies who may have been thinking of switching to 157 nm for their photolithographic needs. Steppers, especially in the production of electronics components require a high degree of cleanliness. Clean room facilities are incompatible with microscopic debris being ejected from the films as they are exposed.

We can note that ablation does not interfere with the dye C6 or the sensor C4TIPS ability to detect protons or fluoride. Ablation may remove up to 10% of the films thickness but leaves enough material to monitor acid or fluoride generation in the exposed areas. Prolonged exposure may lead to irreversible film degradation but this extensive exposure would not be economically favored in an industrial setting. Whether or not the acid is generated in the whole thickness of the film is not known. We do not have the imaging capabilities to develop the films after exposure and investigate the depth of the patterns. Proper masks for use at 157 nm have not been developed until now. However, we can be assured that acid is generated by the PAG following irradiation at 157 nm in the exposed areas.

Solution work at test wavelengths has however put a damper on the possible use of fluorinated photoresists. The fact that HF is most certainly produced by HFP moieties contained in test photoresist, is something that companies will have to consider for the development of photoresists for use at the wavelength of 157 nm. Photoresist formulations that are developed for 157 nm contain a HFP moiety in their formulation because it gives higher transparency at 157 nm. The fluorinated monomers confer transparency to the resist; which is a requirement at 157 nm because of the high absorbance of most materials at that

wavelength. HFP has been found to trap electrons generated by 1,4-DMB in methanol with a rate constant of 6.6 x 10^{10} $M^{-1}s^{-1}$. Generation of HF in production facilities is something that has to be avoided because of the corrosive nature of the acid. The rate constant for electron trapping by benzyl acetate we determined is in the same range as those reported for esters, but more than one order of magnitude smaller than the rate constant for trapping by HFP.

We have shown that acid can be formed after irradiation at 157 nm of photoresist containing PAGs. While the photolithographic process is known to work at other longer wavelengths, we have shown that acid can also be generated using the photolithographic process at this short and very energetic wavelength.

We have also shown that acid can be generated after irradiation at 157 nm of polymer formulations that do not contain PAGs. In these cases the onset of fluorescence detection and formation of a positive image requires a much higher dose of irradiation.

We propose that HF is formed by photoejection of an electron in the non-fluorinated moieties of fluorinated photoresists, followed by deprotonation at the ionization site.[13] The non-fluorinated moieties have the highest absorbance in the fluorinated photoresist making them more likely to release an electron upon exposure at 157 nm. The electron generated will be trapped by the fluorinated moieties. This has been demonstrated by the model systems in solution, where we have shown that HFP is a better electron trap than the ester, which is the other moiety present in the FP. The fluorinated moieties will subsequently release a fluoride and in the presence of the proton generate HF.

2.7 References

(1) Thompson, L. F.; Willson, C. G.; Bowden, M. J. *Introduction to microlithography* Washington D. C., 1994.

(2) Lewotsky, K. *Optical Engineering* **2001**, *1*, 20.

(3) Kim, S. K.; Guo, J.; Bashin, J. S.; Zewail, A. H. *J. Org. Chem.* **1999**, *64*, 5256.

(4) Leigh, W. J.; Cook, B. H. *J. Phys. Chem.* **1999**, *100*, 9202.

(5) Bloomstein, T. M.; Rotschild, m.; Kunz, R. R.; Goodman, R. B.; Palmaci, S. T. *J. Vac. Sci. Technol. B* **1998**, *17*, 3273.

(6) Liberman, V.; Bloomstein, T. M.; Rotschild, M.; Sedlacek, J. H.; Uttaro, R. S.; Bates, A. K.; Van Peski, C.; Orvek, K. *J. Vac. Sci. Technol. B* **1999**, *17*, 3273.

(7) Feke, G. D.; Grober, R. D.; Pohlers, G.; Moore, K.; Cameron, J. F. *Anal. Chem.* **2001**, *73*, 3472-3480.

(8) Dagani, R. *C & EN* **2003**, *181*, 44-49.

(9) Reichmanis, E.; Houlihan, F. M.; Nalamasu, O.; Neenan, T. X. *Chem. Mater.* **1991**, *3*, 394-407.

(10) Pohlers, G.; Scaiano, J. C. *Chem. Mater.* **1997**, *9*, 3222-3230.

(11) Coenjarts, C.; Cameron, J.; Pohlers, G.; Scaiano, J. C.; Zampini, A. *J appl Polym Sci* **2000**, *78*, 1897-1905.

(12) Scaiano, J. C.; Laferrière, M.; Ivan, M. G. *Macromolecules* **2003**, *36*, 6692-6694.

(13) Ivan, M. G.; Laferrière, M.; Sanrame, C. N.; Scaiano, J. C. *Chem. Mater.* **2006**, *18,* 2635-2641.

(14) Csete, M.; Bor, Z. *Applied Surface Science* **1998**, *133*, 5-16.

(15) Lippert, T.; Dickinson, J. T. *Chem. Rev.* **2003**, *103*, 453-485.

(16) Kawamura, Y.; Toyoda, K.; Namba, S. *Appl. Phys. Lett.* **1982**, *40*, 374.

(17) Bituyrin, N.; Luk'yanchuk, B. S.; Hong, M. H.; Chong, T. C. *Chem Rev* **2003**, *103*, 519-552.

(18) Hubert, C.; Fiorini-Debuisschert, C.; Maurin, I.; Nunzi, J.-M.; Raimond, P. *Adv. Mater.* **2002**, *14*, 729-731.

(19) Tanaka, M.; Wong, A. P.; Rehfeld, F.; Tutus, M.; Kaufmann, S. *J. Am. Chem. Soc.* **2004**, *126*, 3257-3260.

(20) Masnovi, J.; Maticic, J. *J. Am. Chem. Soc.* **1988**, *110*, 5189-5191.

(21) Christensen, H. C.; Sehested, K.; Hart, E. J. *J. Phys. Chem.* **1973**, *77*, 983-987.

(22) Boate, D. R.; Johnston, L. J.; Scaiano, J. C. *Can. J. Chem.* **1989**, *67*, 927-932.

(23) Anandhi, R.; Umapathi, S. *J. of Raman Spectrosc.* **2000**, *31*, 331-338.

(24) Shoute, L. C. T.; Mittal, J. P. *J. Phys. Chem.* **1993**, *97*, 8630-8637.

(25) Grabner, G.; Rausher, W.; Zechner, J.; Getoff, N. *J.C.S. Chem. Comm.* **1980**, 222-3.

Chapter 3
Laser Flash Photolysis with 157 nm

Table of Contents

Chapter 3
Laser Flash Photolysis with 157 nm

3.1 Introduction

Flash photolysis is a technique that was developed in the late 1940s by Norrish and Porter for which they received the Nobel prize in 1967.[1] Laser flash photolysis (LFP) was then developed in the mid 60s. This technique is used to measure the absorbance of transient species that are created by laser pulses. The technique is described in more details in Chapter 1. We were interested in using 157 nm as the excitation wavelength for laser flash photolysis of compounds that could be used in photolithography at 157 nm. We wanted to get more information on processes and mechanisms by the study of the transient species that would be created at that very energetic wavelength.

The challenge was to develop an experimental setup and find the appropriate materials for use at 157nm. In Section 3.2, a description of the chamber we built for laser flash photolysis specifically for use at 157 nm as well as a description of the cell holder we developed will be given. Section 3.3 will describe the experiments that were performed and present a discussion of the results.

Many different chromophores were utilized for the study of the feasibility of laser flash photolysis (LFP) using 157 nm as the excitation wavelength. o-Methyl acetophenone (OMAP) is among the chromophores tested. Lifetimes for the

photoenol from OMAP vary with the isomer of the enol.[2] The lifetime of the anti enol isomer is longer because it requires bond rotation before undergoing H-abstraction followed by relaxation to the ground state as can be seen in Scheme 3.1.

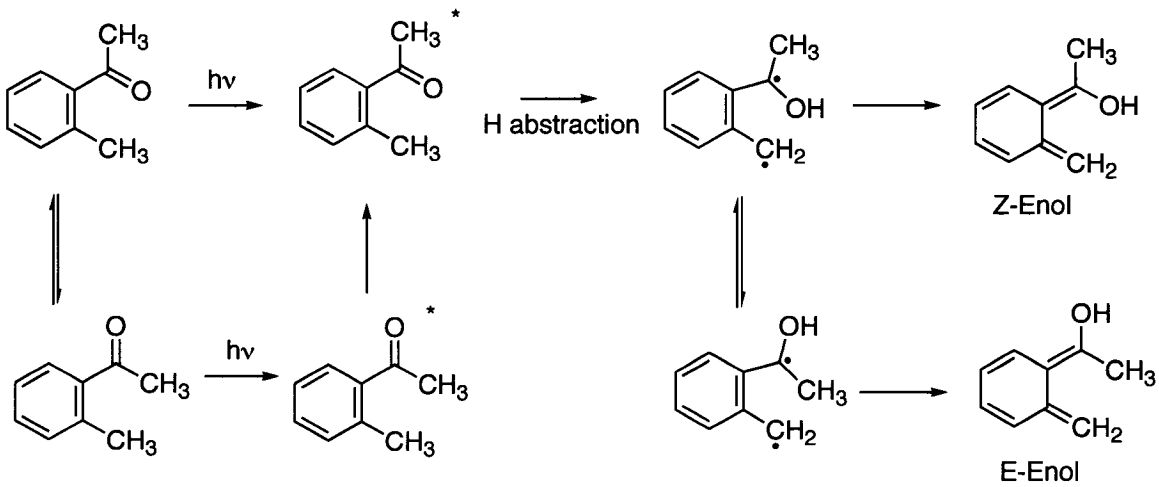

Scheme 3.1 *The enol isomers OMAP have different lifetimes. The Z-enol has a shorter lifetime than the E-enol.*

Xanthone, 1,4-dimethoxybenzene and pyrene are chromophores that have been studied by laser flash photolysis at wavelengths other than 157 nm. We chose these chromophores because of their known properties. Fluorinated solvents were also tested as these have some of the lowest reported absorbances at 157 nm.

In Section 3.4, the challenges and the future of LFP with 157 nm will be discussed.

3.2 Experimental Setup

3.2.1 Laser

Over the course of these experiments two different laser sources for 157 nm were used. The initial laser was an MPB Technologies Inc. MSX-250 Excimer. Laser specifically designed for use at 157 nm. The laser source was later changed to a GDS Lumonics laser filled with a fluorine mixture designed to generate 157 nm. This laser initially designed for use at 193 nm and 248 nm was modified for use at 157 nm by changing the mirrors and the recipe for the gas mixture.

3.2.2 Sample Chamber

The setup we used was changed many times over the years but the general idea was the same. The sample chamber was connected to the laser source by a sealed tube. The sample chamber was also connected to a N_2 source in order to be deaerated. The sample stage from the mini laser flash system (MLFP) from Luzchem described in Chapter 1, was also installed in the sample box. Great care was taken to seal as best as possible all the connections to the box in order to get the least amount of oxygen and water vapour inside our sample chamber, since both have strong absorptions at 157 nm.

The final sample box was constructed out of plexiglass, see Figure 3.1, where the sample could be monitored visually. It was possible to check if the cell

was still full or if the alignment of the monitoring beam and laser relative to the sample was good.

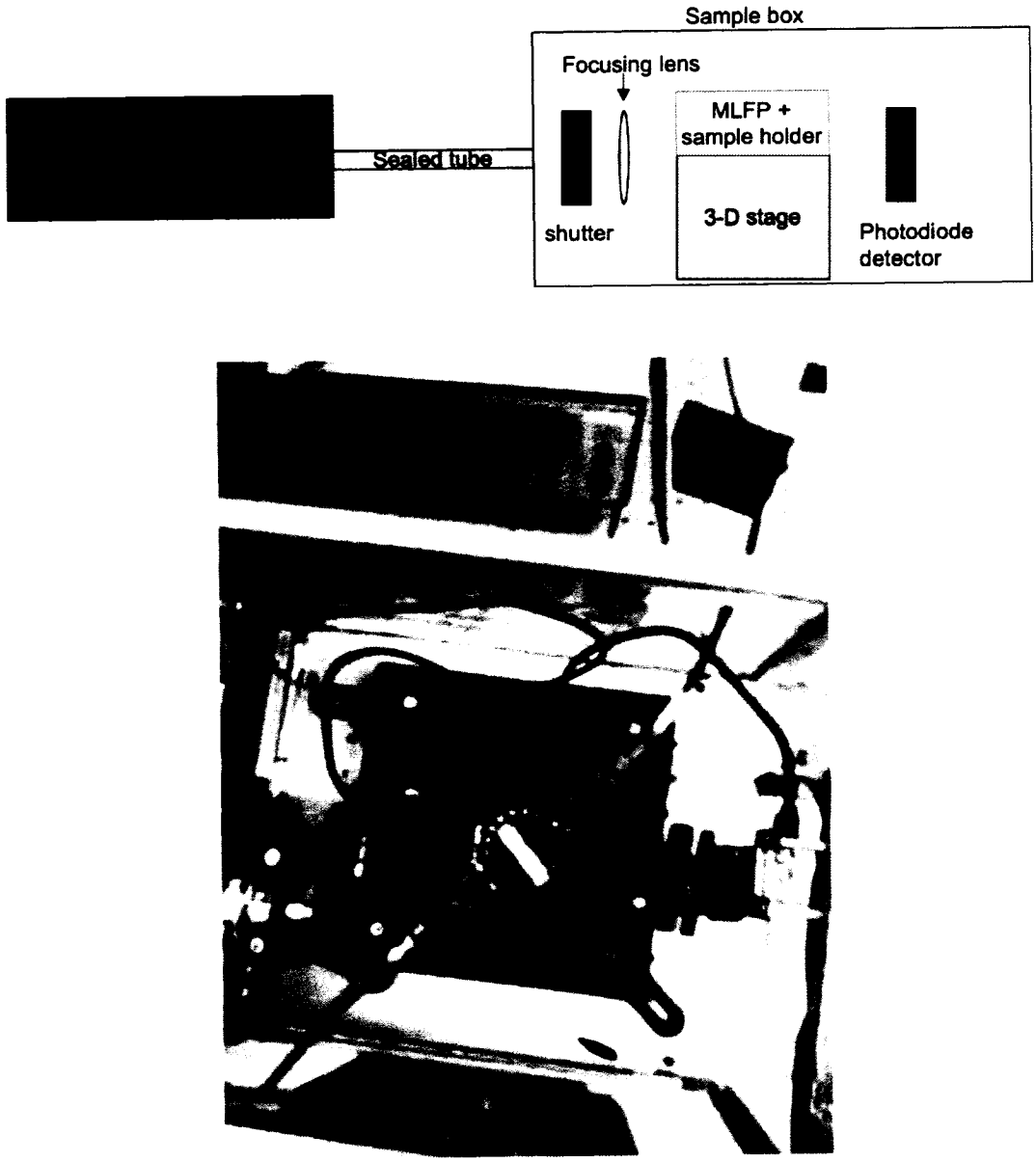

Figure 3.1 *Final setup, side view diagram and top view photograph.*

3.2.3 Sample Holder

CaF_2 cells were used for solution work. It was very important to find a material that was transparent at 157 nm. Calcium fluoride (thickness 1mm) lets about 80 % of the light through at 157 nm.[3] CaF_2 cells that are polished on 4 sides are not commercially available, we had to use cells with only two polished windows. An IR demountable cell from Aldrich was the first cell utilized. It has two 32 mm CaF_2 windows. The front window has two drilled holes for liquid injection. We discontinued its use because of problems with leaks and the fact that it was too thick to use for LFP.

Sealed cells with two CaF_2 windows were then purchased from Wilmad. They have pathlengths of 0.5 mm and 1 mm. They consist of two CaF_2 rectangular windows with a metal spacer in between. The front window has two drilled holes for liquid injection. Teflon stoppers for the cells were machined in order to reduce the amount of leakage we were experiencing. They are the most suitable liquid sample cuvettes we could find for use at 157 nm.

Films were spin coated on quartz disks or CaF_2 windows.

3.2.4 Setup

Several improvements were made over time. A piece of metal grooved with the right width to hold the CaF_2 sealed cell was made. This prevented the cell from moving during the experiments and allowed reproducible placement of the sample cell for subsequent experiments. The grooved piece of metal was on a slide and

let the sample move between the monitoring beams.. Figure 3.2 is a drawing of the sample holder.

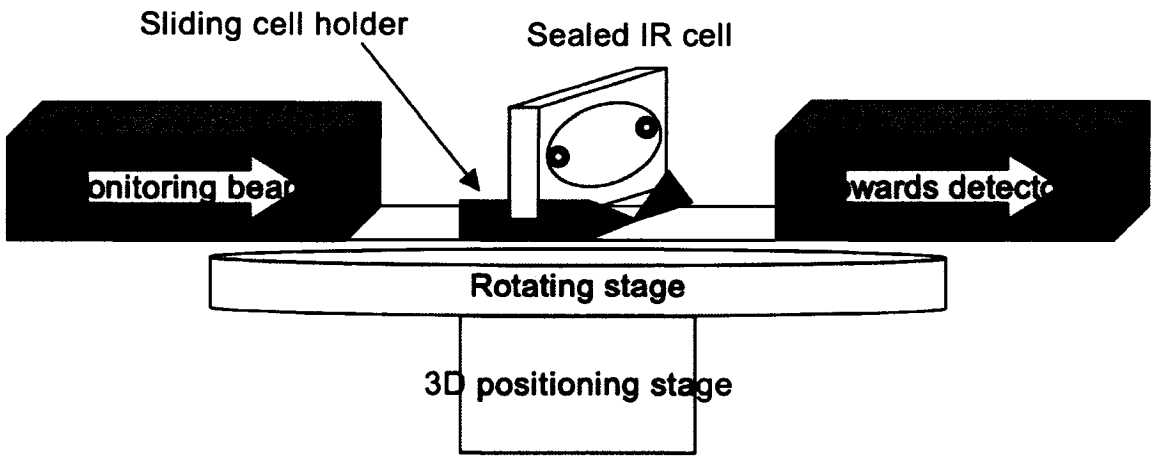

Figure 3.2 *Drawing of cell holder*

Eventually, both the monitoring beam fiber connectors and the sample holder were installed on a rotating stage. This allowed us to change the angle of the sample differently relative to the laser beam while retaining the cell's position on the sliding groove relative to the monitoring beam constant.

The diameter of the optic fiber that was transporting the signal back to the oscilloscope was also changed. By increasing the fiber diameter it was possible to maximize the overlap between the monitoring beam and the laser beam. The amount of signal that was sent to the detector was increased.

A CaF_2 lens with a 100 mm focal distance in order to focus more tightly the laser onto the sample was added at the entry of the sample box after the shutter.

This allowed us to focus the laser beam on the sample with the same order of magnitude as the diameter of the monitoring beam, maximizing our signal.

The sample holder was finally installed on a 3-D stage, see Figure 3.2. This was most helpful in positioning the sample, it could be moved closer to the laser beam and it could be moved up and down to help focus the beam at the same height than the monitoring beam with great precision.

LFP was done at 90 ° or using a front face approach. A concern was at this point that the light that traveled through the CaF_2 cell would get refracted. As the laser beam passed through the first window of the cell, it would get refracted and be off center. This would be a concern when trying to overlap the monitoring beam and the laser. The monitoring beam and the laser beam could not merely be centered on the surface of the cell. We had to make sure that the overlap happened inside the cell at the sample. The sealed cells had very small spacers, 0.5 and 1 mm. We had to make sure there was overlap in this small area.

3.2.5 Trigger

A high-speed Silicon detector, DET 210, from Thorlabs was purchased. The photodiode has a spectral response of 200-1100 nm with a peak wavelength of 730 ± 30 nm. The Lumonics laser generates a beam of red light at 722 nm from fluorine, as well as the 157 nm wavelength. It was positioned after the sample. The laser beam then had to go through the focus lens, the CaF_2 sealed cell containing the sample and then reach the photodiode. The proper alignment of the photodiode with the laser beam was critical.

3.3 Results and discussion

3.3.1 Experimental

Acetonitrile, perfluorohexane, perfluorononane, 2,2,2-trifluoroethanol (TFE), 1,1,1,3,3,3-hexafluoropropan-2-ol (HFP), xanthone, ortho-methyl acetophenone (OMAP), 4-methoxyacetophenone, 1,4-dimethoxybenzene (1,4-DMB) decafluorobenzophenone (DFBP), were purchased from Aldrich. Poly hexafluoropropylene oxide was purchased from Scientific Polymer Products Inc. The fluorinated polymer (FP), XP0921 was supplied by Rohm & Haas Electronic Materials.

Films were prepared by spin coating onto 1-inch quartz or CaF_2 disks.

3.3.2 Laser Flash Photolysis with Films

The first experiments were performed with films. Xanthone, frequently used as a standard in LFP, was incorporated in a polyhexafluoropropylene oxide film, and in a fluorinated polymer XP0921 film. Saturated solutions of xanthone in HFP and in XP0921 were also spin coated or left to dry on the disks in order to obtain a high concentration of xanthone in the films and maximize the chances of seeing a signal. Following LFP at 157 nm, the expected absorbance around 630 nm for the triplet of xanthone could not be observed for any of the films. Upon irradiation, the films were blackening and visible ablation was observed on many occasions.

4-Methoxyacetophenone dissolved in HFP and spin coated was also tried. An absorbance at around 390 nm was expected, but not detected. A spectrum of a film made with DFBP and the fluorinated polymer XP0921 was recorded and no features were observed.

Laser flash photolysis of a film of xanthone in FP was tested with a different excitation wavelength of 355 nm. The laser energy was 9 $mJcm^{-2}$. This is more than the energy delivered by 157 nm during the average LFP experiments, 4 $mJcm^{-2}$. With the excitation wavelength of 355 nm we could observe the triplet for xanthone at 610 nm, see Figure 3.3. The energy delivered by 157 nm for LFP is probably not sufficient to generate an absorbance signal with thin films.

Huge peaks for the fluorescence of pyrene in films were observed, a peak at 380 nm for the monomer and a peak at 440 nm for the excimer, as can be seen in Figure 3.4. The fact that we can monitor fluorescence is indicative that the singlet state is reached by irradiation at 157 nm but that detection of the absorbance signal is difficult.

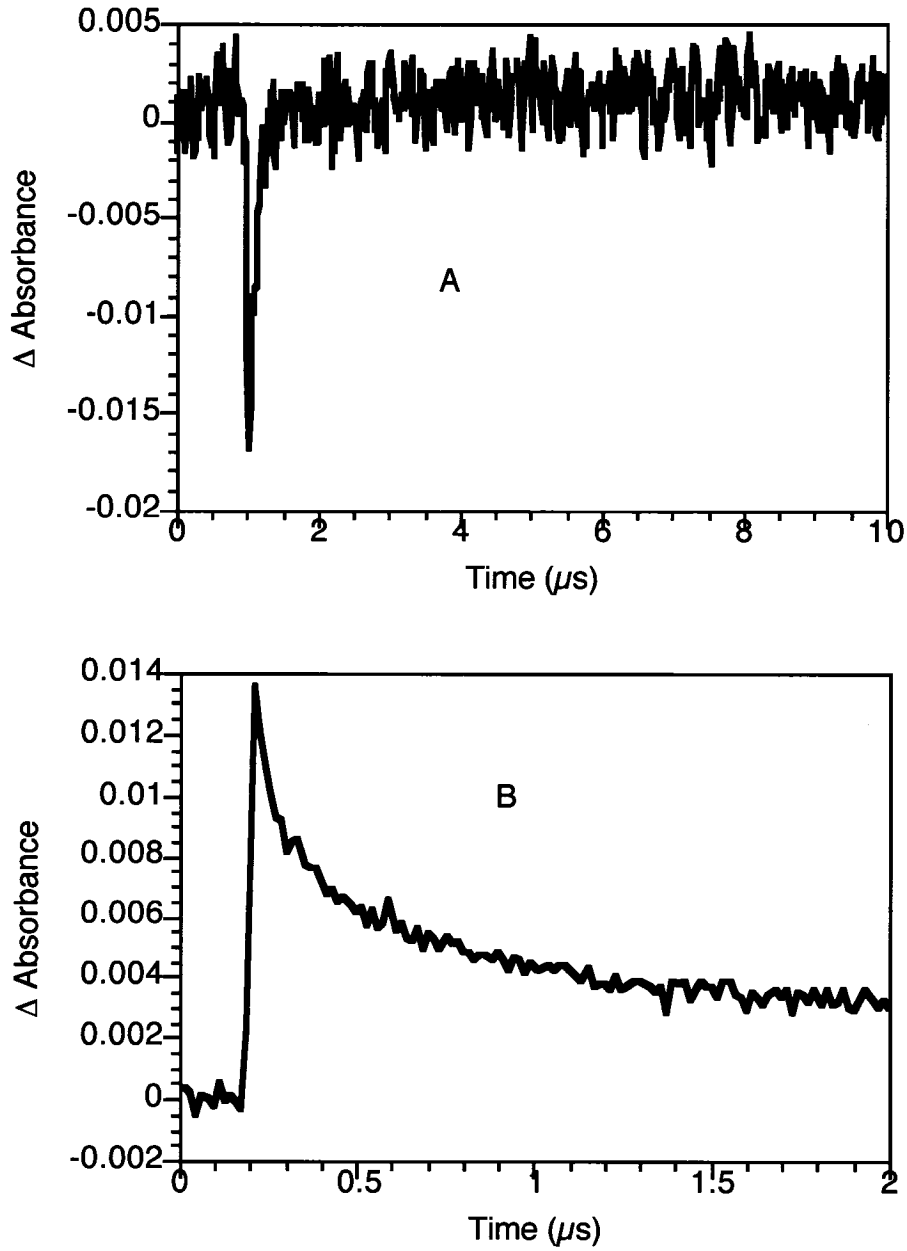

Figure 3.3 *Kinetic decay traces at 610 nm obtained after irradiation at 157nm (A) and 355 nm (B) of a film of xanthone in a fluorinated polymer (FP).*

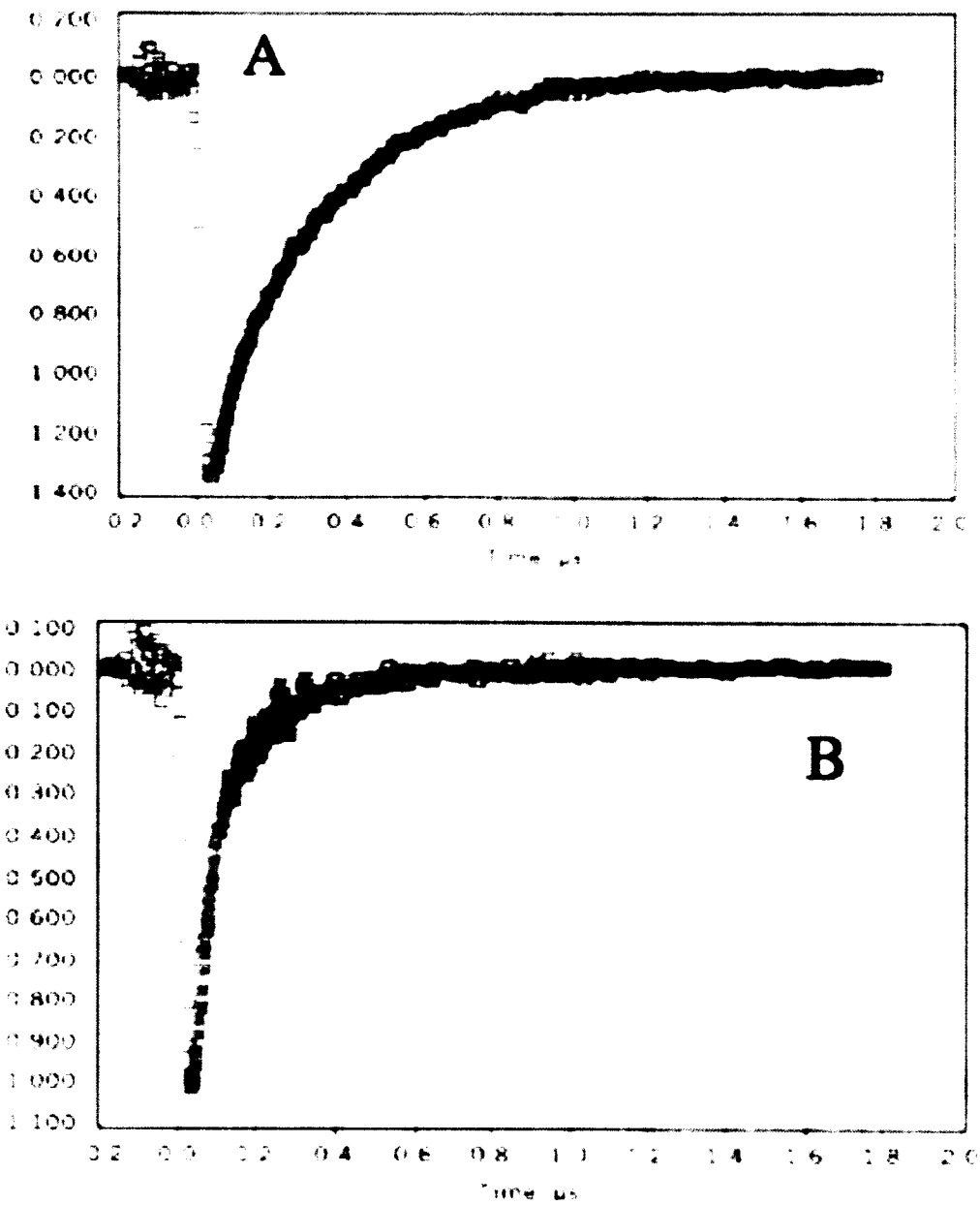

Figure 3.4 *LFP with a 157 nm laser of a film of pyrene in HFP shows fluorescence at 380 nm for the monomer (A) and at 440 nm for the excimer (B) of pyrene.*

3.3.3 Laser Flash Photolysis in Solution

Solutions of xanthone in HFP, 2,2,2-trifluoroethanol (TFE), and perfluorohexane; 1,4-DMB in HFP, perfluorononane, and perfluorohexane; o-methylacetophenone (OMAP) in TFE, decafluorobenzophenone in perfluorononane, perfluorohexane and HFP; and pyrene in TFE were tested for LFP with an excitation wavelength of 157 nm. The typical absorbance peaks that are observed after excitation at longer wavelength were not observed with 157 nm.

Experiments were performed with a 355 nm laser in order to compare the results obtained at 157 nm. A sandblasted CaF_2 window was used in order to reduce the beam energy. The purpose of the window was to reduce the power at 355 nm so as to mimic the energy delivered by the laser at 157 nm. The total energy measured at the entrance of the sample box was reduced from 18 mJ to 3 mJ with the diffuser. The top Δ absorbance was reduced by more than 92%, as can be seen in Figure 3.5. The cell used was the sealed CaF_2 with a 1 mm pathlength and the solution was xanthone in acetonitrile. Even though the intensity of the signal was much smaller, it was still very visible after excitation at 355 nm with the same energy that was available at 157 nm. The energy of 4 $mJcm^{-2}$ at 355 nm delivers more photons than this same energy at a wavelength of 157 nm. This can be a major issue when the intensity of the signal is so small.

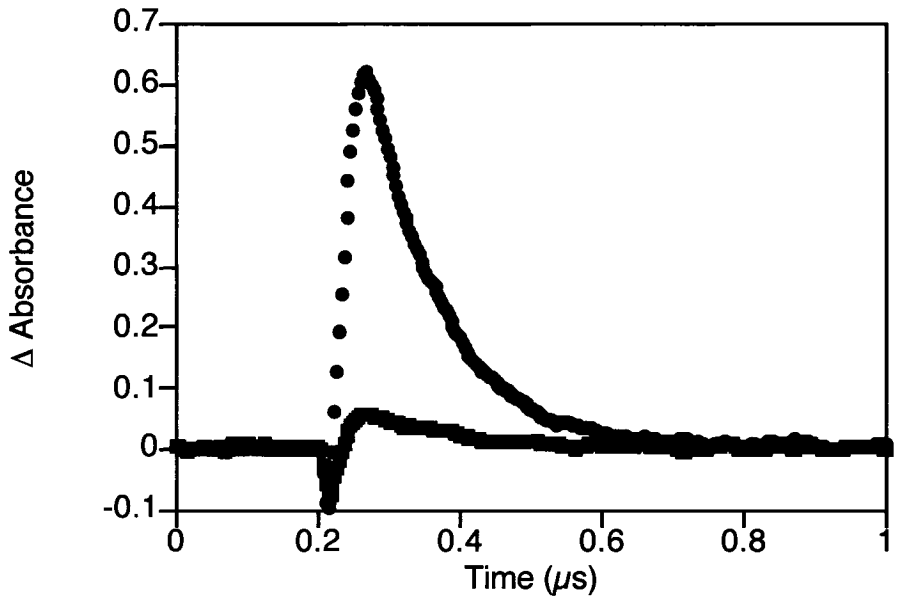

Figure 3.5 *Transient decay obtained for a solution of xanthone in ACN in a 1 mm path length sealed CaF_2 cell with (■) and without (●) a diffuser in front of the 355 nm laser beam .*

With the Lumonics laser, the wavelength could be changed to 248 nm or 193 nm by changing the gas mixture. The system was first aligned at 248 nm then without touching the setup, the wavelength was changed to 157 nm. This was done to ensure that we had the proper alignment at 157 nm. No signals were obtained after switching the laser wavelength back to 157 nm. This was indicative that the pathlength of the laser beam through the sealed CaF_2 cell might not be the same for different wavelengths.

Front face is known to be useful for very concentrated solutions as there is a better overlap of the monitoring beam with the laser beam. It is also useful for very dilute solutions and low energy irradiation as well. Orientation of the CaF_2 sealed

cell relative to the monitoring beam and the laser was critical as was shown by test experiments performed at 308 nm. These initial tests were performed with a sealed CaF_2 cell with a 0.5 mm pathlength. OMAP in TFE was tested with front face configuration for LFP with 157 nm. Figure 3.6 shows a typical kinetic trace at 380 nm for OMAP after excitation at 157 nm.

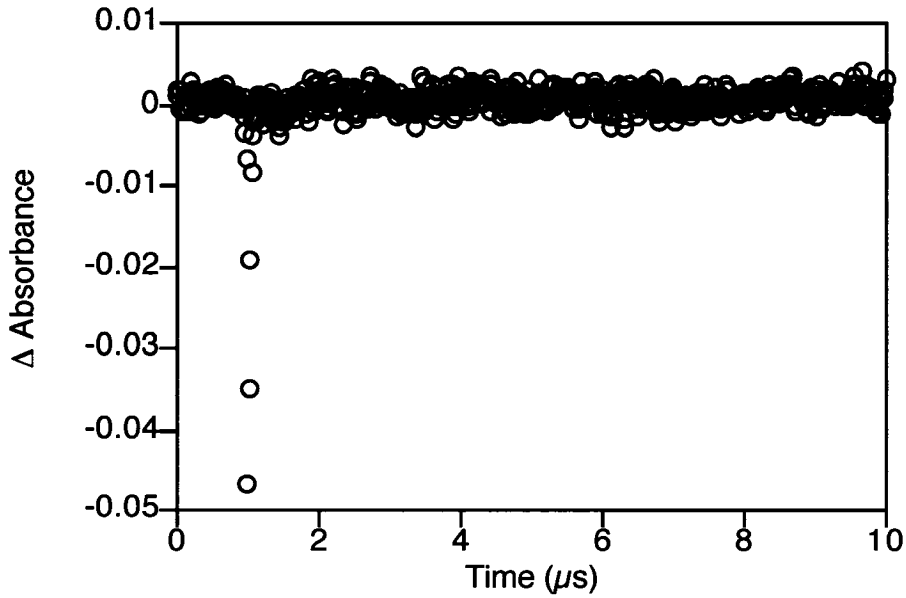

Figure 3.6 *Kinetic traces at 380 nm obtained during laser flash photolysis of OMAP in TFE with 157 nm laser excitation.*

The fluorescence of the monomer and the excimer of pyrene in a solution of TFE could be observed but no signal for the triplet could be monitored with 157 nm laser excitation, see Figure 3.7.

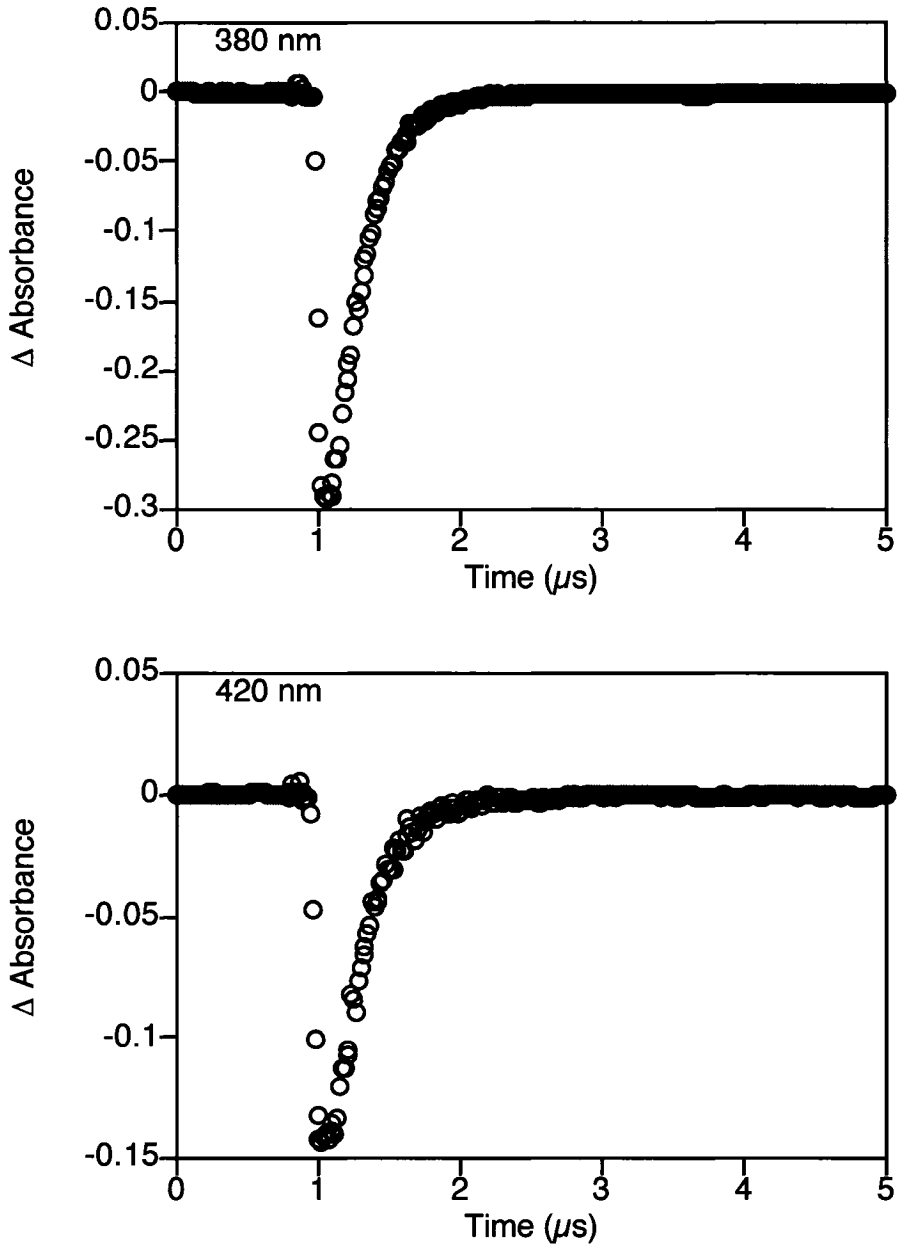

Figure 3.7 *LFP with a 157 nm laser of a solution of pyrene in TFE reveals fluorescence at 380 nm (top) for the monomer and at 420 nm for the excimer (bottom).*

A large blue fluorescence was also visible during irradiation at 157 nm of xanthone solutions. The fluorescence of xanthone in HFP was measured, see

Figure 3.8 in the fluorimeter with an excitation wavelength of 310 nm. Solutions of xanthone in HFP were exposed for 2 hours and 17 hours in a photoreactor with 8 lamps of 300 nm. The solution was injected after exposure into a GC-MS. The spectra obtained were identical for the exposed solutions and for the blank, which was kept in the dark. It was concluded that xanthone did not form significant amounts of product with HFP upon exposure at least at 300 nm.

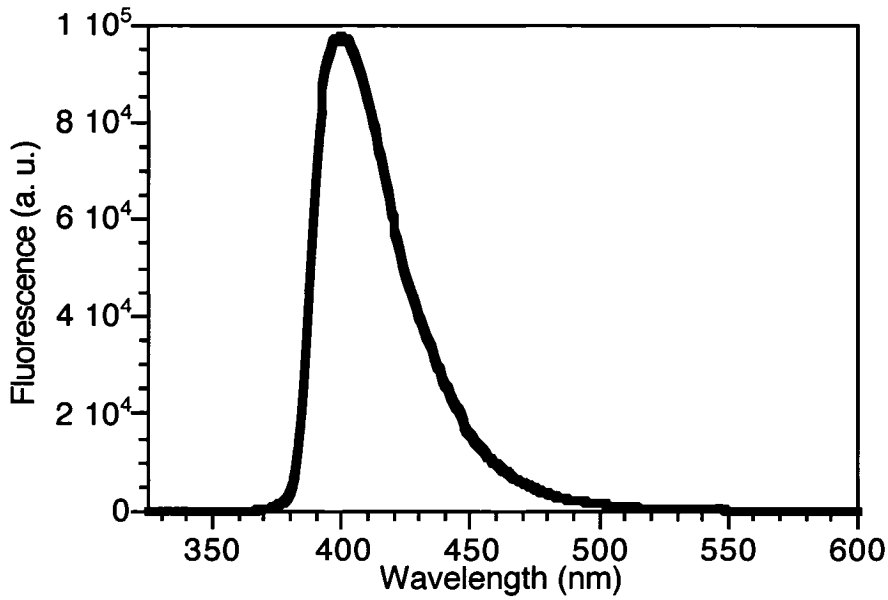

Figure 3.8 *Fluorescence spectra of a solution of xanthone in HFP.*

Tests at 157 nm with xanthone and acetonitrile were made because the high absorbance of the solvent would lead to the formation of bubbles. Gas evolution is observed in the region where the laser hits the sample. This is very useful in order to obtain the best overlap possible between laser and monitoring beam as the origin of the bubbles in the sample corresponds to the laser beam, which was

otherwise transparent. The average power was 3-3.5 $mJcm^{-2}$, measured after the focusing lens.

3.3.4 Subtraction Plots

Xanthone was dissolved in perfluorononane. The CaF_2 sealed cell with a pathlength of 0.5 mm was used with a front face configuration. The kinetic decay traces of perfluorononane alone and of xanthone in perfluorononane were recorded at 610 nm. The two traces are subtracted, see Figure 3.9. The absorbance of the solvent is very high and is hiding the signal from xanthone. The subtraction shows a decay that is consistent with known decay traces of xanthone obtained by LFP at longer wavelengths. The subtraction gives a clear signal at 610 nm.

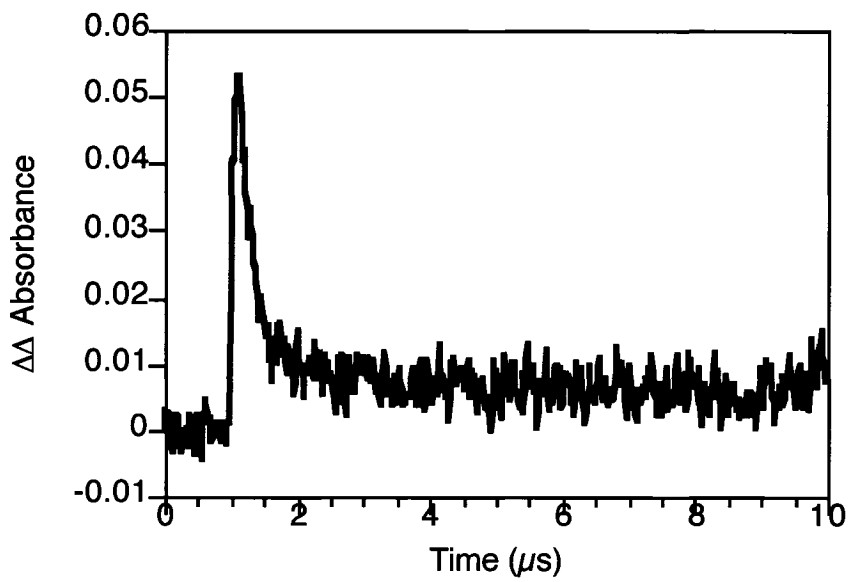

Figure 3.9 *Subtraction of kinetic decay traces obtained by LFP at 157 nm of the solvent and xanthone in perfluorononane at 610 nm.*

The lifetime derived from this signal is 300 ns and is compatible with the known lifetimes of xanthone. Xanthone has a lifetime of 8300 ns in acetonitrile and of 60 ns in n-heptane.[4] This is the first lifetime determined at 157 nm to our knowledge by laser flash photolysis. However, this result could not be reproduced.

3.3.5 Shock Waves

Shock waves will be generated when a sample has an absorbance that is too high. Figure 3.10 shows a sample spectrum of decafluorobenzophenone in perfluorononane demonstrating the generation of shock waves. The speed of sound in that solvent can be calculated from the known pathlength and the time elapsed between each waves. As can be seen from this spectrum, the high absorbance of most of the chromophores and solvents at 157 nm was a source of problems.

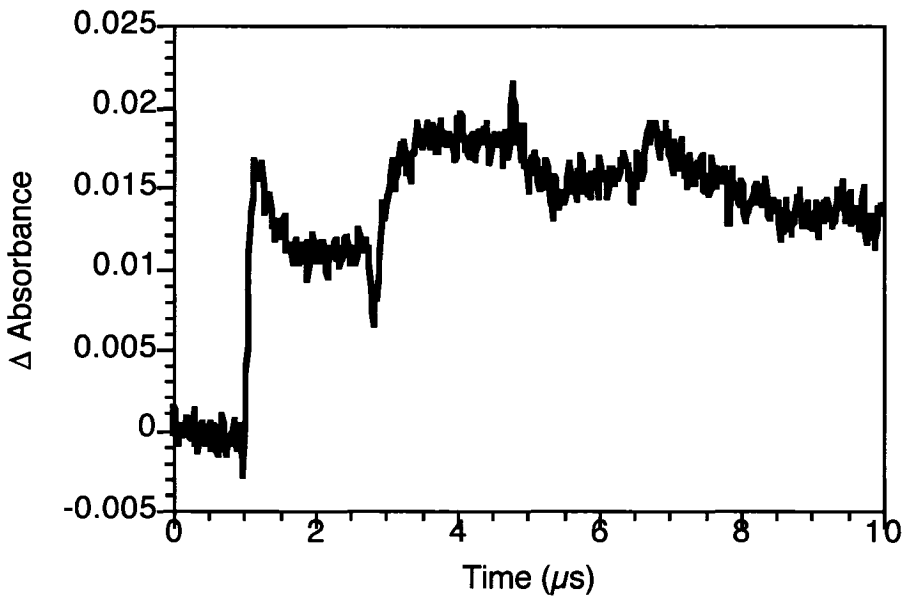

Figure 3.10 *Decafluorobenzophenone in perfluorononane monitored at 550 nm after excitation at 157 nm in a 0.5 mm CaF_2 sealed cell. Shockwaves are spaced 1.75 μs.*

3.4 Discussion

We have attempted to do laser flash photolysis using 157 nm as the wavelength of excitation. 157 nm is a very energetic wavelength, 7.88 eV or 182 $kcalmol^{-1}$. One of the major experimental problem was the fact that the energy delivered to the sample by the laser wasn't sufficient to generate a signal but at the same time was too energetic, because of the high absorbance of the sample, generating local heating in the solvent. This could be seen by the presence of bubbles forming in the path of the laser beam. These bubbles were giving rise to interferences in the signal during LFP measurements. Subtracting the solvent only trace from the trace for both solvent and analyte cannot be done reliably as bubble formation is not controllable in a reproducible manner.

A peak for xanthone was obtained with LFP at 157 nm by subtracting the solvent. The fact that this could not be reproduced is due to many reasons. The energy required to achieve a signal at 157 nm could not be generated with the two lasers that were used at 157 nm. The energy delivered by a laser at 355 nm of comparable energy was sufficient only to generate a weak signal. Generation of local heat in the solvent was interfering with the measurements. The energy delivered to the sample was too low to generate a strong signal but high enough to generate interfering bubbles due to local overheating of the solvents. This problem could be solved by lowering the absorbance of the sample. Unfortunately we could not measure the absorbance of our samples at 157 nm. Fluorescence of pyrene was monitored at 157 nm indicating that the singlet state of the chromophore was

generated but no signal was detected. This could point to a problem of detection in our setup. Birefringence of CaF_2 has led the photolithographic industry to cease research at 157 nm. The fact that our cells were made of CaF_2 could have been a major problem with the detection of a signal. The laser beam as well as the monitoring beam would have to go through the CaF_2 cell during the measurements. The cell was oriented at 45° relative to the laser beam during LFP experiments. Due to birefringence the laser beam probably did not go through the cell following a straight path. This could have led to major misalignments and an incomplete overlap of the monitoring beam with the laser beam. The fact that the experiments had to be conducted under N_2 did not simplify the experimental procedure.

Water has been shown to have a high absorbance at 157 nm and to undergo photodecomposition with a high quantum efficiency.[5] The solubility of water is low in fluorinated solvents but trace amounts could have been a source of problems.

Technical difficulties may also have included problems with the trigger system itself. The photodiode that was set to trigger on the 722 nm light generated by the Lumonics laser. This could have been delayed relative to the light at 157 nm and led us to acquire the signal too late. These are experimental problems that would have to be investigated more thoroughly.

The future of this project relies on finding chromophores and solvents that are less opaque at 157 nm. Finding a material that is transparent and is not birefringent at 157 nm to replace the CaF_2 cells would also be important. LFP at

157 nm has proven to be very difficult experimentally because of the high absorbance of most organic compounds at 157 nm. A project that is currently in development in Prof. Scaiano's group is the use of hollow core photonic crystal fibres (PCF) as sample cells where LFP at 157 nm could be effected by side irradiation and the signal detected with the light guiding modes of the fibres.

3.5 References

(1) Porter, G. *Proceedings of the Royal Society of London. Series A, Mathematical and Physical Sciences* **1950**, *200*, 284-300.

(2) Netto-Ferreira, J. C.; Scaiano, J. C. *J. Am. Chem. Soc.* **1991**, *113*, 5800-5803.

(3) French, R. H.; Wheland, R. C.; Jones, D. J.; Hilfiker, J. N.; Synowicki, R. A.; Zumsteg, F. C.; Feldman, J.; Feiring, A. E. *Proc. SPIE* **2000**, *4000*, 1491-1502.

(4) Scaiano, J. C. *J. Am. Chem. Soc.* **1980**, *102*, 7747-7753.

(5) Getoff, N.; Schenk, G. O. *Photochem. Photobiol.* **1968**, *8*, 167.

Chapter 4
Fluorescence Properties of Quantum Dots in Solution

Table of contents

Chapter 4
Fluorescence Properties of Quantum Dots in Solution

4.1 Introduction

Quantum dots are semiconductor nanoparticles whose radii are smaller than the radii defined by the exciton Bohr radius. Bulk semiconductors are characterized by a gap between the valence band and the conduction band. As the diameter of the quantum dots gets smaller the band gap gets larger. This is what imparts these nanoparticles their special optical properties. Their absorbance and fluorescence properties are size dependent. Metallic nanoparticles do not demonstrate such a strong variation in their fluorescence or absorbance spectra with size. Capping of quantum dots with a material of higher band gap results in an increase in the quantum yield of fluorescence.[1,2] Single quantum dots are known for a phenomenon called blinking; individual quantum dots will stop fluorescing intermittently for varying periods of time, up to several seconds.[3] This property is still not well understood.

The fluorescence quenching of CdSe quantum dots by nitroxides[4,5] as well as the development of radical sensors called prefluorescent probes[6] will be discussed. We will show that there is a quantum dot size dependence on the fluorescence quenching by nitroxyl free radicals. We will discuss the effect of the amino-moiety on fluorescence by comparing the effect of quenching by 4-amino-TEMPO, cyclohexylamine and TEMPO. In Chapter 5, the enhancement of the

fluorescence of quantum dots incorporated in polymer films will be discussed. We will show in chapter 6 that the incorporation of quantum dots in photonic crystal fibers can lead to the development of multiplex sensors.[7]

Quantum dots (QD's) have sparked a lot of interest because of the size-dependence of their optical properties.[8] Their absorbance spectra show a broad of absorption peak making them attractive for simultaneous excitation of different sizes of quantum dots. This feature has been exploited for the development of quantum dot tagged microbeads use for multiplexed optical coding of biomolecules.[9] Many sensing and imaging applications have been proposed in recent years.[10-12] Applications of quantum dots require surface functionalization, for example, biological applications require a water-soluble surface and solar cells require an electron conductive surface.[13] We have examined the properties of CdSe quantum dots in solution by fluorescence spectroscopy, time-resolved fluorescence, and electron spin resonance (ESR).

Fluorescence Quenching

Quenching of the fluorescence of CdSe QD's by cyanide ions has been reported.[10] The TOPO coating of CdSe QD's was replaced by a layer of 2-mercaptoethane sulfonate. Quenching by cyanide ions results in an upward curving Stern-Volmer plot. Wuister et al. have shown that replacing the TOPO ligands on CdSe quantum dots by allylmercaptan or aminoethanethiol leads to a decrease in fluorescence.[14] An increase in fluorescence is observed for CdTe quantum dots covered with trioctylphosphine and dodecylamine ligands after exchange with thiols.[14] The difference is explained by the lower valence band

position of CdSe quantum dots that can trap the photogenerated holes of the thiols, reducing the fluorescence emission.[14] Wang et al. replaced the TOPO ligand on CdSe/ZnS quantum dots with a multidentate ligand, poly(dimethylaminoethyl methacrylate) resulting in a 30% decrease in luminescence intensity.[13] Kalyuzhny and Murray report that the photoluminescence of CdSe nanocrystals increases when they are covered with trioctylphosphine, hexadecylamine, pyridine and acetates and that they observe a decrease with thiols.[15] Talapin et al. report that replacement of the TOPO ligand on CdSe quantum dots by primary amines such as allyamine and dodecylamine leads to an increase in the fluorescence of the quantum dots.[16] Addition of n-butylamine to CdSe QD decreases the fluorescence intensity; it is thought that n-butylamine occupies hole sites blocking the recombination process.[17] Another group reports that addition at low concentration of n-butylamine to CdSe QD enhances the fluorescence intensity.[18]

In this work the fluorescence quenching by TEMPO (2,2,6,6-tetramethylpiperidine-*N*-oxide free radical) and 4-amino-TEMPO of different sizes of CdSe quantum dots was examined by fluorescence spectroscopy. The effect of cyclohexylamine on the fluorescence of CdSe quantum dots was also examined. Cyclohexylamine was chosen to separate the effect of the paramagnetic species on the quenching of fluorescence since it bears a structure similar to 4-amino-TEMPO but without the free radical moiety, see Scheme 4.1

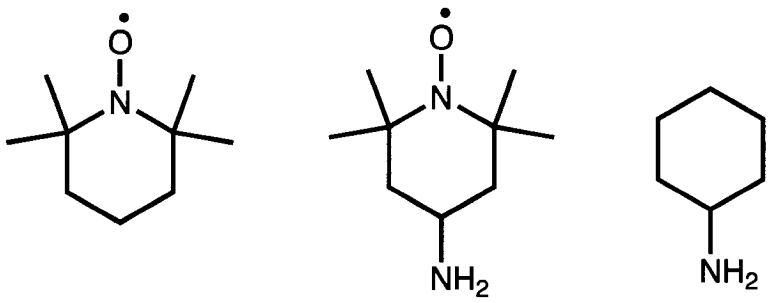

Scheme 4.1 *Structure of TEMPO, 4-amino-TEMPO, and cyclohexylamine.*

Stern-Volmer Plots

The intensity of fluorescence of many fluorophores in solution decays monoexponentially.[19] Dynamic quenching refers to collisional encounters between fluorophore and quencher that deactivate the fluorescence of the excited state fluorophore.[20] Fluorescence lifetimes become shorter. Static quenching refers to collisional encounters between the quencher and the fluorophore that lead to the formation of a non-fluorescent complex.[20] Static quenching does not affect the fluorescence lifetime of the chromophore as only the uncomplexed chromophores will fluoresce in the presence of quencher. In some cases of dynamic quenching, upon addition of quenchers, the decay becomes non-exponential due to transient effects in diffusion.[19] In this case, dynamic quenching can be described by inclusion of time-dependence in the model derived by Smoluchowski or by the distance-dependent quenching (DDQ) model.[19,21] This model gives a rate constant that is exponentially dependent on the distance between the fluorophore and the quencher.[21]

A Stern-Volmer treatment is used to analyze fluorescence quenching. Stern-Volmer plots are linear if quenching involves a single excited state and proceeds by only static or dynamic quenching.[20] The data can then be fitted according to Equation 4.1

(4.1) $$\frac{I_0}{I} = 1 + K_{SV}[Q]$$

where I_0 is the intensity of fluorescence in the absence of quencher and I is the intensity of fluorescence in the presence of quencher, K_{SV} is the Stern-Volmer constant and [Q] is the concentration of quencher. The quantum yield of fluorescence Φ is proportional to the fluorescence intensity such that the ratio I_0/I is equal to Φ_0/Φ.

In the case of dynamic quenching K_{SV} is defined by Equation 4.2

(4.2) $$K_{SV} = k\tau_0$$

where *k* is the rate constant for quenching and τ_0 is the lifetime of the chromophore in the absence of quencher. In the case of static quenching, K_{SV} can be described as an association constant between the chromophore and the quencher.[20]

When there is a mixture of static and dynamic quenching, one obtains upward curving Stern-Volmer plots, that can be described according to Equation 4.3.[20]

(4.3) $$\frac{I_0}{I} = (1 + K_D[Q])(1 + K_S[Q])$$

where K_D and K_S are the Stern-Volmer constants for dynamic and static quenching respectively.

Downward curving Stern-Volmer plots are indicative of either two different chromophores or chromophores with sites that have different accessibility. In the presence of two sites but with different accessibility, the Stern-Volmer plot can be fitted to the following Equation. 4.4.[17]

(4.4) $$\frac{\Phi_F^0}{\Phi_F} = \frac{1}{\frac{f_1}{(1+K_{SV1}[Q])} + \frac{f_2}{(1+K_{SV2}[Q])}}$$

where f_1 and f_2 are the relative fractional portions of fluorescence attributed to the different sites and K_{SV1} and K_{SV2} are the Stern-Volmer constants for quenching for each site.

If a chromophore has two different sites and one of the sites is not accessible, the Stern-Volmer equation can be modified according to Equation 4.5.[18,20,22]

(4.5) $$\frac{I_0}{\Delta I} = \frac{1}{f_a K_a [Q]} + \frac{1}{f_a}$$

where f_a is the fraction of accessible sites and K_a is the rate constant for quenching of these sites.

Perrin Model

When large amounts of quencher are required to quench the fluorescence, it can be inferred that static quenching does not occur through formation of a ground-state complex.[20] When static quenching occurs only by a loose association, Equation 4.3 can be replaced with Equation 4.6. The quenching in this case is only apparent static quenching.

(4.6) $$\frac{I_0}{I} = (1 + K_D[Q])e^{V[Q]}$$

where V is the static quenching constant and can be represented by a volume.[23] This volume can be viewed as a sphere of action similar to the Perrin model. Quenchers present in this volume with the chromophore in its center will quench the fluorescence in an apparent static quenching process.[20] Chromophores that do not have a quencher in their sphere of action will fluoresce. A radius of action, r, can be derived from this volume, see Equation 4.7.

(4.7) $$V = N_A \frac{4}{3}\pi r^3$$

A simple Perrin model will be described by an exponential dependence with concentration, see Equation 4.8, where α is N_aV and N_a is Avogadro's number and V is the volume

(4.8) $$\frac{I_0}{I} = e^{\alpha[Q]}$$

Prefluorescent probes

Prefluorescent probes are typically organic fluorophores that have their fluorescence quenched by being covalently bound to a nitroxide free radical. In the presence of carbon-centered free radicals, the nitroxide moiety reacts to produce a diamagnetic alkoxyamine. This restores the fluorescence of the probe. These probes have been used to detect radicals and antioxidants in homogeneous and heterogeneous media.[5,24,25]

The fluorescence of quantum dots is quenched by binding of the amino moiety of 4-amino-TEMPO to the quantum dots surface. Fluorescence is restored when photogenerated radicals from AIBN react with the quantum dot-4-amino-TEMPO complex, see Scheme 4.2.

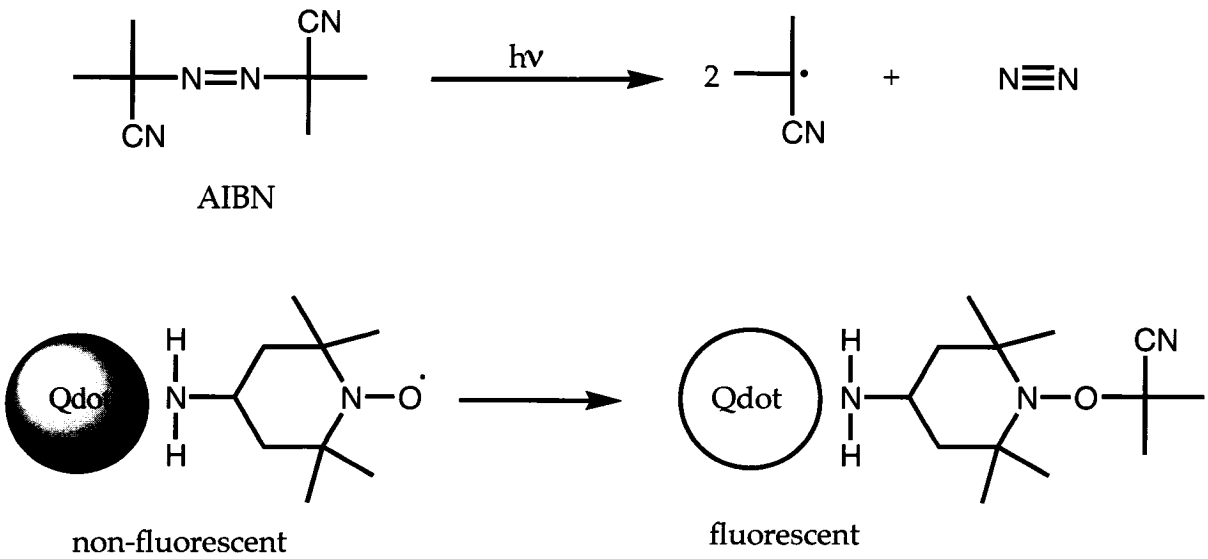

Scheme 4.2 *Proposed mechanism for the fluorescence recovery of the complex quantum dot-4-amino-TEMPO in the presence of photogenerated radicals from AIBN.*

4.2 Experimental

CdSe core quantum dots were purchased from Evident Technologies. They are covered with trioctylphosphine oxide (TOPO) and were supplied in toluene solutions. Different sizes were purchased: Amaranth green, 2.4 nm in diameter, hawkweed orange, 3.2 nm, begonia red, 5.2 nm and, aster red 6.7 nm. The solutions contained 2.5 mg of quantum dot per ml.

Quantum dots were also synthesized in our laboratory following a method described by Peng and Peng.[26] CdSe quantum dots covered with TOPO and dispersed in toluene were prepared. The sizes of the nanoparticles and their concentration were determined using a calibration described by Yu *et al.*[27]

TEMPO, 4-amino-TEMPO (4AT), cyclohexylamine were purchased from Aldrich, and toluene, HPLC grade, was purchased from EMD.

Fluorescence was measured using a PTI spectrofluorimeter. Time resolved data was acquired with a laser flash photolysis system described in Chapter 1. EPR measurements were performed using a JEOL FA-100 X-Band EPR spectrometer equipped with a JEOL ES-UCX2 cylindrical cavity. Irradiation was done with a Luzchem Xenon illuminator with a filter cutting wavelengths below 345 nm or one 350 nm lamp in a Luzchem photoreactor. The spectral profile of the xenon lamp with filter and of one lamp in the photoreactor is shown in Figure 4.1

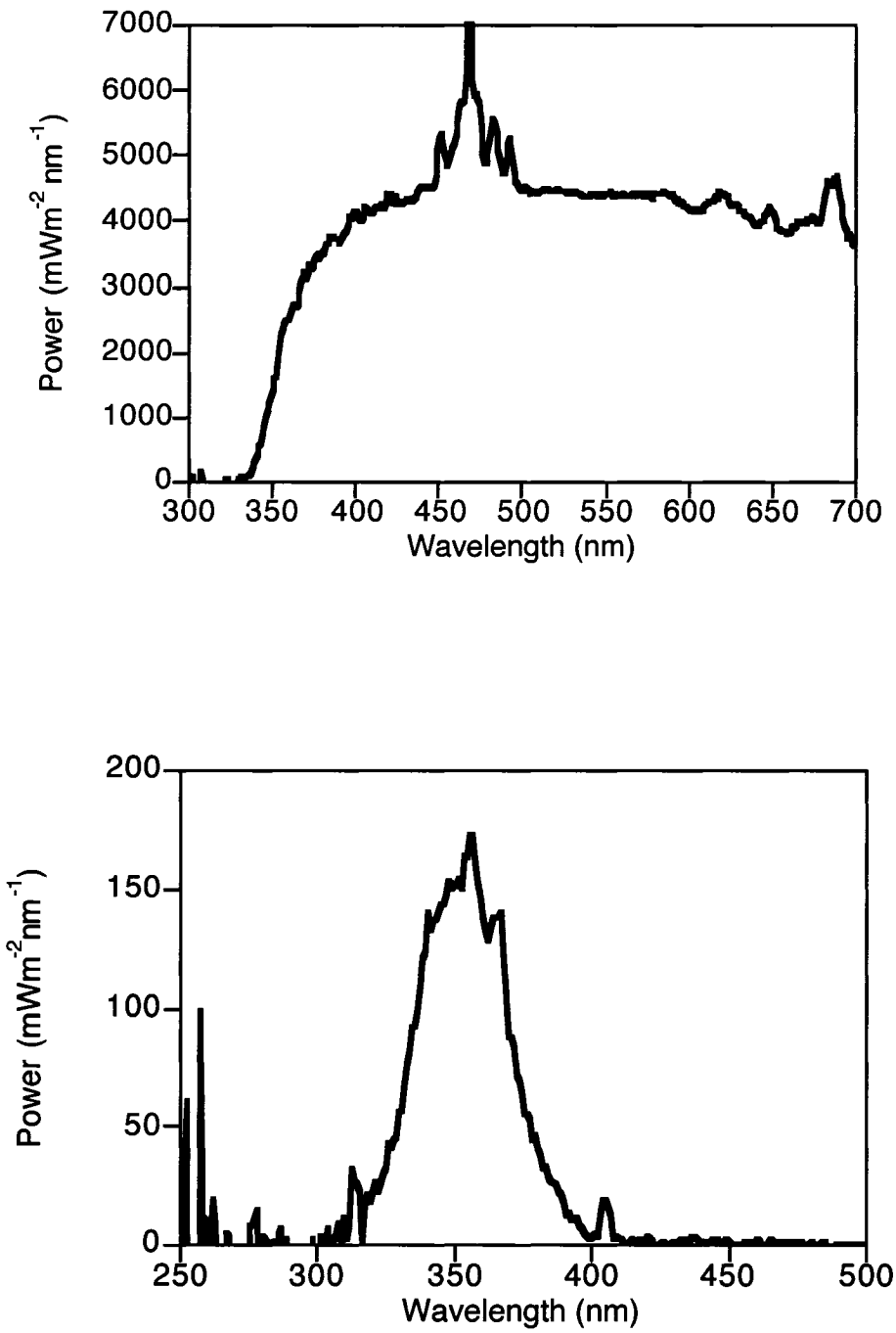

Figure 4.1 *Spectral features of the Luzchem Xenon illuminator with a 345 nm filter, (top) and of 1 lamp in the photoreactor (bottom)*

4.3 Properties of CdSe Quantum Dots

4.3.1 Absorbance and Fluorescence of CdSe Quantum Dots

Quantum dots purchased from Evident have absorbance and fluorescence spectra that are in accordance with the published spectra on the company's website. The absorbance and fluorescence spectra illustrate the differences between the different sizes of QD's, see Figures 4.2-4.3. The smaller QD's have a peak in their absorbance spectra, which is blue shifted relative to the larger quantum dots peak. This peak in the absorbance spectra is used to determine the size of the QD's.[27]

The fluorescence spectra also show for these three different sizes of QD's well separated peaks. This allows the use of different sizes of quantum dots in the same solution with minimal overlap. The absorbance spectra shows that a single wavelength of excitation can be used, provided it is shorter than the longest band of the smaller QD's in the solution. This allows simultaneous excitation of all the QD's sizes in solution. The fluorescence spectra show well separated fluorescence peaks for all the sizes in solution. This can be useful in sensing applications were different size QD's can be used and monitored separately.

The QD's that were synthesized in our laboratory by two postdoctoral fellows and a summer student also have absorbance and fluorescence spectra that are identical to those of the QD's that were purchased. Their UV-visible absorbance spectra allowed determination of their sizes. We did not observe any

differences in the properties of the QD's synthesized in our laboratory with those purchased from Evident, other than the differences that would be observed from batch to batch independent of the source of the QD's.

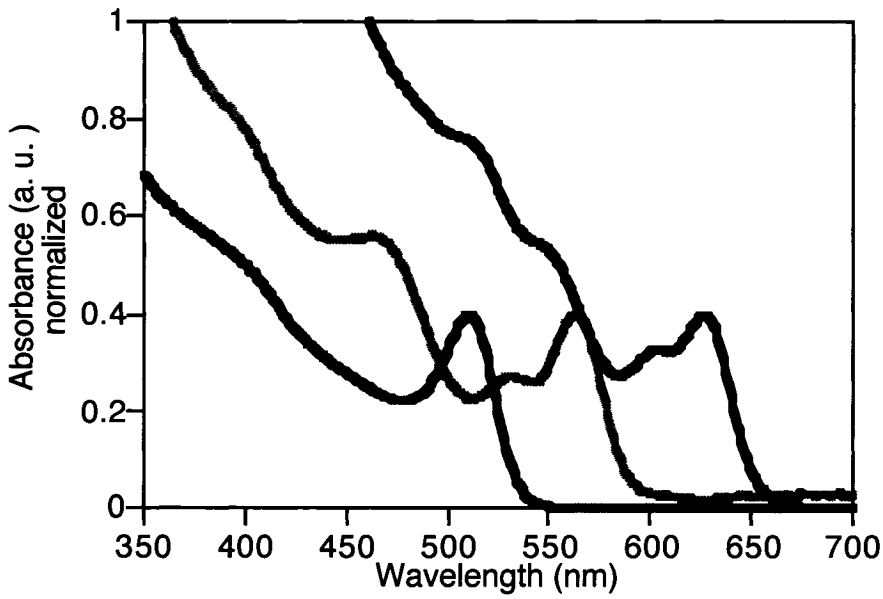

Figure 4.2 *Normalized absorbance spectra of CdSe QD's coated with TOPO from Evident, amaranth green (2.4 nm), hawkweed orange (3.2 nm) and aster red (6.8 nm)*

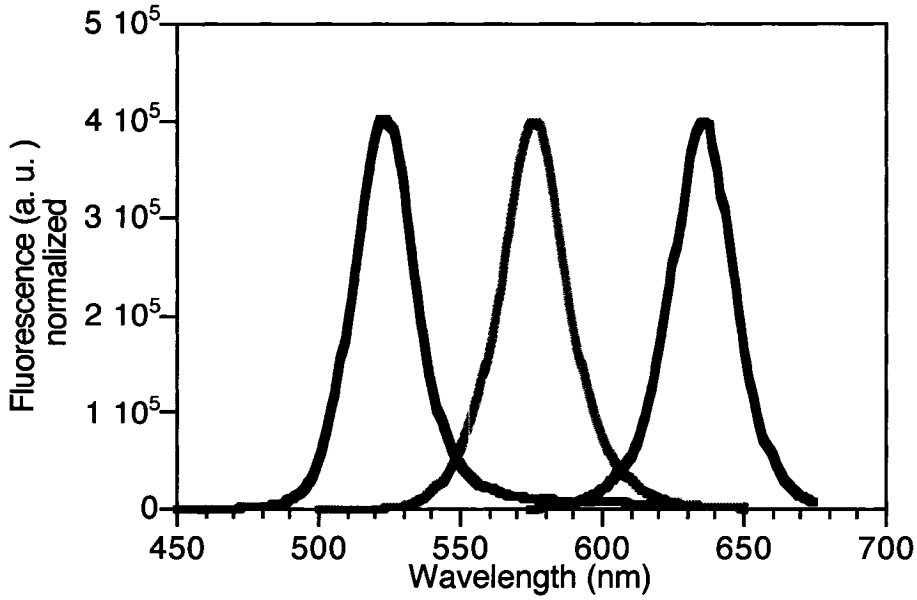

Figure 4.3 *Normalized fluorescence spectra of CdSe QD's coated with TOPO from Evident, amaranth green (2.4 nm), hawkweed orange (3.2 nm) and aster red (6.8 nm)*

4.4 Fluorescence Quenching by TEMPO

4.4.1 Correction for the Absorbance of TEMPO

The initial fluorescence quenching experiments of quantum dots fluorescence was monitored with an excitation wavelength of 380 nm. The amount of TEMPO required to quench the fluorescence was enough to interfere with the absorbance of the quantum dots in solution. The molar absorption coefficient for

TEMPO was measured at 380 nm to be 1.75 $M^{-1}cm^{-1}$. The value is obtained from the slope of the fit as determined by Equation 4.9, where the pathlength is 1 cm.

(4.9) $$\varepsilon = \frac{A}{[\text{TEMPO}] * 1cm}$$

A formula was derived to correct the fluorescence measurements for the high absorbance of TEMPO at the excitation wavelength. The absorbance measured from the center of the cell, where the fluorescence measurements are done, is half the absorbance measured through the whole cell. The total light absorbed at the center is calculated with Equation 4.10.

(4.10) $$1 - T = 1 - 10^{-A_{total}/2}$$

The correction factor to be applied to I_0/I for the Stern-Volmer plots is given by Equation 4.11. The total light that would be absorbed by quantum dots in the absence of TEMPO is given by the numerator and the total light that is absorbed by quantum dots in the presence of TEMPO is given by the denominator.

(4.11) $$\text{correction factor} = \frac{\frac{A_{\text{quantum dots}}}{A_{\text{total}}}\left(1 - 10^{-A_{\text{total}}/2}\right)}{1 - 10^{-A_{\text{quantum dot}}/2}}$$

This correction factor is used because the absorbance of TEMPO at the excitation wavelength, 380 nm is too high relative to the absorbance of the quantum dots to be ignored. The absorbance of TEMPO was recorded for different concentrations of TEMPO as can be seen in Figure 4.4. The absorbance was

plotted against TEMPO concentration at the wavelength of excitation (380 nm), see Figure 4.5. The absorbance of TEMPO was used to calculate the correction factor.

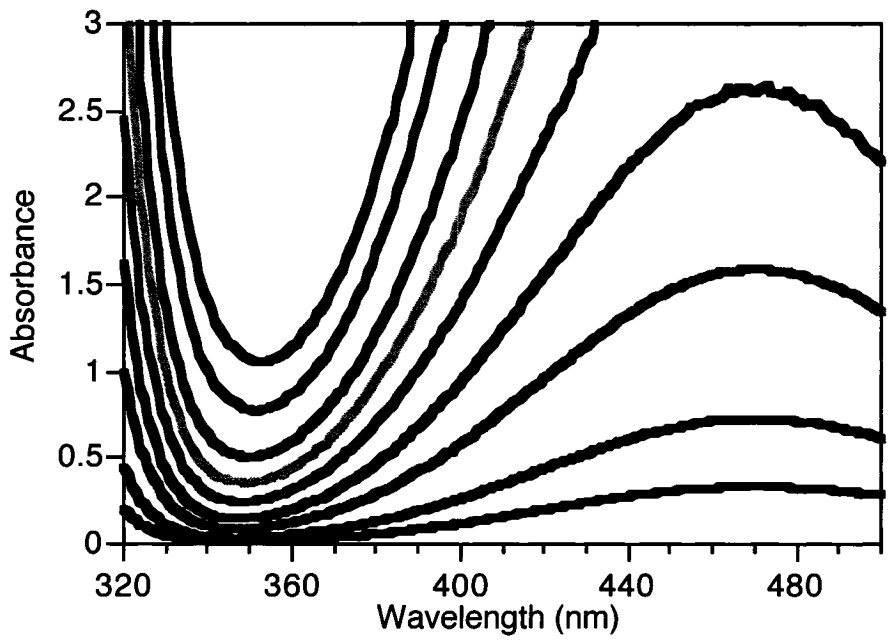

Figure 4.4 *Absorbance of TEMPO in toluene measured at different concentrations ranging from 0.03 M to 1.44 M.*

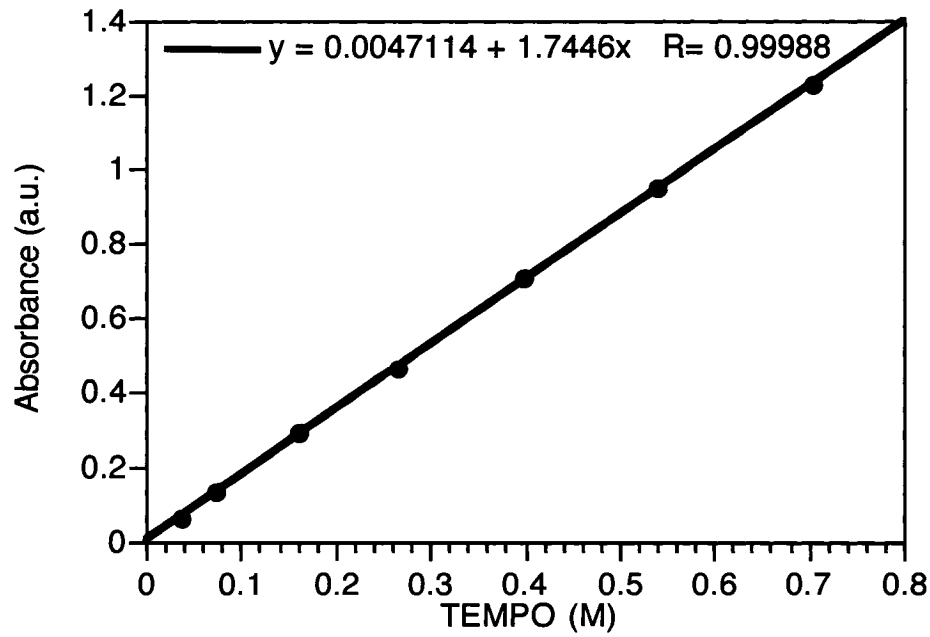

Figure 4.5 *Fit of TEMPO absorbance at 380 nm against TEMPO concentration gives a good linear relationship*

The fit from this plot was used to derive the absorbance of TEMPO at all the concentrations used for Stern-Volmer plots. The later experiments were done with an excitation wavelength of 355 nm where the absorbance of TEMPO is minimal and can be ignored relative to the absorbance of the quantum dots.

4.4.2 Quenching of CdSe Amaranth Green Quantum Dots

The fluorescence of CdSe amaranth green quantum dots, 2.4 nm in diameter, was quenched by addition of TEMPO in solution. The quantum dots

were diluted in toluene to 4.1x 10^{-6} M. TEMPO was added directly to the cell and the fluorescence was measured after each addition. The fluorescence spectra for different TEMPO concentrations are shown in Figure 4.6. The data is treated in a Stern-Volmer fashion, shown in Figure 4.7. The Stern-Volmer treatment gives an upward curving plot at the fluorescence maximum, 525 nm.

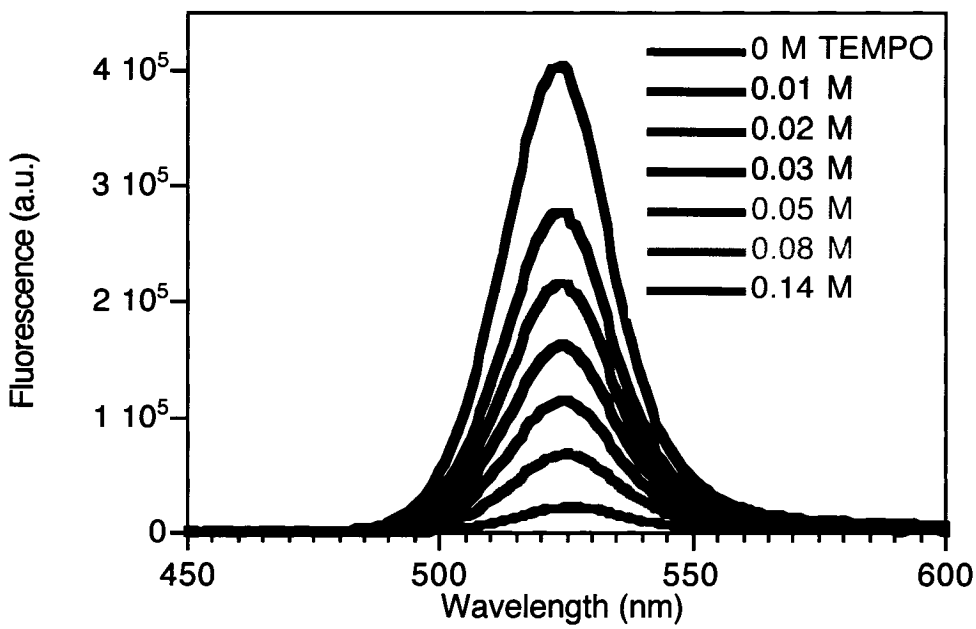

Figure 4.6 *Fluorescence spectra of a toluene solution of 4.1 μM CdSe amaranth green quantum dots after addition of different concentrations of TEMPO.*

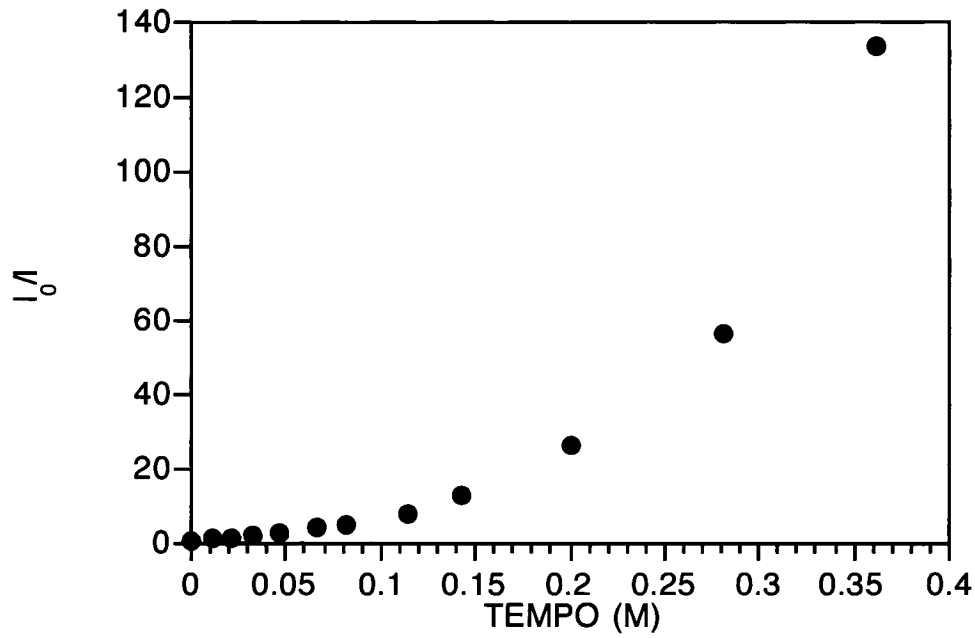

Figure 4.7 *Stern-Volmer plot of the fluorescence data for addition of TEMPO to CdSe amaranth green quantum dots.*

4.4.3 Quenching of CdSe Amaranth Green and Hawkweed Orange Quantum Dots

The fluorescence peaks for amaranth green and aster red quantum dots from Evident Technologies are sufficiently well separated that we can use a mixture of the different size quantum dots, excite them with a single wavelength and obtain well-separated fluorescence peaks that can be analysed separately.

A solution of hawkweed orange, 3.2 nm in diam. and amaranth green, 2.4 nm in diam. was prepared in toluene. The solution was 3.7 x 10^{-6} M for each quantum dot color. TEMPO was added directly to the cell containing the equimolar

solution of green and orange quantum dots. Representative spectra for different concentrations of TEMPO are shown in Figure 4.8. The peak at 525 nm is assigned to the fluorescence of the green quantum dots and the peak at 575 nm is assigned to the fluorescence of the orange quantum dots. The data is analysed with a Stern-Volmer treatment, see Figure 4.9. The values of I_0 are taken at the maximum for the green quantum dot and taken at 590 nm for the orange peak in order to minimize any overlap.

Stern-Volmer plots show a positive deviation from linearity.

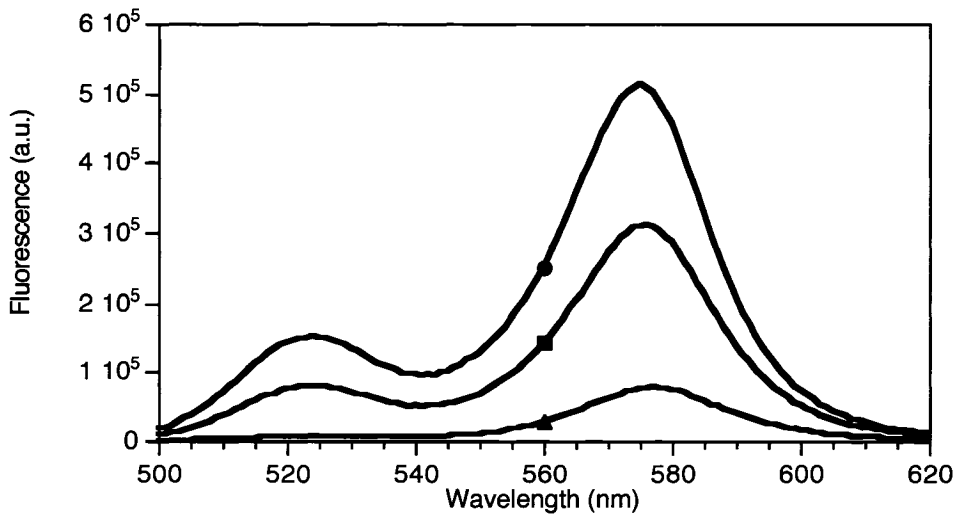

Figure 4.8 *Fluorescence spectra of a toluene solution of amaranth green and hawkweed orange quantum dots, 3.6 x 10^{-6} M, showing a decrease in fluorescence after addition of TEMPO, 0 M (●), 0.04 M (■) and 0.2 M (▲).*

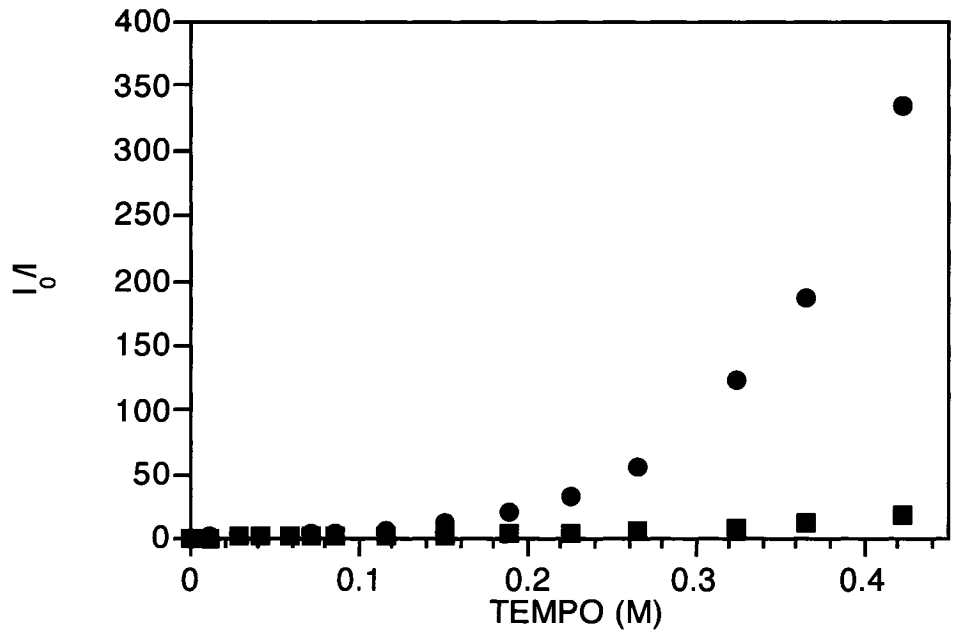

Figure 4.9 *Stern-Volmer plot derived from the fluorescence intensities at 525 nm (●) and 590 nm (■).*

4.4.4 Quenching of Aster Red Quantum Dots

The fluorescence of aster red quantum dots, 6.8 nm in diameter was quenched by addition of TEMPO in a toluene solution. The quantum dots were diluted in toluene to 1.78 x 10^{-7} M. TEMPO was added directly to the cell and the fluorescence was measured after each addition. Representative fluorescence spectra for different TEMPO concentrations are shown in Figure 4.10. The data is treated in a Stern-Volmer fashion, shown in Figure 4.11. The Stern-Volmer treatment at the fluorescence maximum, 535 nm, gives an upward curving plot.

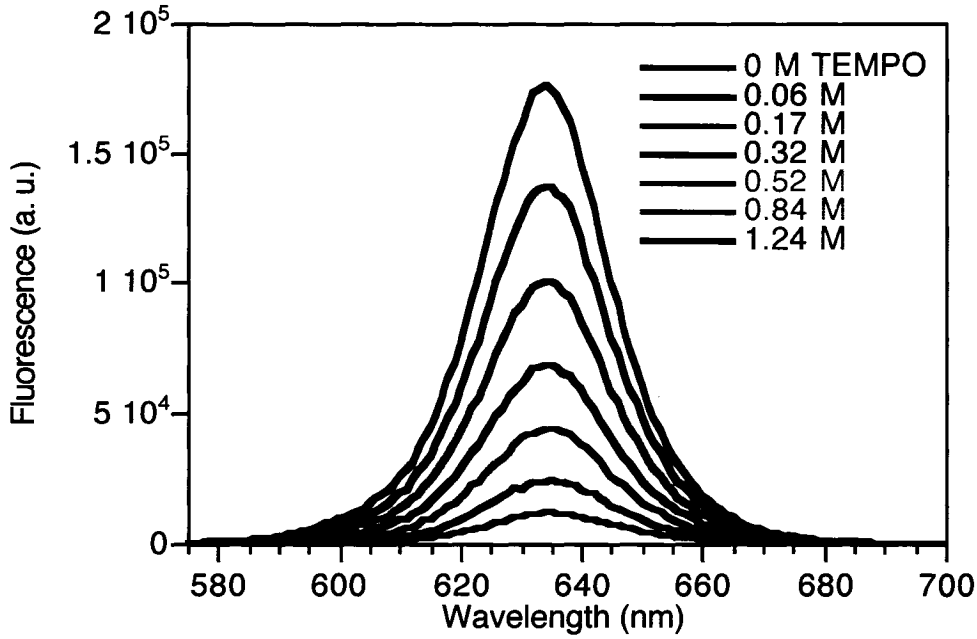

Figure 4.10 *Fluorescence spectra of a toluene solution of 0.18 μM aster red quantum dots after addition of different concentrations of TEMPO.*

The Stern-Volmer plot show a positive deviation from linearity but the curvature is significantly less than with the smaller CdSe quantum dots.

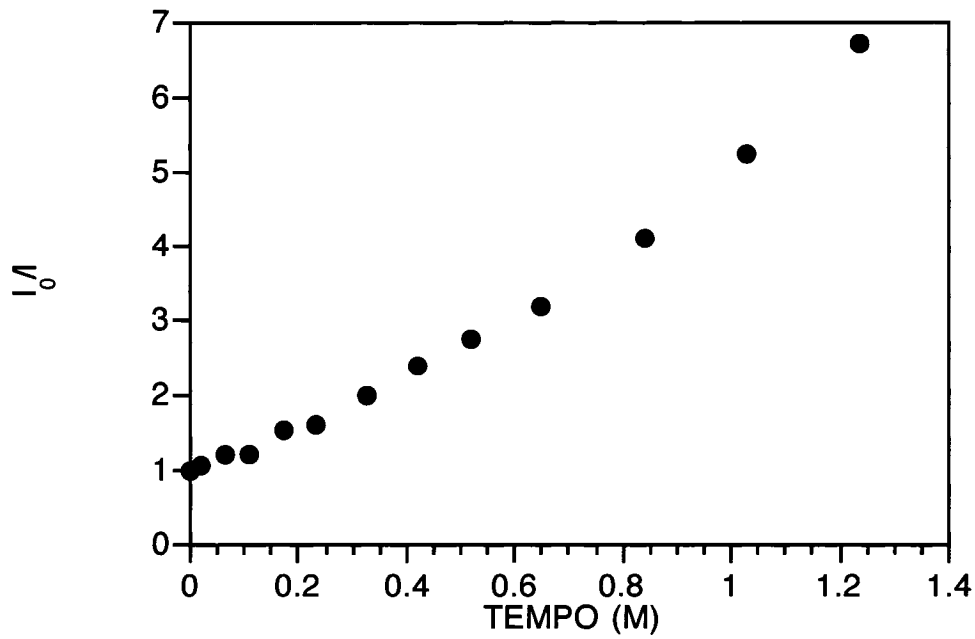

Figure 4.11 *Stern-Volmer plot of the fluorescence data for addition of TEMPO to CdSe aster red quantum dots.*

4.4.5 "Reverse" Perrin Model

Figure 4.12 shows three plots for quenching by TEMPO of amaranth green (3.7×10^{-6} M), hawkweed orange (3.7×10^{-6} M) and aster red (1.8×10^{-7} M) QD's. Fitting to Equation 4.8 gives values of α of 1.6, 6.4 and 13.7 M^{-1} for aster red, hawkweed orange and amaranth green QD's respectively.

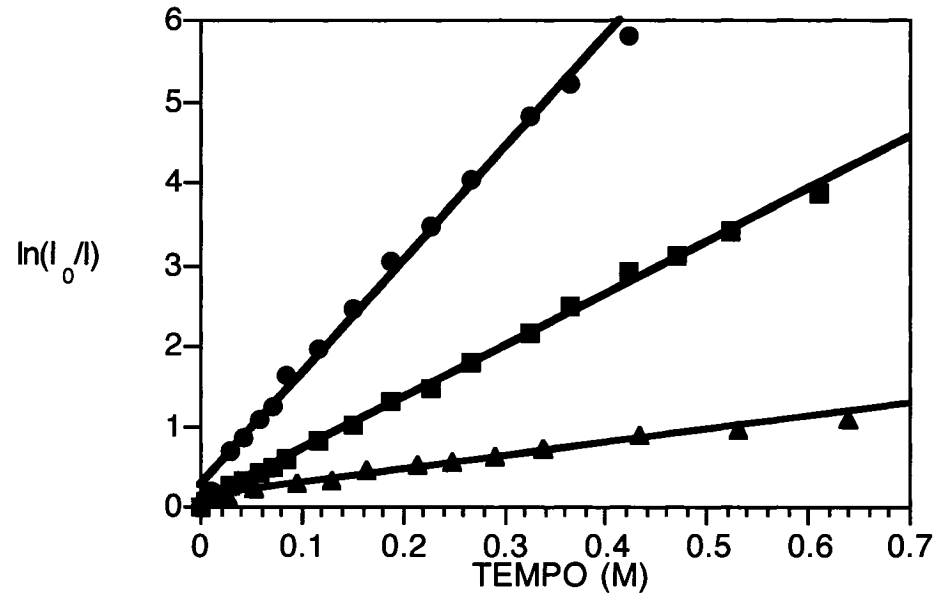

Figure 4.12 *Quenching by TEMPO of amaranth green (●), hawkweed orange (■) and aster red quantum dots (▲).*

According to the Perrin model and Equation 4.7, the calculated radii from the values of α are 1.8, 1.5 and 0.9 nm, for particles of 2.4, 3.2 and 6.7 nm in diameter, respectively. The radius calculated for the larger QD is smaller than the radius of the nanoparticle. The interpretation of the results with the Perrin model would imply that the quenching occurs inside the nanoparticle, that the quencher would have to penetrate the QD to quench. Conceptually, the more penetration required, the less effective the quenching is, but it is easier to visualize the quenching using the "reverse" Perrin model.

The quenching radii calculated with the Perrin model are properties of the quencher and fluorophore pair. The same quencher will possess a different

quenching radius depending on its interaction with the different fluorophores. In this case, if the calculated radius is assigned to the quencher instead of the chromophore, we can better visualize the interaction between quencher and chromophore, we call this a "reverse" Perrin model. Figure 4.13 depicts to scale the QD's and the sphere of action surrounding the quencher. We can see that the smaller quantum dots are more efficiently quenched by TEMPO than the larger QD's. The volume surrounding the quencher can better interact with the smaller quantum dot, it reaches across a larger volume for the smaller QD. The quenching of the fluorescence of the QD is related to size and curvature.

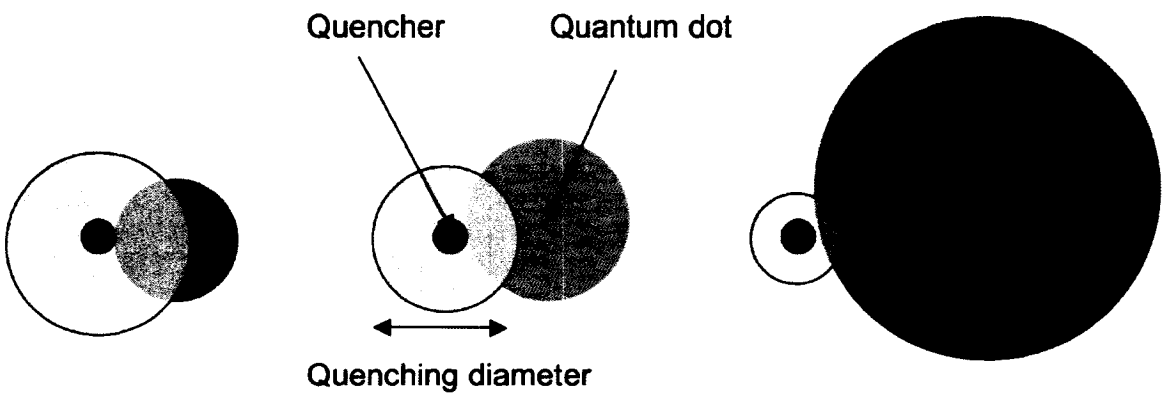

Figure 4.13 *Graphical depiction of the "reverse" Perrin model with the sphere of action surrounding the quencher, TEMPO, and its interaction with different size QD's, amaranth green (2.4 nm diam), hawkweed orange (3.2 nm diam.) and aster red (6.7 nm).*

4.4.6 Quenching of Green 505 in a Deaerated Solution

The effect of the absence of oxygen on the fluorescence quenching of small green quantum dots by TEMPO was tested by using deaerated solutions of toluene and quantum dots. A solution of 5.2 x 10^{-6} M quantum dots was deaerated with nitrogen before quenching the fluorescence with TEMPO. The quantum dots used in this experiments were synthesized in our lab. Their fluorescence maximum is at 505 nm. Steady-state fluorescence measurements were made in alternation with time-resolved fluorescence measurements. The time-resolved fluorescence results are presented in Section 4.4.7.

The fluorescence spectra are shown in Figure 4.14 for different concentrations of TEMPO.

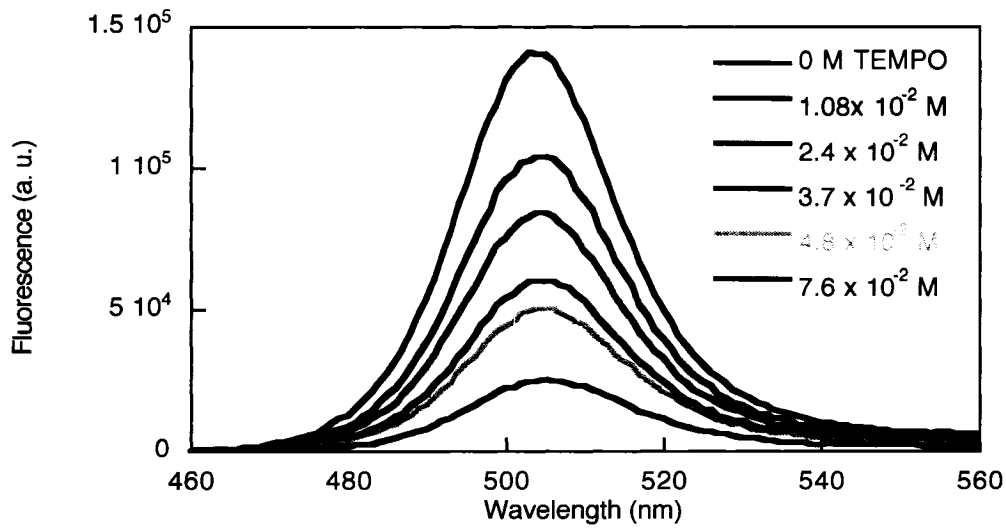

Figure 4.14 *Fluorescence of green 505 quantum dots in a deaerated solution is quenched upon addition of TEMPO.*

The Stern-Volmer treatment of the data at the fluorescence maximum results in an upward-curving plot, see Figure 4.15.

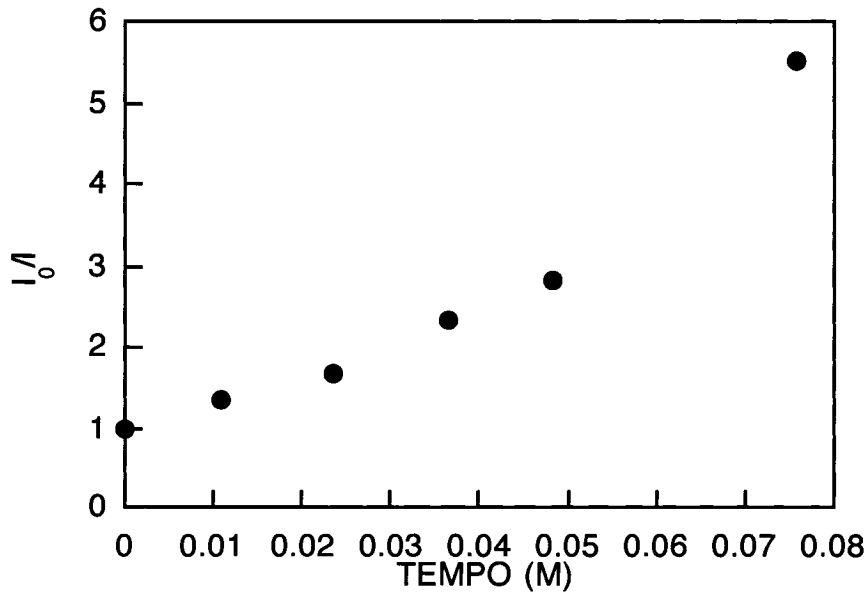

Figure 4.15 *Stern-Volmer plot of the fluorescence quenching by TEMPO at the fluorescence maximum, 505 nm.*

A fit of the Stern-Volmer plot using Equation 4.8 gives a value of α equal to 22.03 M^{-1}. This value corresponds to a Perrin-like radius of 2.06 nm according to Equation 4.7. No corrections were necessary for the absorbance of TEMPO as the wavelength of excitation was chosen as 355 nm, a minimum in the absorbance of TEMPO. The range of concentrations of TEMPO used for this experiment was such that the absorbance of TEMPO was always small enough, compared to the

absorbance of quantum dots, to be ignored. TEMPO absorbance is about 0.05 at 0.07 M and the quantum dot absorbance is greater than 0.4.

4.4.7 Time-resolved Fluorescence

Quantum dots synthesized in our laboratory with an emission maximum at 505 nm (green 505) were used for the following experiments. The excitation wavelength is 355 nm and the laser pulse is 7 ns long. A solution of QD's in toluene 5.2 x 10^{-6} M was prepared and deaerated with N_2. This experiment was done in alternation with steady-state measurements. The steady-state results are reported in the previous section 4.4.6. Figure 4.16 shows time-resolved fluorescence decay traces for selected concentrations of TEMPO.

The different spectra were fitted with biexponential decays. The fit for the short lifetimes is within the experimental limit of the experimental setup. However the fits clearly show that as TEMPO is added to the QD solution, the longer lifetimes are affected, see Table 4.1. They get shorter with increasing TEMPO concentration. The biexponential fit is only an approximation to the real kinetic decay of QD's in solution.

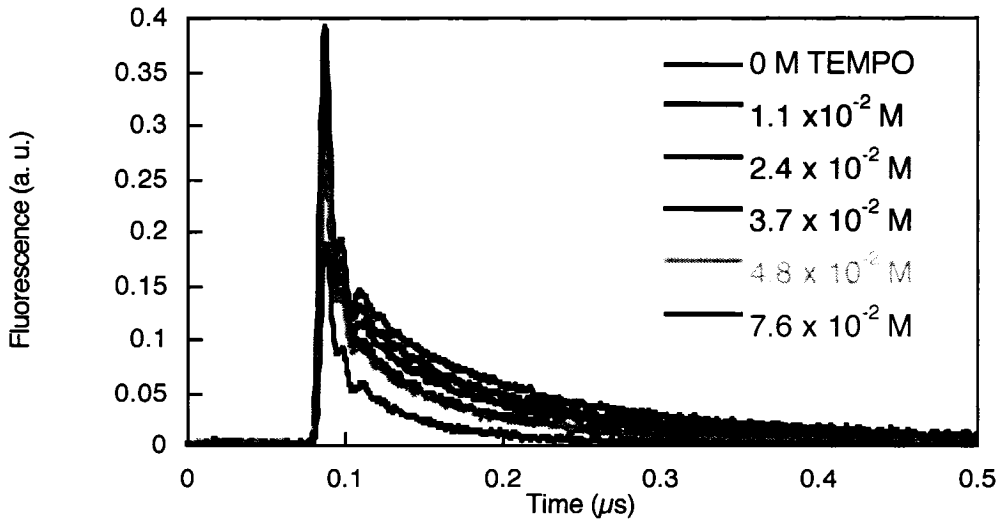

Figure 4.16 *Fluorescence time resolved decay traces for a solution of 5.2 x 10^{-6} M green 505 QD's after addition of different concentrations of TEMPO.*

Table 4.1 summarizes the fits to the curves of fluorescence decay for all the concentrations of TEMPO used.

Table 4.1 *Fluorescence lifetimes*

TEMPO (M)	*0*	*1.1 x 10^{-2}*	*2.4 x 10^{-2}*	*3.7 x 10^{-2}*	*4.8 x 10^{-2}*	*7.6 x 10^{-2}*
Lifetimes (ns)	4.3	4.1	4.3	5.1	5.4	4.3
	112.0	96.9	86.9	72.8	73.0	48.4

4.4.8 Size Dependence of Quenching

The width of the fluorescence peaks is related to a particle size distribution within each peak. The smaller dots fluoresce at shorter wavelengths than the bigger QD's. We have reported that the fluorescence quenching of quantum dots by TEMPO is size dependent.[4] This effect can also be seen with the Stern-Volmer plots. If you make three Stern-Volmer plots, one at the fluorescence maximum and two others on each side of a fluorescence peak obtained by quenching one size QD's with TEMPO, you can observe that the three Stern-Volmer plots will not be superimposed. Stern-Volmer plots will show significant differences for differences of only 15 nm in emission wavelength. The Stern-Volmer plot taken at the shorter wavelength exhibits more quenching that the one taken at a longer wavelength. This property reflects on a smaller scale the differences observed for fluorescence quenching of QD's that emit at 520 nm (green), 580 nm (orange) and 620 nm (red). Figure 4.17 shows three Stern-Volmer plots made from the same quenching experiment. The data were taken from the quenching by TEMPO of amaranth green QD at 3 different wavelengths, 510, 525, 540 nm.

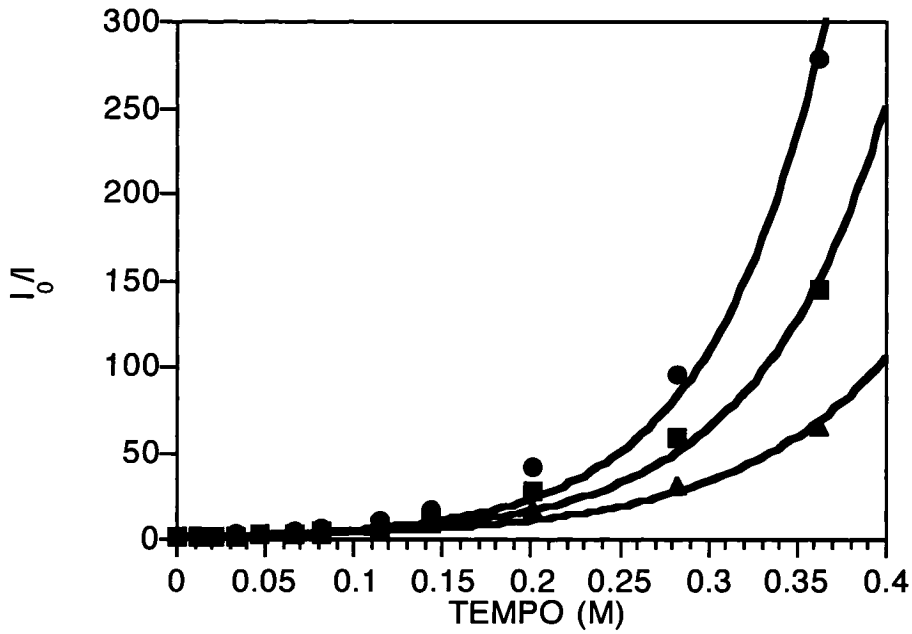

Figure 4.17 *Stern-Volmer plots taken at 510 (●), 525 (■), and 540 (▲) nm for fluorescence quenching by TEMPO of a 4.1 x 10 $^{-6}$ M solution of amaranth green QD's.*

Fit to Equation 4.8 gives values of α of 15.6, 13.7 and 11.6 M^{-1} for 510, 525 and 540 nm. The same trend can be observed with fluorescence quenching of hawkweed orange QD's by TEMPO, see Figure 4.18 and for fluorescence quenching of aster red QD's, see Figure 4.19. Values of α are 9.8, 8.2 and 6.8 M^{-1} for 560, 575 and 590 nm and α are 1.8, 1.7 and 1.6 M^{-1} for 620, 635 and 650 nm. The exponential fit seems less perfect for the larger aster red QD's but the upward

curving trend is very clear in Figure 4.11. The deviations of points at lower concentrations of TEMPO can be attributed to experimental errors.

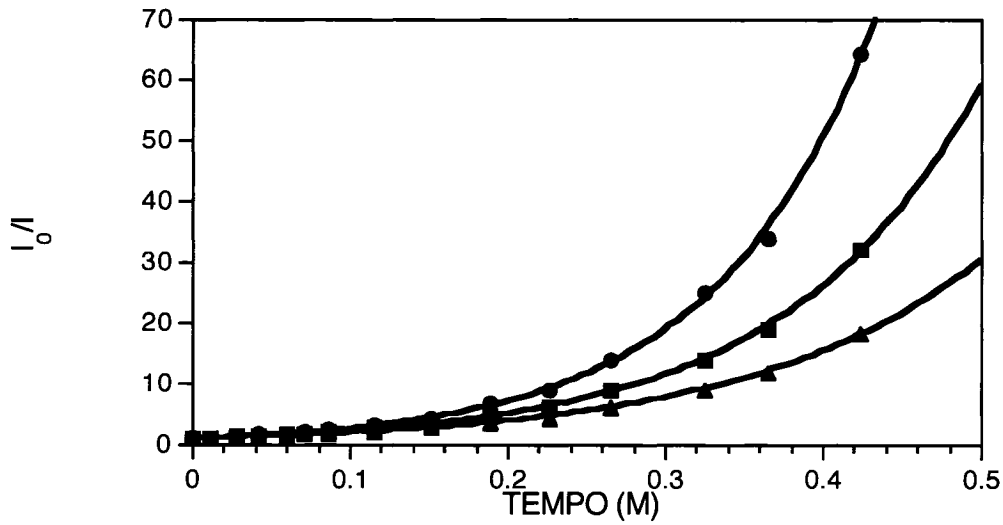

Figure 4.18 *Stern-Volmer plots taken at 560 (●), 575 (■), and 590 (▲) nm for fluorescence quenching by TEMPO of a 4.1 x 10 $^{-6}$ M solution of hawkweed orange QD's.*

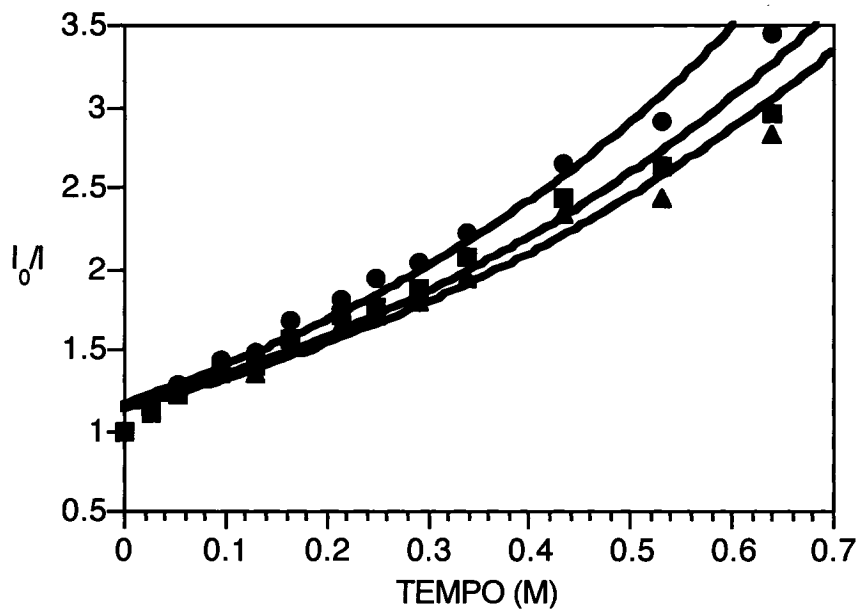

Figure 4.19 *Stern-Volmer plots taken at 620 (●), 635 (■), and 650 (▲) nm for fluorescence quenching by TEMPO of a 1.8 x 10 $^{-7}$ M solution of aster red QD's.*

Figure 4.20 shows the variation of α, the Perrin model parameter, with the emission wavelength for the quenching of CdSe QD by TEMPO. As the emission wavelength gets longer the value of α becomes smaller indicating that the smaller QD's corresponding to shorter emission wavelengths are more efficiently quenched by TEMPO than the larger QD's.

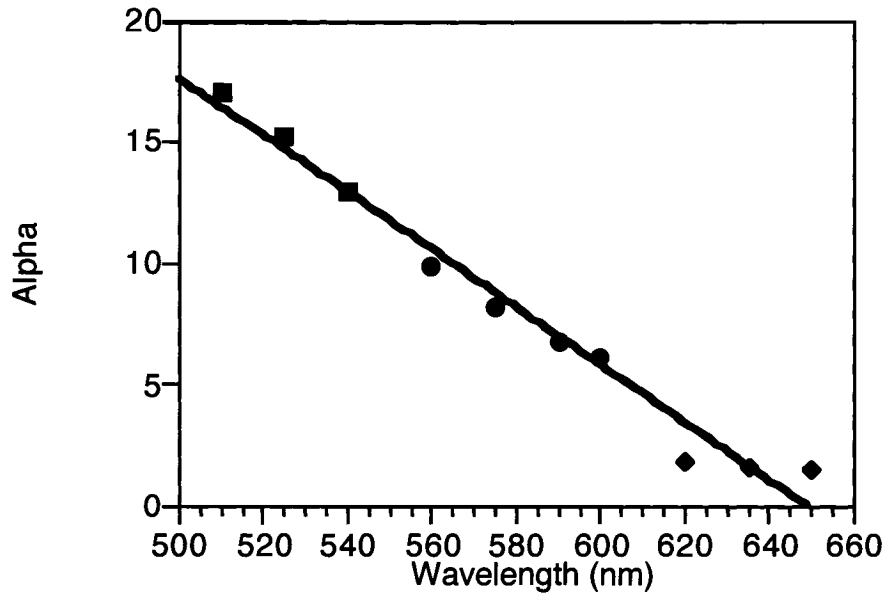

Figure 4.20 *Values of α derived from the Perrin model for quenching by TEMPO of CdSe QD's derived from quenching with amaranth green (■), hawkweed orange (●) and aster red (◆).*

4.5 Fluorescence Quenching by 4-Amino-TEMPO

4.5.1 Electron Spin Resonance Studies

Electron spin resonance (ESR) studies done in our group by Dr Vincent Maurel, a postdoctoral fellow, have shown that there is formation of a complex between 4-amino-TEMPO (4AT) and green QD's. The ESR spectrum of 4AT in toluene shows the characteristic ^{14}N hyperfine splitting of 1.54 (±0.01) mT (Knauer and Napier report 1.546 mT [28]). These experiments were carried out under nitrogen in order to avoid line broadening caused by oxygen. Upon addition of

QD's, line broadening is observed in the ESR spectra, see Figure 4.21. This broadening is indicative of the formation of a complex between the quantum dots and 4AT. This is due to slow tumbling of the nitroxide moiety in the tight layer of TOPO ligands on the QD surface. The QD quencher interactions are different than the ones we observed for quenching by TEMPO. ESR does not indicate formation of a complex between the green quantum dots and TEMPO. The concentration of TEMPO required to quench is at least three orders of magnitude higher than required by 4AT to quench the small quantum dots.

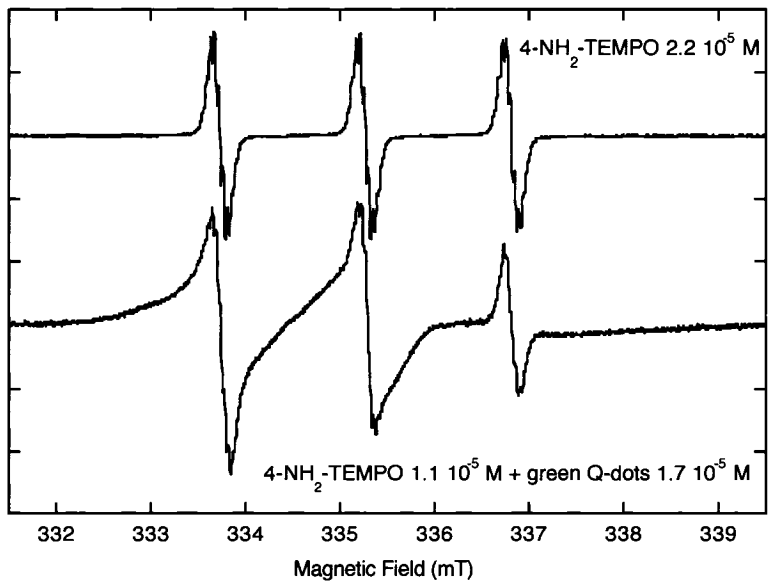

Figure 4.21 *ESR spectra before and after addition of QD's.*

An association constant for the binding of 4AT to green QD (2.4 nm in diameter) was found to be (6.7 ± 3.4) x 10^6 M^{-1}. This association constant was derived from the ESR results. The signal at high field is very weak when the

complex 4AT-QD is formed, it is assumed that this signal at high field is entirely due to free 4AT in solution. By comparison of the peak to peak height at high field of an ESR spectrum of 4AT only ($3.6x10^{-7}$ M) and of a spectrum of 4AT ($3.6x10^{-7}$ M) and QD ($4.3x10^{-7}$ M), the concentration of free 4AT can be determined, 2.2×10^{-7} M. It is also assumed that at these low concentrations only one 4AT molecule binds to a QD. From this value the concentration of complex and free QD in solution can be determined and from this the equilibrium constant of complex formation can be calculated. The 50% relative uncertainty is due to the uncertainty of the concentrations of the QD's and to the determination of the concentration of 4AT from the ESR spectra due to low intensity of the signal at such low concentrations of free 4AT.

Job's method[29] was used to determine the number of 4AT that bind to a small green QD (2.4 nm in diam.) using ESR spectra. The signal at 0.5mT lower than the first peak only shows a weak signal for 4AT. The signal was recorded at this value for different mole fractions of 4AT and QD where the total concentration was maintained constant at 2×10^{-5} M. The value of the signal was recorded for QD and 4AT in solution and the intensity of the signal without QD was subtracted. The resulting plot clearly shows a broad maximum for mole fractions between 0.5 and 0.6. This corresponds to a preferential binding of one or two 4AT per QD, at these concentrations, see Figure 4.22.

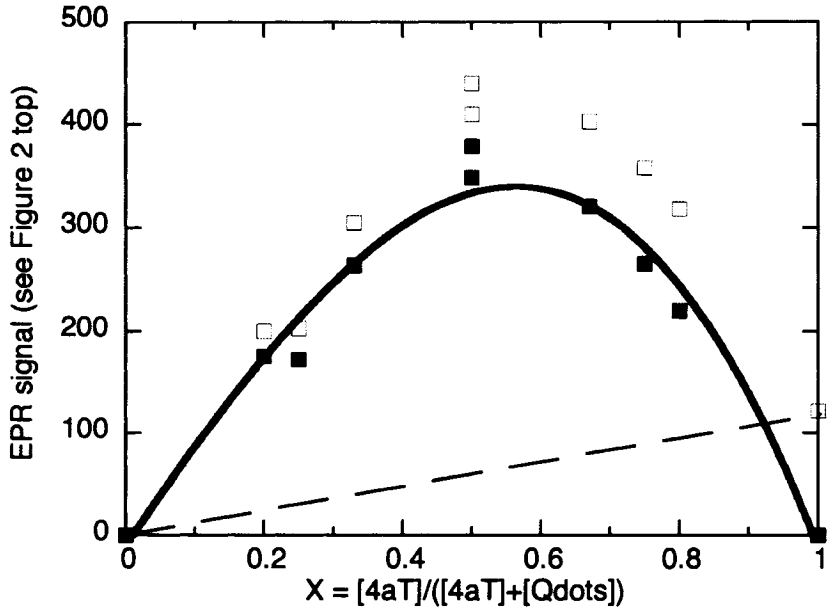

Figure 4.22 *Job's method. Open squares = experimental data; filled squares = data corrected, dashed line = correction function, total concentration is constant [4A] +[QD] = 2x 10 $^{-5}$ M. The full line is a fit to a 3rd order polynomial function and is a visual aid only.*

4.5.2 Quenching of CdSe Amaranth Green Quantum Dots

The fluorescence of green QD's, 2.4 nm in diameter was quenched by addition of 4-amino-TEMPO (4AT) in a toluene solution. Figure 4.23 shows representative spectra for different concentrations of 4AT. Figure 4.24 shows the Stern-Volmer plot at the maximum fluorescence wavelength.

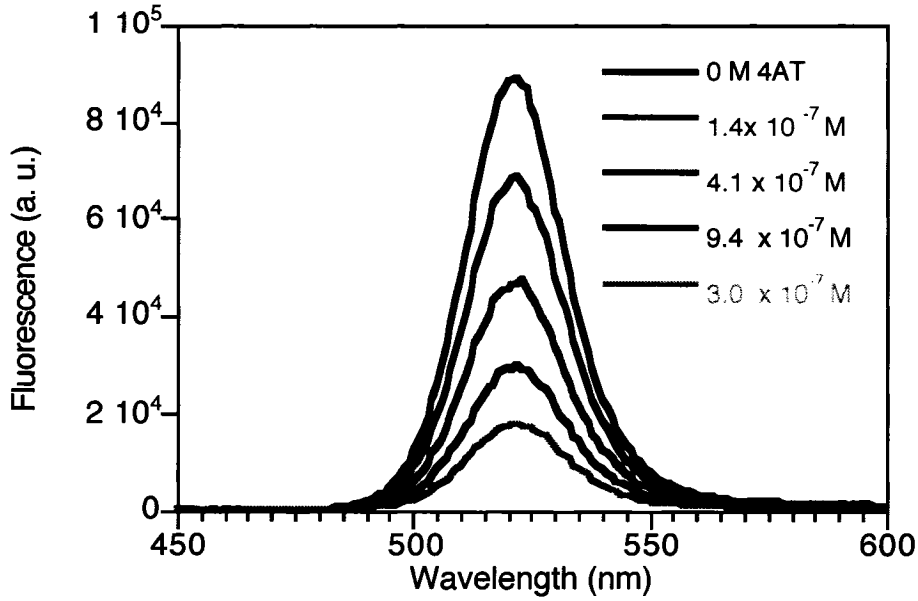

Figure 4.23 *Fluorescence spectra (λ_{exc} 360 nm) of amaranth green QD's 1.2 x 10^{-6} M after addition of 4AT.*

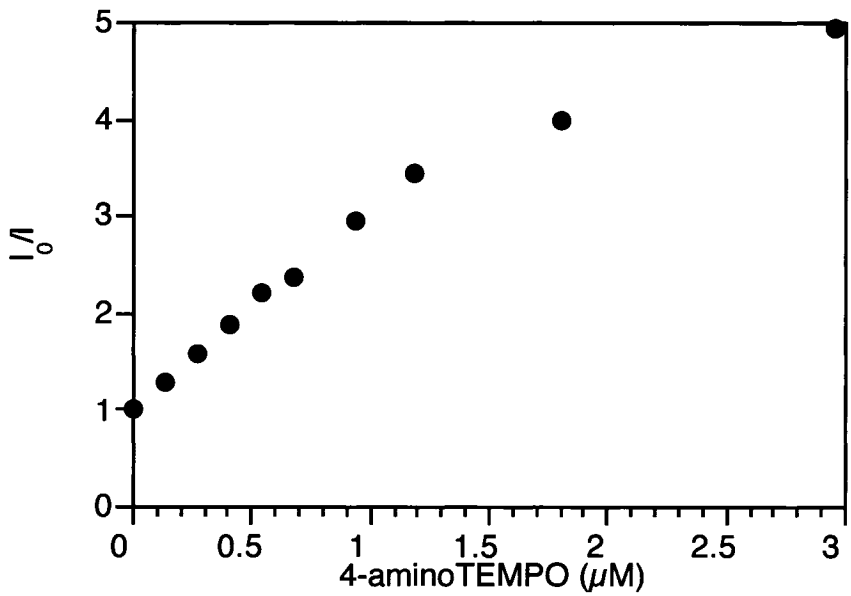

Figure 4.24 *Stern-Volmer plot at the fluorescence maximum for quenching by 4AT of a 1.15 x 10^{-6} M solution in toluene of green QD's.*

Figure 4.25 shows a Stern-Volmer plot obtained for a similar concentration of green QD's, 1.27 x 10^{-6} M for quenching by 4AT.

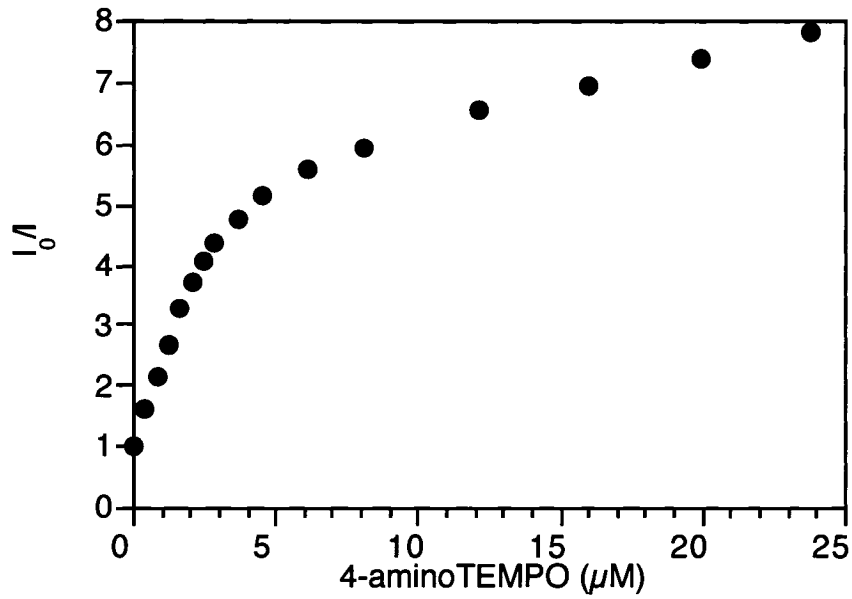

Figure 4.25 *Stern-Volmer plot at the fluorescence maximum for quenching by 4AT of a 1.27 x 10^{-6} M solution in toluene of green QD's.*

Figures 4.24-4.25 show that the results are reproducible, even though there are many instances when experiments with quantum dots can lead to slightly different results depending on aging of the sample or other unknown experimental parameters. The latest experiments were performed by systematically degassing the QD's solutions with N_2 in order to minimize the variability in the results. We also wanted to have similar experimental conditions to the ESR experiments that were done with deaerated solutions.

4.5.3 Quenching of Hawkweed Orange Quantum Dots

The fluorescence of hawkweed orange quantum dots, 3.2 nm in diameter, was quenched by addition of 4-amino-TEMPO (4AT) in a toluene solution. Figure 4.26 shows representative spectra for different concentrations of 4AT. Figure 4.27 shows the Stern-Volmer plot at the fluorescence maximum for hawkweed orange QD's 1.70 x 10^{-6} M quenching by 4AT.

The Stern-Volmer plot is downward curving at low concentrations of 4AT. More 4AT is required to quench the fluorescence of the orange QD's than for quenching of the smaller green QD's fluorescence.

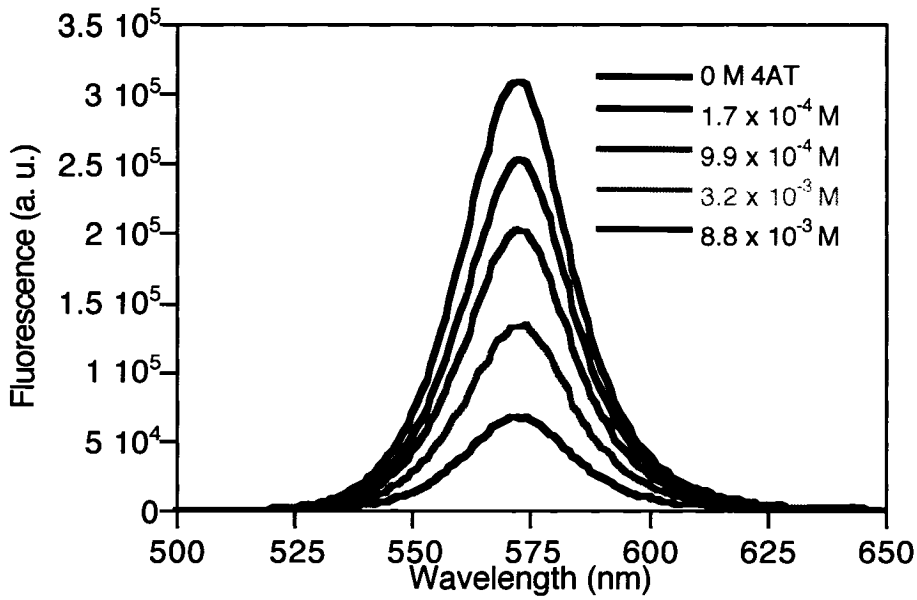

Figure 4.26 *Fluorescence spectra (λ_{exc} 360 nm) of hawkweed orange QD's 1.7 x 10 $^{-6}$ M after addition of different concentrations of 4AT.*

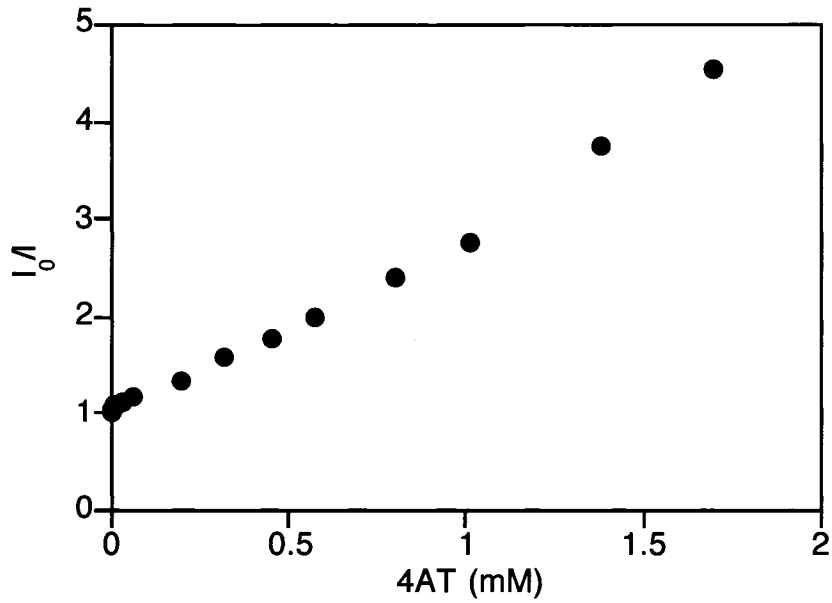

Figure 4.27 *Stern-Volmer plot for hawkweed orange QD's 1.7 x 10 $^{-6}$ M taken at the fluorescence maximum for quenching by 4AT.*

The slope of the Stern-Volmer plot of Figure 4.27 in the linear region at higher concentrations of 4AT is 2 x 10^3 M^{-1} and according to Equation 4.2 would be equal in the case of dynamic quenching to k_q x τ. If we assume that the quenching is dynamic and diffusion controlled, k_q = 10 ^{10} M^{-1} s^{-1} we would find a lower limit lifetime for the QD of 200 ns. The reported lifetimes are in the 20 to 100 ns and our time resolved experiments give lifetimes of 4.3 ns and 112.0 ns, see Table 4.1. Dynamic quenching can be excluded for hawkweed orange QD quenching by 4AT based on these lifetimes. The difference between the quenching for the smaller amaranth green QD's and the larger hawkweed orange quantum dots can be seen by the concentration of 4AT required to quench half the fluorescence of the QD's. For the smaller green QD's, 1.3 x 10 $^{-6}$ M, the concentration of 4AT required is of

0.5 μM, for the orange QD's, 1.7 x 10^{-6} M of similar concentration, the concentration of 4AT required is between about 4 mM, a 100 times more. The difference could in part be attributed to surface curvature and stress, which is greater for smaller QD's and can lead to more facile displacement of the initial ligand TOPO. The Stern-Volmer plots are downward curving at low concentrations of 4AT and are more linear or slightly upward curving at higher concentrations.

4.5.4 Quenching of Aster Red Quantum Dots

The fluorescence of a solution 1.78 x 10^{-7} M of aster red quantum dots, 6.8 nm in diameter, was quenched by addition of 4AT in a toluene solution. Figure 4.28 shows representative spectra for different concentrations of 4AT. Figure 4.29 shows the Stern-Volmer plot at the fluorescence maximum.

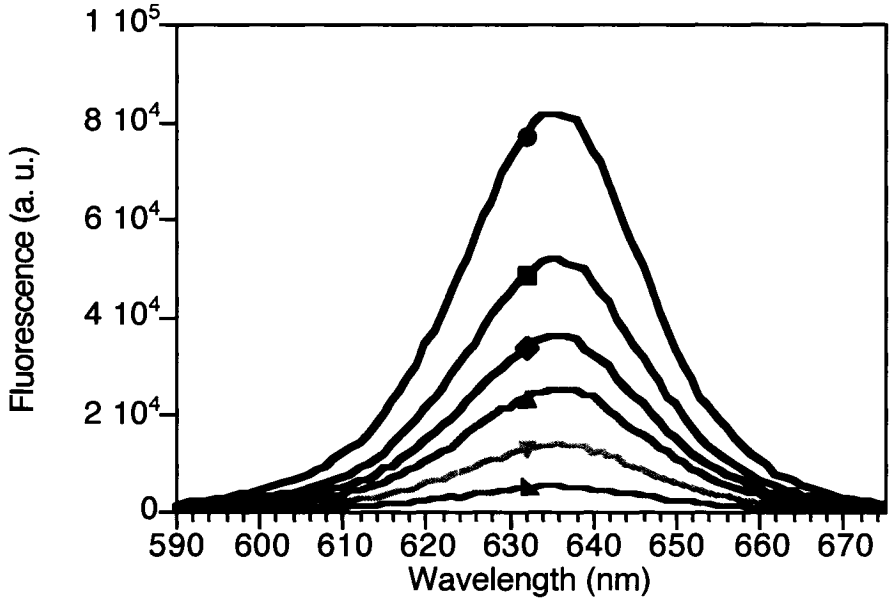

Figure 4.28 *Fluorescence spectra (λ_{exc} 360 nm) of aster red QD's 1.78 x 10 $^{-7}$ M in the presence of 0 M (●), 8.5 x 10 -4 M (■), 1.4 x 10 -3 M (◆), 2.0 x 10 -3 M (▲), 3.4x 10 -3 M (▼), 8.1 x 10 -3 M (◣) 4AT.*

The Stern-Volmer plot is downward curving at low concentrations of 4AT as can be seen in the inset of Figure 4.29. At higher concentration of 4AT, the Stern-Volmer plot seems to be more linear or slightly upward curving.

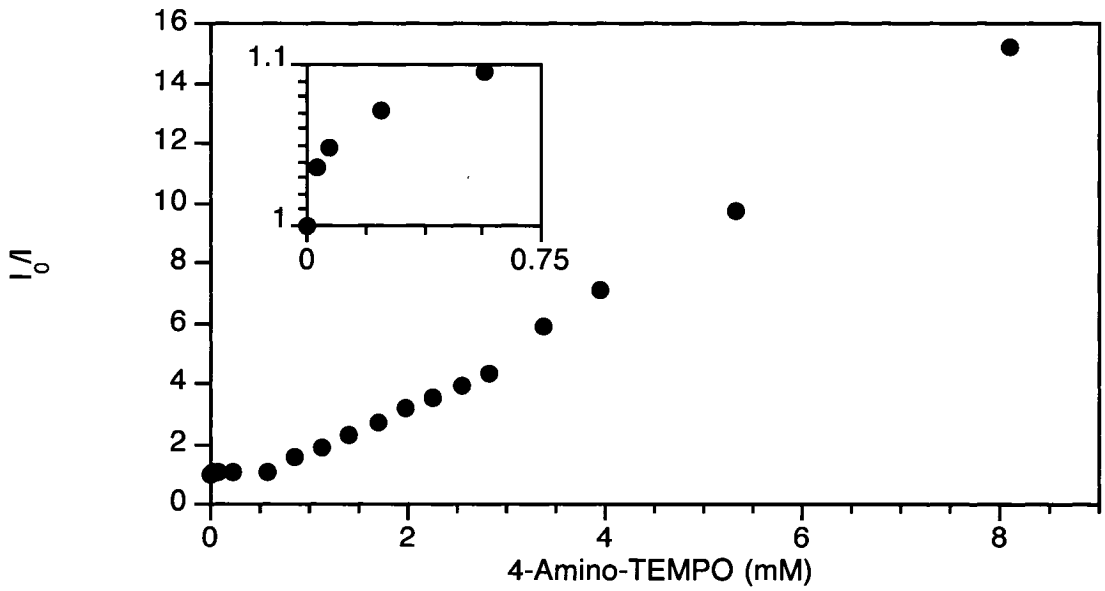

Figure 4.29 *Stern-Volmer plot for quenching by 4AT of 0.2 μM aster red QD's*

4.5.5 Size Dependence of Quenching

A size dependence within each fluorescence peak is also reported for quenching by 4AT of CdSe QD's. Figure 4.31 shows three Stern-Volmer plots obtained for the quenching of amaranth green QD's by 4AT at the fluorescence maximum, 530 nm, and on each side of the peak maximum, 515 nm and 545 nm. We can observe that there is more quenching at the shorter wavelengths, which corresponds to smaller QD's and less quenching at the longer wavelength, which corresponds to larger QD's.

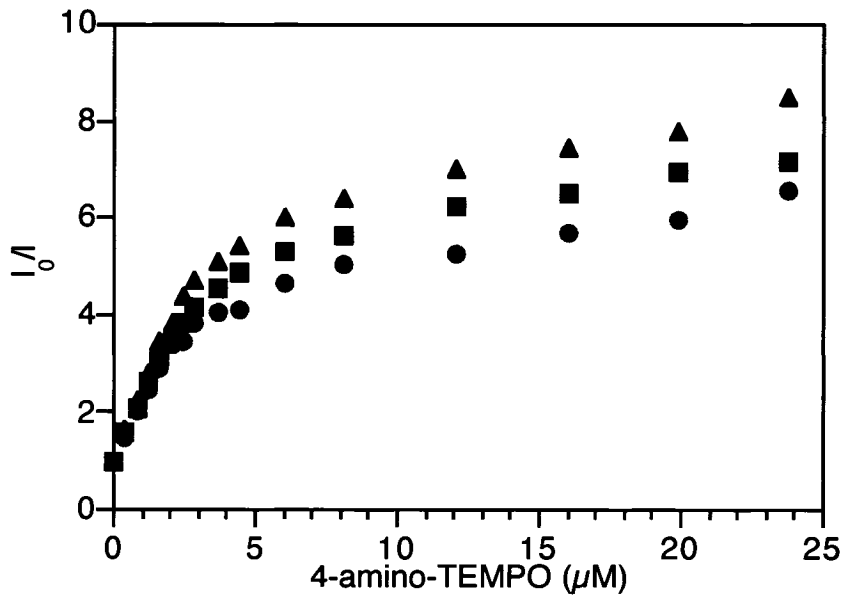

Figure 4.30 *Stern-Volmer plots obtained at 515 nm (▲), 530 nm (■), and 545 nm (●) for the quenching of amaranth green QD's (1.27 x 10 $^{-6}$ M) by 4AT, (λ_{exc} 360 nm).*

The same treatment was done for hawkweed orange and aster red QD's, see Figure 4.31 and Figure 4.32.

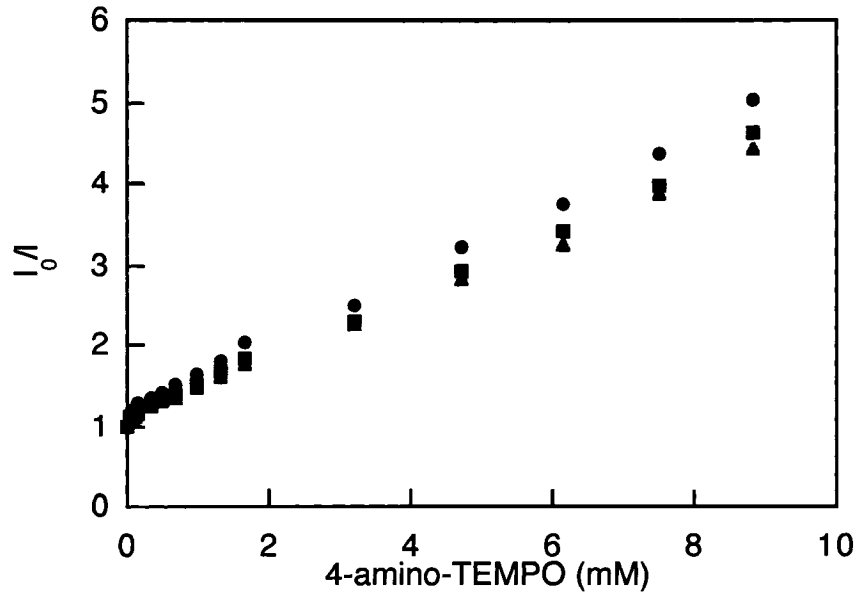

Figure 4.31 *Stern-Volmer plots taken at 560 (●), 575 (■), and 590 (▲) nm for fluorescence quenching by 4AT of a 1.7 μM solution of hawkweed orange QD's. (λ_{exc} 360 nm)*

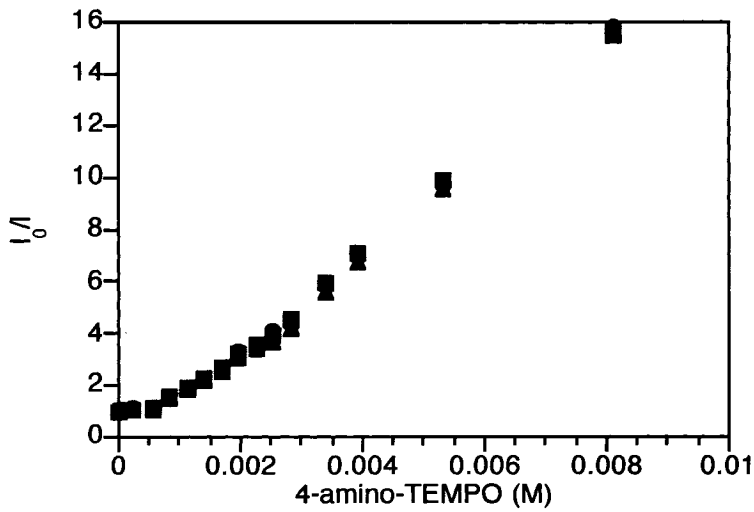

Figure 4.32 *Stern-Volmer plots taken at 620 (●), 635 (■), and 650 (▲) nm for fluorescence quenching by 4AT of an 0.2 μM solution of aster red QD's. (λ_{exc} 360 nm)*

The effect of size on quenching is minimal for the larger aster red quantum dots. The Stern-Volmer plots show only a very slight difference in quenching within 15 nm each side of the maximum. This confirms the relationship between diameter and number of surface defects that allow binding of the amino moiety of 4AT. As the particles gets larger, the change in surface curvature or stress is not as important as with the smaller QD's, this leads to a lesser effect of quenching with size.

4.6 Development of Prefluorescent Probes

4.6.1 Control Experiments

Quantum dots synthesized in our laboratory with an emission maximum at 515 nm were used for the following experiments. An 8.66 x 10^{-6} M solution of green 515 QD's in toluene was exposed to one lamp at 350 nm in the photoreactor for several minutes, see lamp profile in Chapter 1, by small time increments. Typically, the solution was exposed for 15 s then the fluorescence intensity was measured and the same solution was exposed for another 15 or 30 s. This was repeated for a total exposure time of several minutes. The same experiment was also done with a solution containing 8.56 x 10^{-6} M green 515 QD's and 6.12 x 10^{-5} M 4AT. The concentration of 4AT added was sufficient to quench more than half the initial fluorescence of the QD's before addition of 4AT. The results of both experiments are plotted in Figure 4.33.

Fluorescence intensity changes are minimal for the times of exposure used.

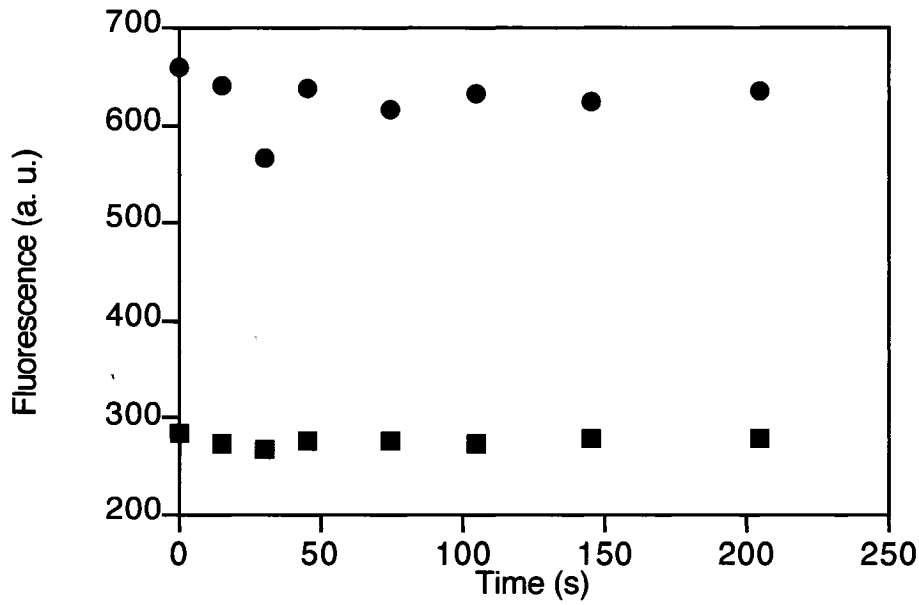

Figure 4.33 *Fluorescence (λ_{exc}=400 nm) intensity variation with time of exposure for a solution of green 515 QD's (●) and a solution of green 515 QD's (■) quenched with 4AT. Exposure was done in the photoreactor with one 350 nm lamp.*

4.6.2 Radical Traps

Addition of AIBN to solutions of green 515 QD's and green 515 QD's containing 4AT does not affect the fluorescence properties of these solutions. Upon exposure to one 350 nm lamp in the photoreactor or to light from a Luzchem Xenon illuminator with a filter cutting wavelengths below 345 nm, AIBN generates radicals in solution. These radicals are expected to react with the free radical

nitroxide moiety of 4AT. Upon exposure, solutions of QD's and 4AT containing AIBN see their fluorescence restored to their initial fluorescence before addition of 4AT.

Figure 4.34 shows the change at the maximum fluorescence intensity with exposure to 1 lamp in the photoreactor of a solution of 7.9 x 10^{-6} M green 515 QD's, 5.7 x 10^{-5} M 4AT and containing AIBN. The maximum intensity of fluorescence of the solution before addition of 4AT and AIBN was 1.03 x 10^{5}. Addition of 4AT quenched the fluorescence to an intensity of 5.2 x 10^{4}.

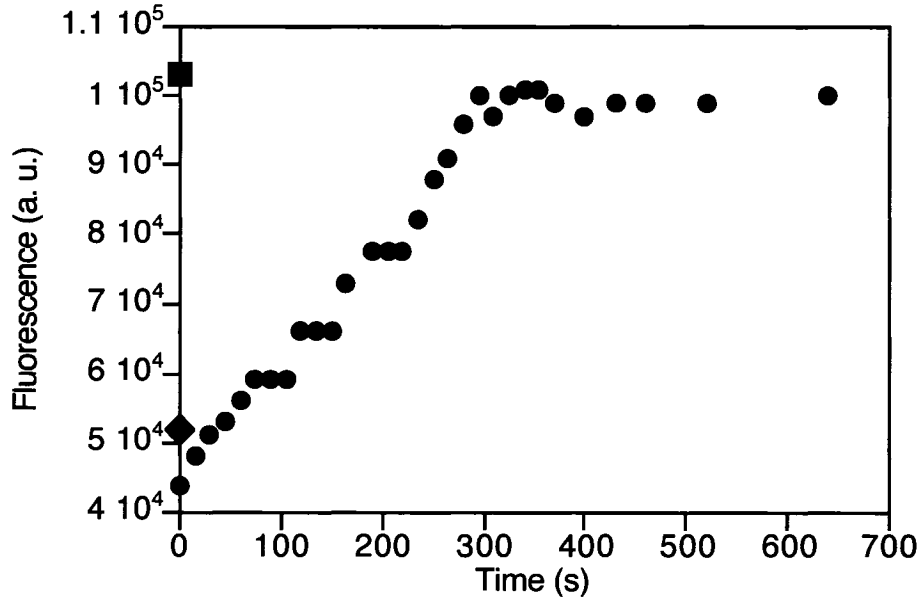

Figure 4.34 *Evolution of fluorescence intensity (●) of a solution of green 515 QD's 7.9 x 10^{-6} M, 4AT 5.7 x 10^{-5} M and AIBN with irradiation time (photoreactor 1 lamp 350 nm). Fluorescence of QD's before (■) and after addition (◆) of 4AT at time 0.*

Addition of AIBN because of a dilution factor and after degassing the solution gave a fluorescence intensity of 4.4×10^4. Upon irradiation in the photoreactor the fluorescence was gradually restored over 300 seconds to almost the initial value of fluorescence before addition of quencher.

A solution of green 515 QD's (7.7×10^{-6} M) with 4AT (7.2×10^{-5} M) was prepared. TEMPO was added but at a concentration, 5.5×10^{-5} M, that does not significantly quench the fluorescence of the solution. The experiment was designed to verify if AIBN would react preferentially with the free radicals in solution, such as the TEMPO radicals first and then react with the free radicals of 4AT presumably bound to the QD. This would manifest by an induction period before recovery of fluorescence. The concentration of 4AT and TEMPO being similar, if the radical from AIBN reacts indiscriminately with the bound 4AT or the unbound TEMPO, the recovery of fluorescence should be slowed down compared to when only 4AT is present. Upon addition of AIBN there was a slight decrease in fluorescence that can be attributed to a dilution factor as well as to the fact that the solution was degassed for more than 20 minutes. Upon irradiation, with the Luzchem illuminator, the fluorescence was restored to 80% of the fluorescence of QD's green 515 alone, see Figure 4.35. Prolonged irradiation, after the initial 200 s. induced a decrease in the fluorescence intensity. This could be explained by the fact that irradiation with the lamp and the filter induces at prolonged exposure a decrease in fluorescence. The experiment was redone but irradiation was made in the photoreactor with one 350 nm lamp, see Figure 4.36. Irradiation in the photoreactor with one 350 nm lamp was shown not to induce significant loss of

fluorescence after 250 s of exposure. The quantum dots for this experiment have a maximum fluorescence peak at 520 nm.

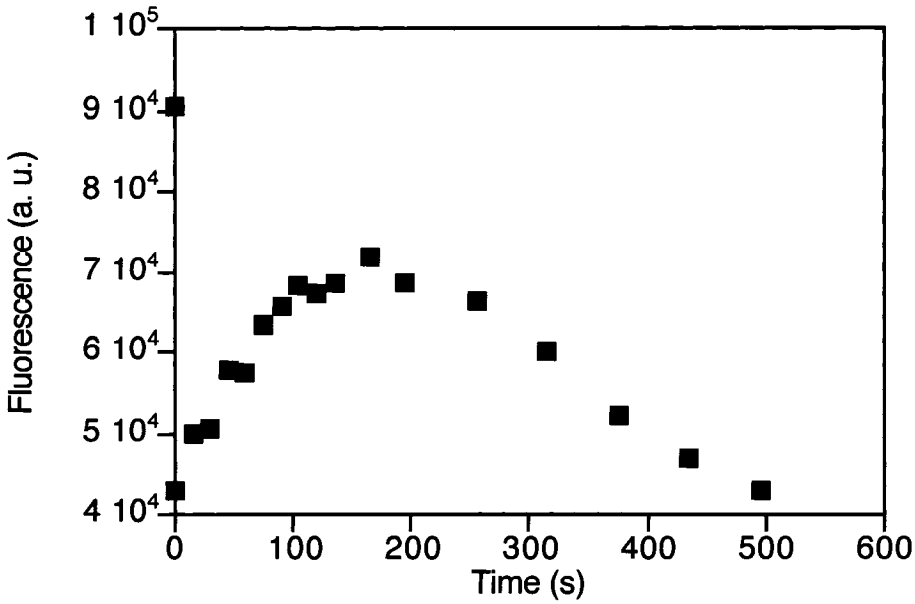

Figure 4.35 *Fluorescence of a 7.7 x 10^{-6} M green 515 QD's, 7.2 x 10^{-5} M TEMPO and 5.5 x 10^{-5} M 4AT solution with AIBN is restored with irradiation times totaling less than 200 s (Luzchem Xe illuminator). Prolonged exposure with the lamp leads to decreases in fluorescence.*

There is an observable delay, see Figure 4.36, in the fluorescence recovery for the solution that contains TEMPO compared to the solution that contains only the QD and the 4AT and AIBN.

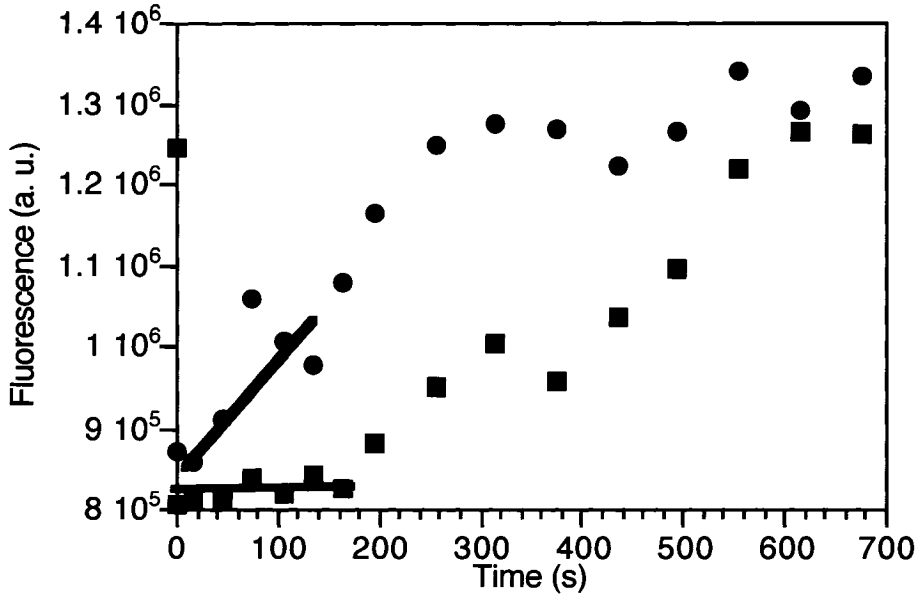

Figure 4.36 *Evolution of fluorescence intensity of a solution of green 520 QD's 7.9 μM + 66 μM 4AT and AIBN (●) and of an identical solution but with 70 μM TEMPO (■) with irradiation (350 nm) time. At time 0, before addition of 4AT and TEMPO the fluorescence intensity of both solutions was identical.*

Two opposing factors are at play, enhancement of fluorescence by complexation of the radical from AIBN with 4AT on the surface of the QD's and decrease in the intensity of fluorescence by irradiation of the QD's or of the 4AT-QD complexes. Figure 4.35 shows that the increase in fluorescence occurs in the first 150 seconds while irradiation in the photoreactor shows an increase over 300s, see Figures 4.34 and 4.36. No induction period for the quenching of fluorescence was observed when the samples where irradiated with the Xe lamp and filter. The intensity of irradiation is larger with the lamp than with irradiation in the photoreactor and may be destroying the sample.

4.7 Effect of Cyclohexylamine on Fluorescence

Cyclohexylamine is a molecule that has a structure similar to 4AT but lacks the paramagnetic moiety. Tests with cyclohexylamine will clarify the effect of the amino moiety on the fluorescence quenching of QD's by 4AT.

The fluorescence of a solution of green 515 QD's (8.7×10^{-6} M) in toluene was measured before and during addition of cyclohexylamine (CHA). A slight decrease, 12%, in the intensity of fluorescence was observed after 30 equivalents of CHA were added, as can be seen in Figure 4.37. The decrease is complete for a concentration of 5×10^{-5} M CHA or 6 equivalents. The decrease in fluorescence being less facile after 6 equivalents of CHA may point to the fact that after a certain concentration, CHA might bind by displacing the TOPO molecules on the surface. The first CHA molecules that quench the fluorescence would bind to the QD surface in holes in the TOPO ligand layer.

The effect of adding cyclohexylamine to the same concentration of quantum dot (8.6×10^{-6} M) but quenched partially with 4AT (6.1×10^{-5} M) is to increase the fluorescence of the solution, see Figure 4.37. The increase is complete after 0.0001M CHA or 11 equivalents. The increase in fluorescence would be indicative that CHA displaces 4AT from the QD surface. CHA decreases only slightly the fluorescence of the QD while 4AT decreases it significantly. The fluorescence increase observed would point to a displacement of 4AT leading to an increase in fluorescence of the QD that is partially offset by the binding of CHA, leading to a

small decrease in fluorescence. Cyclohexylamine when added in excess to the QD-4AT complex, which shows ESR band broadening, was shown to restore the signal to a width typical of free 4AT in solution. This supports the hypothesis that cyclohexylamine displaces 4AT.

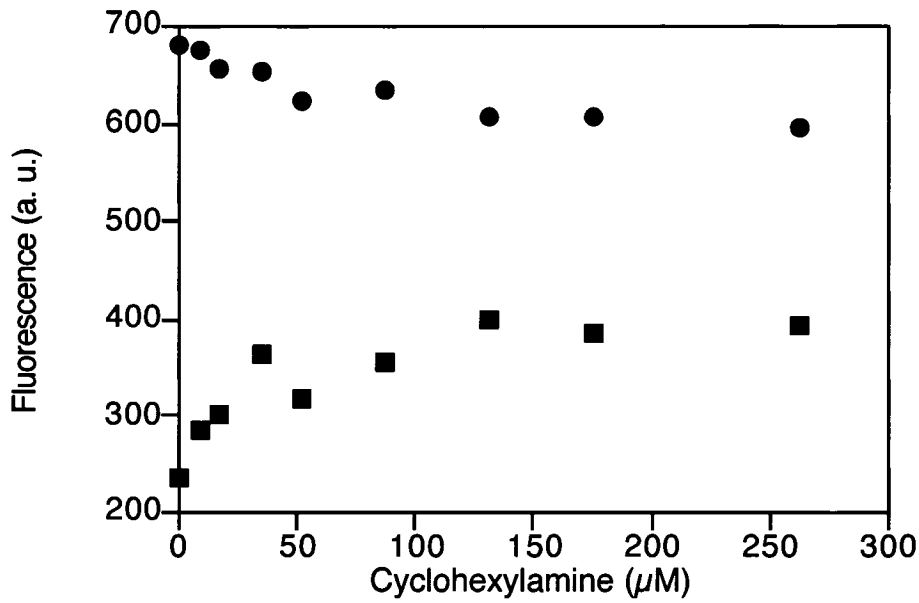

Figure 4.37 *Fluorescence changes with addition of cyclohexylamine to a solution of QD's 8.7 x 10^{-6} M (●) and QD's 8.6 x 10^{-6} M and 4AT 6.1 x 10^{-5} M (■).*

The two curves do not meet at the final concentration of CHA added of 2.6 x 10^{-4} M. The concentration of CHA is probably not sufficient to displace all the 4AT bound to the QD and furthermore the displaced 4AT in solution could quench the fluorescence of the QD in the same manner as TEMPO does.

4.8 Two-Photon Fluorescence Excitation

The fluorescence of solutions of quantum dot in toluene was recorded under 2-photon excitation with a picosecond laser pulse from an Nd-YAG laser emitting at 1064 nm. The laser beam was focused with a lens onto the samples, which were contained in 10 x 10 mm quartz cuvettes.

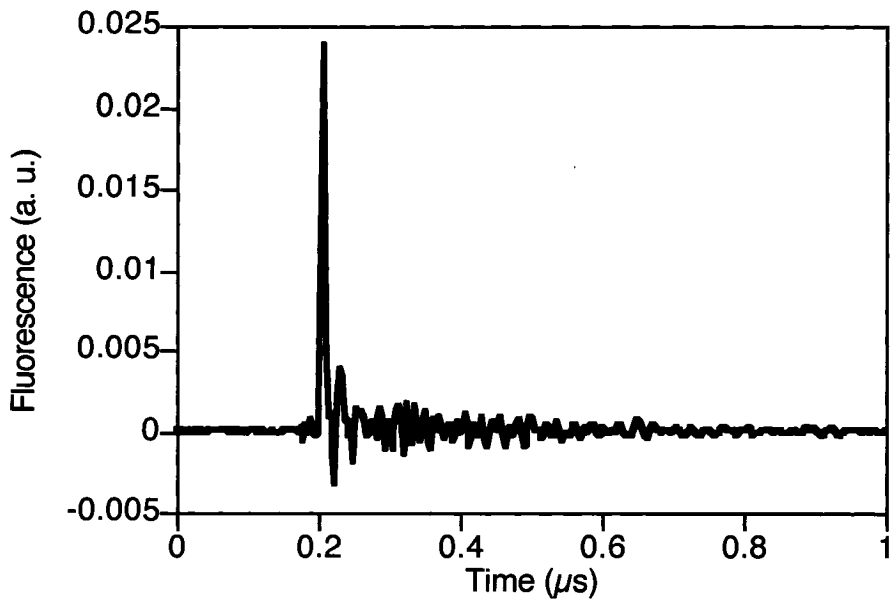

Figure 4.38 *Amaranth green QD's fluorescence at 520 nm after excitation with a 1064 nm laser pulse.*

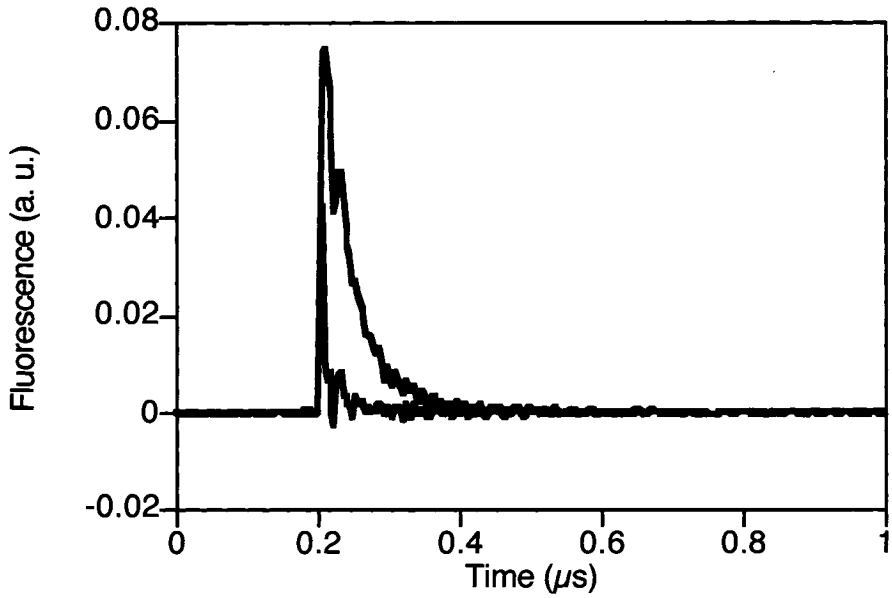

Figure 4.39 *Hawkweed orange QD's fluorescence at 580 nm after excitation with a 1064 nm laser pulse. The more intense curve is for a ~20x more concentrated solution.*

Figure 4.38 shows that fluorescence of green QD that emit at 520 nm can be achieved with 1064 nm excitation. Excitation of the QD that emit at a longer wavelength around 530 within the green QD peak will emit under two-photon conditions. The possibility of a three-photon process is not eliminated. Fluorescence can be generated by a two-photon process for hawkweed orange and aster red QD's, see Figure 4.39-4.40. As can be seen in Figure 4.39, the effect of concentration is very important for the intensity of the signal.

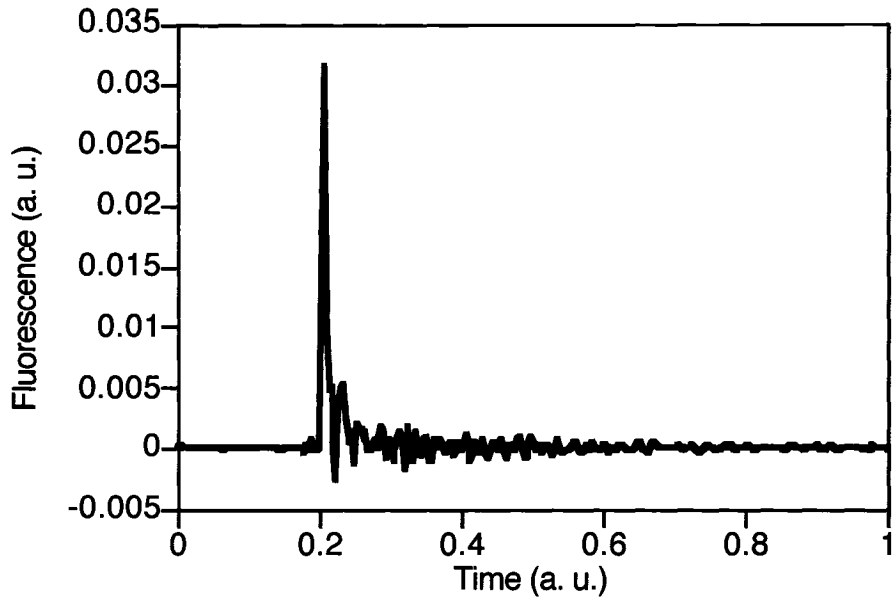

Figure 4.40 *Aster red QD's fluorescence at 610 nm after excitation with a 1064 nm laser pulse.*

4.9 Discussion

Fluorescence quenching by TEMPO

The free radical TEMPO quenches the fluorescence of CdSe quantum dots and the fluorescence quenching is size-dependent. Smaller quantum dots are quenched more efficiently than larger quantum dots. Stern-Volmer plots for quenching by TEMPO reveal an upward curve for all sizes of QD's. This upward curving trend is usually indicative of a combination of static and dynamic quenching or of quenching of two distinct electronic states. However, we could not fit the Stern-Volmer curves for quenching by TEMPO to this model. The data was fitted with a Perrin model. The radius of action of the chromophore, the QD, was found

to be very small, close to the radius of the QD itself. The quenching radius is better described in this case as an action radius for the quencher. We label this view of the Perrin model the "reverse" Perrin model. We have shown that the smaller quantum dots are more efficiently quenched by TEMPO than the larger QD's. In the case of the smaller nanoparticles, TEMPO's radius of action can reach across the molecule. For the larger nanoparticles, the action radius of TEMPO can only reach a small portion of the surface of the QD. The dependence on size could be related to the surface structure as for the smaller QD, the curvature would allow a better access of the quencher through the TOPO ligands. More curvature would expose more of the surface by creating openings in the TOPO ligand shell.

Time-resolved fluorescence quenching reveals at least two different lifetimes, a very short lifetime close to the experimental detection limit of the instrument, and a longer lifetime, 100 ns. Upon fluorescence quenching by TEMPO, the states with the longer lifetimes are quenched preferentially.

Fluorescence Quenching by 4-Amino-TEMPO

4-Amino-TEMPO was also shown to quench the fluorescence of CdSe quantum dots and the quenching was also size dependent. ESR did not reveal binding between TEMPO and the CdSe QD, but did show formation of a complex between 4AT and the QD's. This binding is further confirmed by the different concentrations of TEMPO and 4AT required to quench the QD fluorescence. Table 4.2 summarizes the concentrations required to quench half the fluorescence of different sizes of QD's.

Table 4.2 *Concentration of nitroxide radical required to reduce the quantum dot luminescence by 50%.*

Nanoparticle type	[TEMPO] for $\Phi_0/\Phi = 2$	[4-Amino-TEMPO] for $\Phi_0/\Phi = 2$
2.4 nm (green, λ_{max} 525nm)	2.8×10^{-2} M	6.5×10^{-7} M
3.2 nm (orange, λ_{max} 575 nm)	1.0×10^{-1}M	5.7×10^{-4} M
6.7 nm (red, λ_{max} 630 nm)	3.1×10^{-1} M	1.2×10^{-3} M

We can see that 4AT is more efficient than TEMPO for quenching of the fluorescence of CdSe quantum dots. The concentrations required to quench the fluorescence by half can be up to 5 orders of magnitude smaller for 4AT relative to TEMPO for the smaller quantum dots.

Size Dependence of Quenching

The width of the fluorescence peaks is related to size distribution. The fluorescence spectrum can be seen as a continuum of fluorescence for different sizes of QD's, each size corresponding to a different emission wavelength. The size dependence of quenching by TEMPO and 4AT is so strong that it can be observed within a single peak. The QD's that emit at shorter wavelengths within the same peak show better quenching than those that emit at longer wavelengths. This is easily visualized with the Stern-Volmer plots. Size dependence of quenching is observed for small differences in diameter and can be observed within a 15 nm shift in emission wavelength. The size dependence of quenching within one peak is stronger for the smaller green QD's than for the larger red QD's.

This again shows that as the nanoparticles get larger surface differences get smaller affecting less the quenching process.

Tests with two-photon absorption show that QD's could be used for biological applications where exciting at a longer wavelength is less damageable.

Quenching Mechanism of QD by TEMPO and 4AT

4AT was shown to quench QD fluorescence by formation of a complex through binding of the amino moiety to the QD surface either in vacancies or by displacing TOPO ligands.

Kagan et al. report electronic energy transfer from small QD's to larger QD's in solids.[30] The fluorescence enhancement of the larger QD's and fluorescence decrease of the smaller QD's follows Forster's theory on long range resonance transfer. The absorbance band of TEMPO, centered at 470 nm is at higher energy than the band gap of all the QD's used. The overlap integral is minimal for TEMPO and all the sizes of QD's used for these experiments. Quenching of the fluorescence of the QD's by energy transfer to TEMPO would be an uphill process that would be very unlikely, see Figure 4.41.

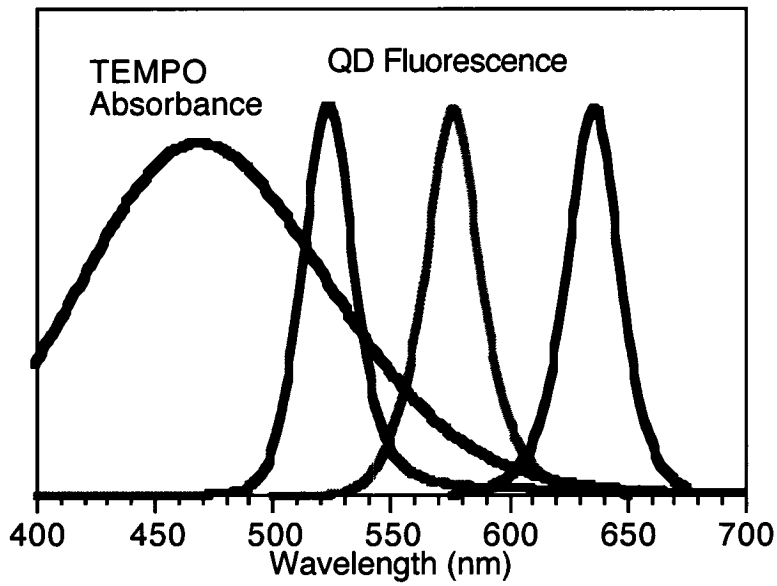

Figure 4.41 *TEMPO absorbance and fluorescence of amaranth green, hawkweed orange and aster red QD's.*

Reabsorption of the emission of the smaller green QD by TEMPO is possible. Calculations have shown that including a factor for the reabsorption does not alter significantly the result already presented, the Stern-Volmer plots for quenching by TEMPO remain upward curving and size dependent. Irreversible electron transfer from TEMPO to the QD would not be favoured in toluene. Quenching by nitroxides is known to be related to the energy of the excited state of the donor.[31,32] A Dexter electron exchange mechanism requires close contact between the donor and the acceptor. The Perrin radii that are obtained from fluorescence quenching by TEMPO are small; for the aster red QD, the Perrin radii

is smaller than the QD radii. This points to the fluorescence quenching being a short-range process such as the Dexter electron exchange. A reversible electron transfer where an electron from the conduction band would be transferred to the SOMO of TEMPO followed by a back electron transfer to the valence band is a more likely mechanism, see Scheme 4.3.

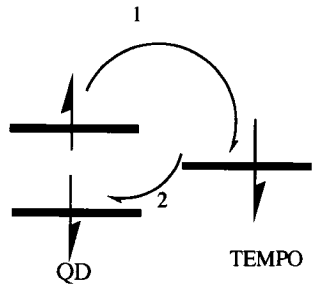

Scheme 4.3 *Reversible electron transfer mechanism*

However this would be indistinguishable from an assisted intersystem crossing. Assisted intersystem crossing would change the multiplicity of the excited QD from a singlet to a triplet rendering the QD non-fluorescent.

We have shown that fluorescence quenching of CdSe quantum dots by 4-amino-TEMPO is static. Dynamic quenching was excluded by ESR, which shows formation of a complex, and by fluorescence quenching. The Stern-Volmer plots derived from 4AT quenching are downward curving. This is usually indicative of quenching of two different chromophores or different accessibility or two different sites on the same chromophore. The first few 4AT molecules could bind to the QD surface on defects in the TOPO ligand shell and subsequent 4AT molecules could bind by displacing TOPO. The slopes in the initial portion of the Stern-Volmer plots

are too steep for dynamic quenching. If we were to assume that quenching is diffusion limited, $k_q=10^{10}$ $M^{-1}s^{-1}$, the slope which is equal to the product of k_q and the lifetime of the QD would give a lifetime many orders of magnitude larger than the reported values for CdSe QD's.[33-35]

Prefluorescent Probes

The use of the 4-amino-TEMPO-Quantum dot complex as a prefluorescent probe was explored. The binding of 4AT to a QD only partially quenches the fluorescence of the QD. The complex has a residual fluorescence. This can be understood by observation of the Stern-Volmer plots that are downward curving. Addition of additional 4AT at larger concentrations leads to only marginally more quenching. This quenching differs from the quenching of an organic fluorophore where upon the encounter of the chromophore and quencher the fluorescence is completely quenched. In the presence of photochemically generated radicals from AIBN, the fluorescence of the 4AT-QD complex is restored to the level of fluorescence of the QD alone. Binding of cyclohexylamine to QD was shown not to affect significantly the fluorescence of QD's but to increase slightly the fluorescence of the 4AT-QD complexes by displacing 4AT. The displacement of 4AT by cyclohexylamine was shown by ESR. The formation of an alkoxyamine upon binding of the carbon free radical that is shown not to affect significantly the fluorescence of the QD, can explain the fluorescence recovery of the 4AT-QD complex in the presence of carbon centered free radicals.

4.10 References

(1) Hines, M. A.; Guyot-Sionnest, P. *J. Phys. Chem.* **1996**, *100*, 468-471.

(2) Bruchez, M. J.; Moronne, M.; Gin, P.; Weiss, S.; Alivisatos, A. P. *Science* **1998**, *281*, 2013-2016.

(3) van Sark, W. G. J. H. M.; Frederix, P. L. T. M.; Bol, A. A.; Gerritsen, H. C.; Meijerink, A. *CHEMPHYSCHEM* **2002**, *3*, 871-879.

(4) Laferrière, M.; Galian, R. E.; Maurel, V.; Scaiano, J. C. *Chem. Commun.* **2006**, 257-259.

(5) Ricci, A.; Chrétien, M. N.; Scaiano, J. C. *Chem. Mater.* **2004**, *16*, 2669-2674.

(6) Maurel, V.; Laferrière, M.; Billone, P.; Godin, R.; Scaiano, J. C. *J. Phys. Chem. B* **2006**, *110*, 16353-16358.

(7) Galian, R. E.; Laferrière, M.; Scaiano, J. C. *Mater. Chem.* **2006**, *16,* 1697-1701.

(8) Alivisatos, A. P. *J. Phys. Chem.* **1996**, *100*, 13226-13239.

(9) Han, M.; Gao, X.; Su, J. Z.; Nie, S. *Nat. Biotechnol.* **2001**, *19*, 631-637.

(10) Jin, W. J.; Fernandez-Arguelles, M. T.; Costa-Frenandez, J. M.; Pereiro, R.; Sanz-Medel, A. *Chem. Commun.* **2005**, *7*, 883-885.

(11) Tomasulo, M.; Yildiz, I.; Raymo, F. M. *J. Phys. Chem. B* **2006**, *110*, 3853-3855.

(12) Mulder, W. J. M.; Koole, R.; Brandwijk, R. J.; Storm, G.; Chin, P. T. K.; Strijkers, G. J.; de Mello Donega, C.; Nicolay, K.; Griffioen, A. W. *Nano Lett.* **2006**, *6*, 1-6.

(13) Wang, X.-S.; Dykstra, T. E.; Salvador, M. R.; Manners, I.; Scholes, G. D.; Winnik, M. A. *J. Am. Chem. Soc.* **2004**, *126*, 7784-7785.

(14) Wuister, S. F.; de Mello Donega, C.; Meijerink, A. *J. Phys. Chem. Bde mello* **2004**, *108*, 17393-17397.

(15) Kalyuzhny, G.; Murray, R. W. *J. Phys. Chem. B* **2005**, *109*, 7012-7021.

(16) Talapin, D. V.; Rogach, A. L.; Kornowski, A.; Haase, M.; Weller, H. *Nano Lett.* **2001**, *1*, 207-211.

(17) Landes, C.; Burda, C.; Braun, M.; El-Sayed, M. A. *J. Phys. Chem. B* **2001**, *105*, 2981-2986.

(18) Sharma, S. N.; Pillai, Z. S.; Kamat, P. V. *J. Phys. Chem. B* **2003**, *107*, 10088-10093.

(19) Zelent, B.; Kusba, J.; Gryczynski, I.; Johnson, M. L.; Lakowicz, J. R. *J. Phys. Chem.* **1996**, *100*, 18592-18602.

(20) Lakowicz, J. R. *Principles of fluorescence spectroscopy*; 2nd ed.; Kluwer Academic / Plenum: New York, 1999.

(21) Lakowicz, J. R.; Kusba, J.; Szmacinski, H.; Johnson, M. L.; I., G. *Chemical Physics Letters* **1993**, *206*, 455-463.

(22) Matsumoto, H.; Matsunaga, T.; Sakata, T.; Mori, H.; Yoneyama, H. *Langmuir* **1995**, *11*, 4283-4287.

(23) Effink, M. R.; Ghiron, C. A. *The journal of physical chemistry* **1976**, *80*, 486-493.

(24) Aspée, A.; Maretti, L.; Scaiano, J. C. *Photochem. Photobiol. Sci.* **2003**, *2*, 1125-1129.

(25) Garcia Ballesteros, O.; Maretti, L.; Sastre, R.; Scaiano, J. C. *Macromolecules* **2001**, *34*, 6184-6187.

(26) Peng, Z. A.; Peng, X. *J. Am. Chem. Soc.* **2001**, *123*, 183-184.

(27) Yu, W. W.; Qu, L.; Guo, W.; Peng, X. *Chem. Mater.* **2003**, *15*, 2854-2860.

(28) Knauer, B. R.; Napier, J. J. *J. Am. Chem. Soc.* **1976**, *98*, 4395-4400.

(29) Hill, Z. D.; MacCarthy, P. *J. Chem. Educ.* **1986**, *63*, 162-167.

(30) Kagan, C. R.; Murray, C. B.; Nirmal, M.; Bawendi, M. G. *Phys. Rev. Lett.* **1996**, *76*, 1517-1520.

(31) Watkins, A. R. *Chem. Phys. Lett.* **1974**, *29*, 526-528.

(32) Gijzeman, O. L. G.; Kaufman, F.; Porter, G. *J. Chem. Soc. Faraday Trans. 2* **1973**, *69*, 727-737.

(33) Kloepner, J. A.; Bradforth, S. E.; Nadeau, J. L. *J. Phys. Chem. B* **2005**, *109*, 9996-10003.

(34) Fisher, B. R.; Eisler, H.-J.; Stott, N. E.; Bawendi, M. C. *J. Phys. Chem. B* **2004**, *108*, 143-148.

(35) Javier, A.; Magana, D.; Jennings, T.; Strouse, G. F. *Appl. Phys. Lett.* **2003**, *83*, 1423-1425.

Chapter 5
Fluorescence Properties of Quantum Dots in Films

Table of contents

Chapter 5
Fluorescence Properties of Quantum Dots in Films

5.1 Introduction

Quantum dots (QD's) have been incorporated into thin polymer films and photoenhancement of their fluorescence has been reported.[1-5] Bakalova et al. report that there is an enhancement of fluorescence of CdSe quantum dots in solution after prolonged exposure to UV irradiation in organic solvents.[6] Irradiation of up to 500 minutes in 1-butanol, chloroform and hexane of CdSe quantum dots capped with TOPO leads to an initial increase in fluorescence followed by a decrease in intensity. They also see an effect on fluorescence with the presence of free Cd^{2+} or Se^{2-} ions in solution. They explain this phenomenon by two opposing factors, UV irradiation degrades the QD's and decreases the fluorescence but liberation of free Cd or Se ions in solution leads to passivation of the surface and enhances fluorescence. The size dependence of the fluorescence enhancement is explained by the fact that smaller dots have a higher surface tension so they would adsorb more of the free ions in solution that passivate traps. Smaller dots show a bigger enhancement than larger QD's.

Jones et al report that the fluorescence of CdSe/ZnS core-shell quantum dots, core diameter 3.3 nm, covered with TOPO in toluene or hexane solutions is enhanced with irradiation above the band gap energy, 438 nm.[7] They explain this by the non-radiative decay of excitons to trap states that live long enough to

thermalize to spin allowed states. They also state that photoinduced rearragement of the TOPO molecules on the surface can stabilize the trap states giving more time for the thermalization process to occur.

Cordero et al. report that luminescence of QD in monolayers can be enhanced by the interaction of water molecules adsorbed on the surface upon irradiation.[1] These monolayers are prepared by a Langmuir-Blodgett method and are of CdSe QD capped with hexadecylamine. They suggest that the water molecules adsorbed on the QD surface passivate surface traps increasing the fluorescence but oxidation of QD creates surface defects decreasing the fluorescence. They also report that smaller quantum dots oxidize faster than larger ones. They observe a fluorescence increase in smaller dots followed by a decrease within 15 seconds but for larger dots the increase they observe is over almost 200 seconds.

Muller et al. studied the effect of oxygen and water on single CdSe/ZnS QD's capped with TOPO.[4] The quantum dots were prepared in a polystyrene film. Since it has been observed that air doesn't induce an increase in fluorescence intensity but requires the presence of water, they propose that there is an electron transfer from the nanocrystal core to oxygen. This passivates the surface traps increasing the fluorescence of the QD's. The effect of water is to make the LUMO of O_2 broader facilitating electron transfer which otherwise would be slightly uphill.

Nazzal et al. report that nanocrystals lose their fluorescence intensity and have a broader peak upon casting into thin polymer films.[5] Irradiation of the films

during 5 minutes increases the fluorescence and restores the peak width to what they observed for the QD's in solution. They attribute this recovery to surface reconstruction and optimization of surface-ligand passivation by photon-phonon coupling.

Hess et al. also report that the fluorescence of QD's decreases upon casting into films. They explain the loss of fluorescence by the disordering of the ligand layer.[2] The photorecovery is explained by the fact that electrons may get trapped in antibonding orbitals of strained surface bonds weakening them and leading to return to the highly fluorescent state. The dynamics of the recovery they observe leads to the conclusion that there is a wide distribution of energy barriers to phonon- assisted photo-transformation.

Kimura et al. report that photoionization of a certain number of QD's in a film occur.[3] These ionized QD's do not fluoresce but the adjacent QD's that were not ionized see a decrease of their ionization probability due to an electrostatic blockade. The quantum dots that cannot be ionized have a greater probability of fluorescing and increase overall the total fluorescence. This effect requires close proximity of the QD's for the electrostatic effect to take place.

The explanations reported for the photoinduced recovery of fluorescence in films and in solution are varied. There is however an agreement that the fluorescence of QD's in films is decreased relative to the fluorescence in solution. There is also an agreement that irradiation of QD's in films leads to a fluorescence enhancement.

Representative fluorescence images of thin polymer films containing CdSe quantum dots and the effect of irradiation on the fluorescence intensity will be presented. Different polymers have been used to prepare thin films with quantum dots, see Scheme 5.1.

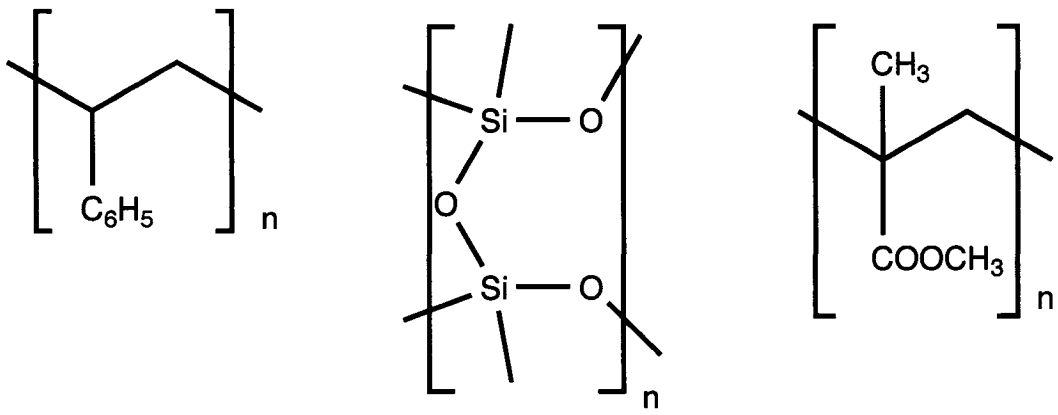

Scheme 5.1 *Structure of polymers used to prepare films containing CdSe quantum dots, from left to right, polystyrene, polymethylsilsesquioxane and polymethylmethacrylate.*

Understanding the enhancement of fluorescence obtained with these thin polymer films that contain quantum dots is necessary if these films are to be utilized as novel materials. The results are qualitative but are a step towards a better understanding of the behavior of quantum dots incorporated in films.

5.2 Experimental

Amaranth green (2.4 nm in diam., emission 520 nm), hawkweed orange (3.2 nm in diam., emission 570 nm), and begonia red (5.2 nm in diam., emission 620 nm) CdSe quantum dots were purchased from Evident. Members of the group have synthesized quantum dots according to a method described by Peng and Peng.[8] They are referred to by their wavelength of fluorescence (green 505 and green 515). Their concentrations were determined according to a formula derived by Yu et al.[9]

Polystyrene (PS) was purchased from Aldrich. Polymethylmethacrylate (PMMA) was purchased from Polysciences Inc. Polymethylsilsesquioxane (PMSSQ) was a gift from Rohm and Haas. PMMA and PS solutions were prepared in toluene (Omnisolv, EMD) and PMSSQ solutions were prepared in 2-heptanone (99%, Sigma-Aldrich). Quantum dots were added to solutions of polymer or polymers were dissolved directly in QD's solutions as provided by Evident. Films were prepared by spin coating on 1-inch quartz disks. A post application bake of about 60 seconds at 90° C was performed to evaporate the solvent.

Fluorescence images were taken using a Leica DMLS microscope using a CCD cooled camera Leica DFC300 FX with the microscope filter cube XF02-2 (Omega filters). All images were acquired with a 20x objective except when noted otherwise. Irradiation of the films was done by keeping the fluorescence

shutter open between acquisitions of the fluorescence images. The filter cube XF02-2 has an excitation centered at 365 nm, see Chapter 1 for more details.

5.3 Polystyrene Films

Prolonged UV irradiation in a HTG exposure unit (254 nm) of polystyrene (PS) films generates blue fluorescence. However, irradiation with the microscope (365 nm) for over 20 minutes does not generate a significant amount of blue fluorescence.

Irradiation of green 515 QD's incorporated in a PS film leads to a visible green fluorescence enhancement after 2 minutes of irradiation, see Figure 5.1. After 2 minutes with the shutter open, the intensity of fluorescence of the green quantum dots increases. The film did not cover the whole surface of the disk as can be seen by the darker region in the top left portion of the images.

The fluorescence of hawkweed orange CdSe quantum dots in solution is centered at 570 nm. Polystyrene was dissolved directly in the QD solution, as sold by Evident, in order to obtain the most concentrated solution of QD we could have. In order to detect fluorescence of a thin film, the concentration of QD had to be very high. A film of PS and hawkweed orange quantum dots shows a fluorescence centered at 570 nm.

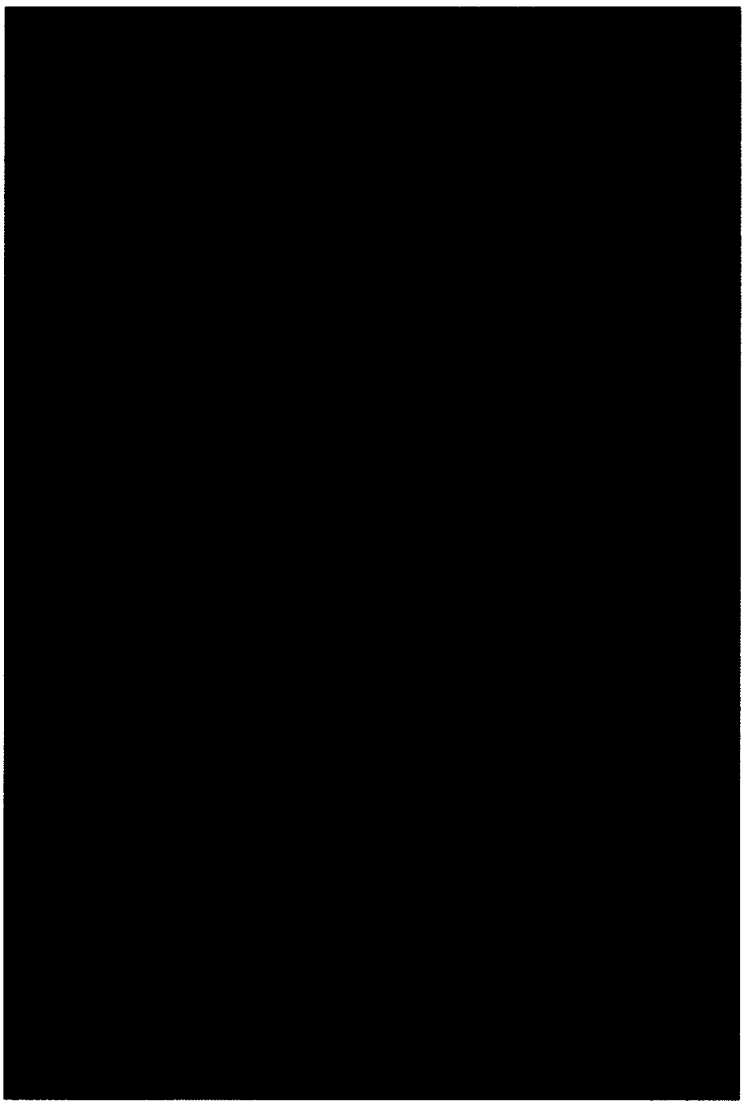

Figure 5.1 *Green 515 CdSe quantum dot film with polystyrene, top initial fluorescence, bottom after 2 minutes of exposure in the microscope.*

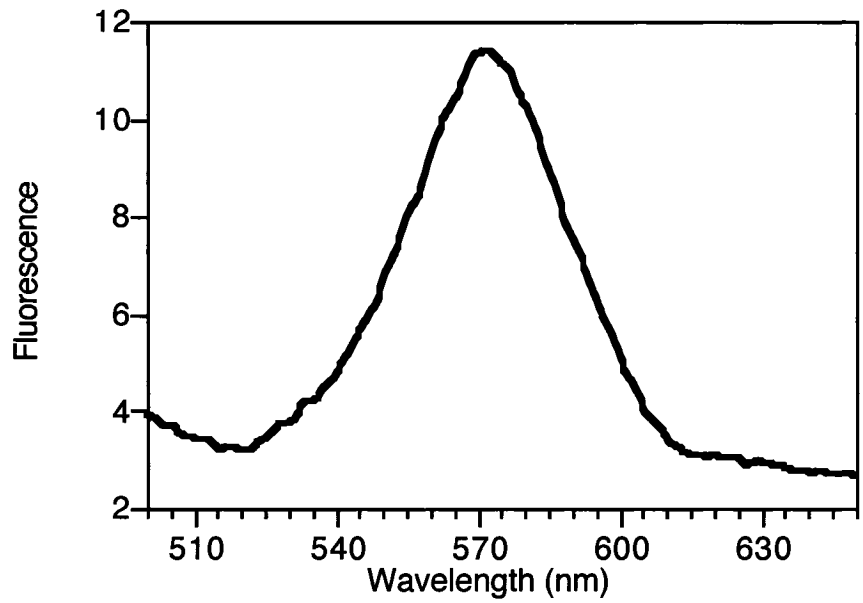

Figure 5.2 *Fluorescence spectra of a polystyrene and orange quantum dots film, excitation wavelength 380 nm.*

Fluorescence enhancements were also observed for films of polystyrene and begonia red QD's after exposure in the microscope. A slight decrease in fluorescence was observed after 1 minute of exposure followed by an enhancement of fluorescence over the next 30 to 40 minutes, see Figure 5.3.

A decrease in red fluorescence was observed after one minute of irradiation of a PS film containing equimolar amaranth green and begonia red QD's. The decrease in red fluorescence is consistent with the observed decrease after one minute of exposure for a film of begonia red QD and PS.

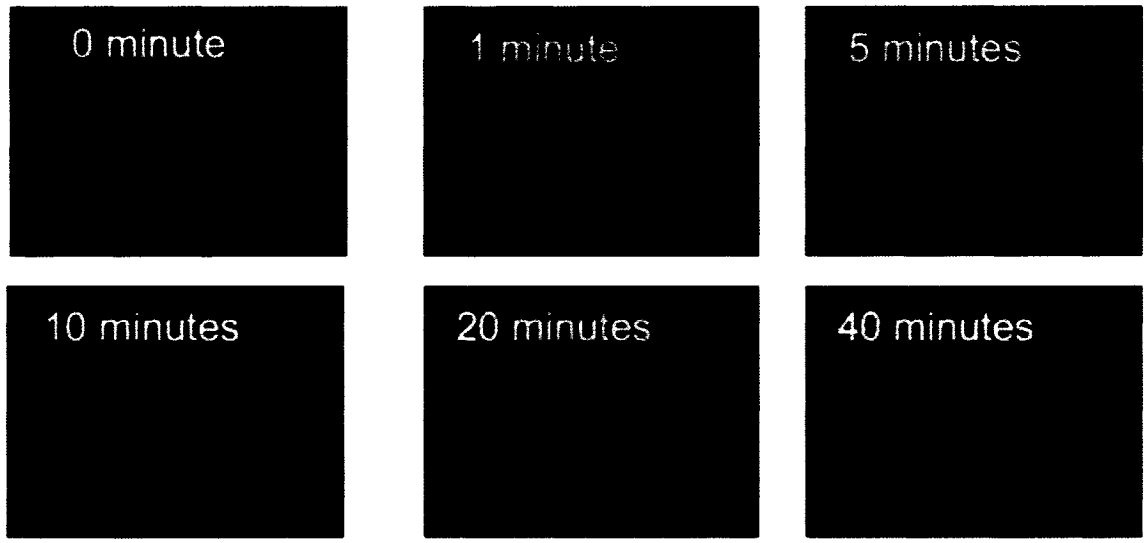

Figure 5.3 *Fluorescence images of a Begonia red and PS film after different irradiation periods under the microscope.*

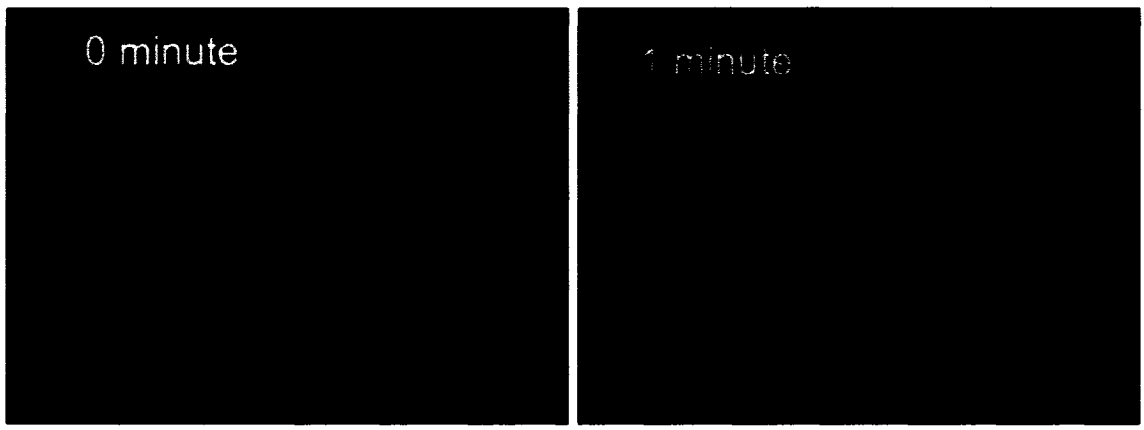

Figure 5.4 *Red fluorescence decrease of an equimolar amaranth green and begonia red QD and PS film after 1 minute of exposure.*

5.4 Polymethylsilsesquioxane Films

A polymethylsilsesquioxane (PMSSQ) film containing green QD was exposed for a five minutes in the microscope. The increase in fluorescence is visible, as can be seen in Figure 5.5.

Figure 5.5 *The fluorescence of a PMMSQ film containing amaranth green QD was enhanced by exposure. Left panel, initial fluorescence, right panel fluorescence of film after 5 minutes of exposure.*

A PMSSQ film containing hawkweed orange QD's was exposed under the microscope for several minutes resulting in an increase in orange fluorescence, see Figure 5.6.

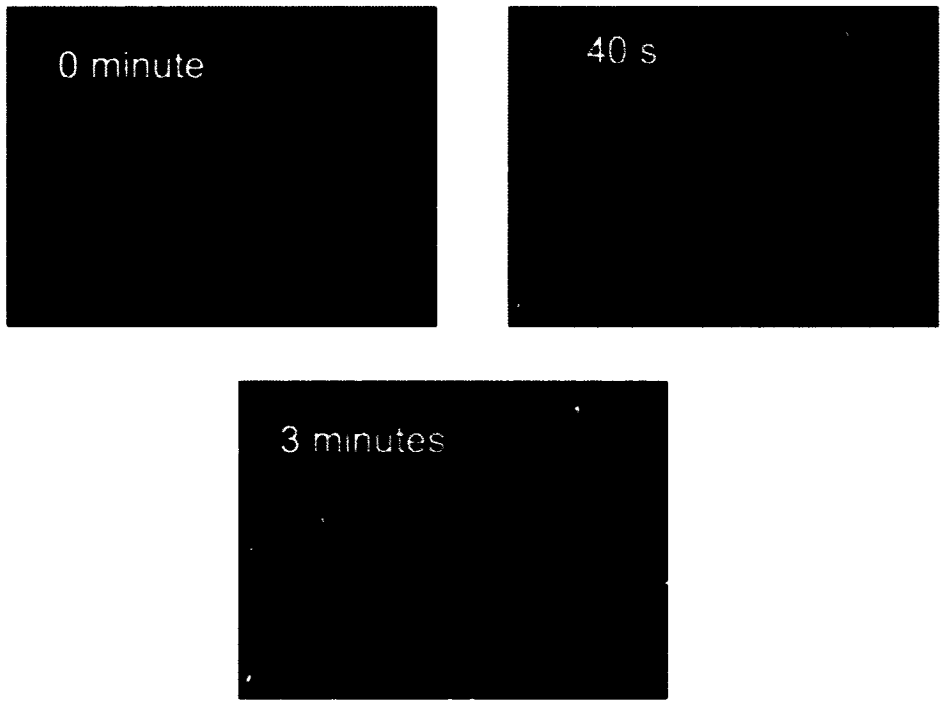

Figure 5.6 *Fluorescence of a PMSSQ film of hawkweed orange QD's was enhanced by irradiation. A 100x objective was used to acquire these images.*

A PMSSQ film of green 505 and begonia red QD'S of the same concentration was prepared. Upon mixing of the two QD's, the solution turned greenish brown. The initial fluorescence was very low. An electron microscope grid was placed on the surface of a PMSSQ film containing amaranth green and begonia red QD's. Figure 5.7 shows the pattern created by irradiation of the film after more than 5 minutes of exposure in the microscope. The dark regions correspond to unexposed regions of the film and are not as fluorescent as the

center of the grids, which are the exposed regions. The mask was removed after irradiation taking precautions not to move the sample so as to be able to image the irradiated region of the film. The use of the mask makes visualization of the enhancement of fluorescence easier by contrasting the exposed and the unexposed areas of the films. In Figure 5.7 the exposed centers of the grid have a reddish fluorescence and the initial fluorescence can be observed in the unexposed areas.

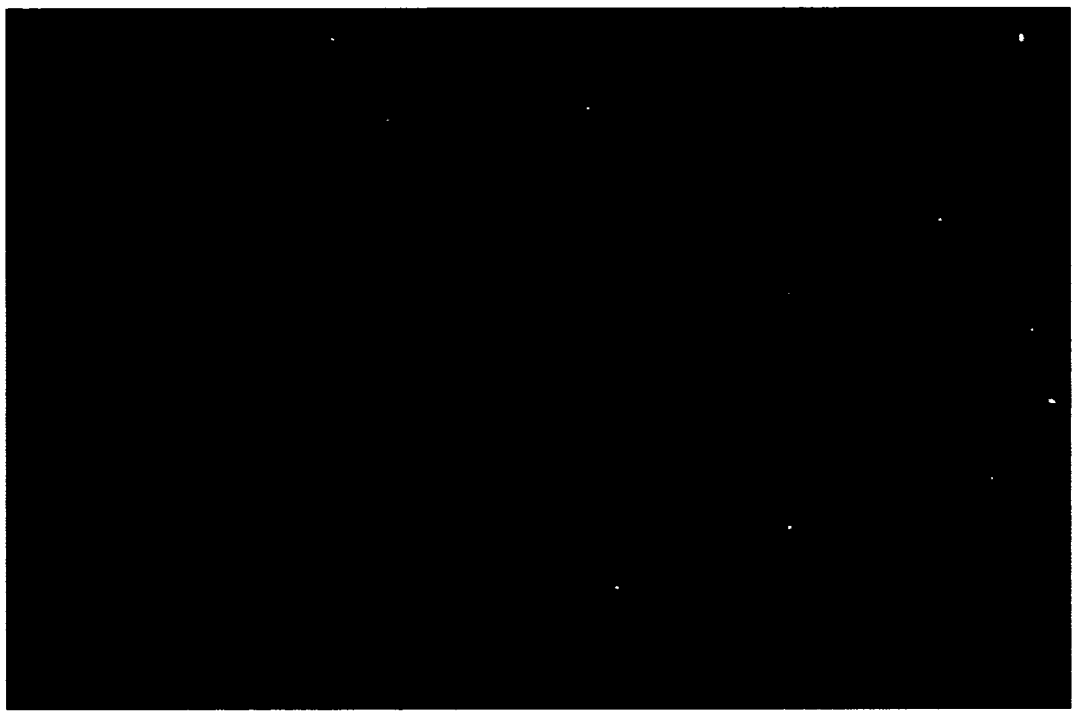

Figure 5.7 *Red fluorescence is enhanced after exposure for more than 5 minutes of a PMSSQ film containing equimolar concentrations of amaranth green and begonia red QD's.*

5.5 Polymethylmethacrylate Films

Films of polymethylmethacrylate (PMMA) only show no fluorescence after 5 minutes of exposure with the shutter open in the microscope.

Exposure for 5 minutes of a PMMA film containing green 515 QD's lead to an enhancement of the green fluorescence, see Figure 5.8. The enhancement of fluorescence was still visible after 48 hours.

Figure 5.8 *Fluorescence image of a film of PMMA and green 515 QD's after 5 minutes of exposure using an electron microscope grid as a mask.*

Fluorescence enhancements were also observed for begonia red QD's incorporated in PMMA films after an exposure of 4 minutes. The initial fluorescence was low and the enhancement was only minimal, see Figure 5.9.

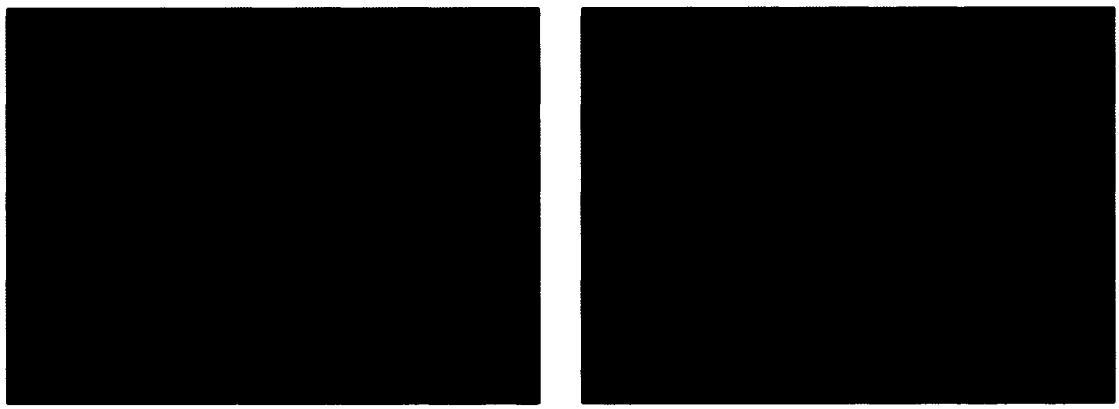

Figure 5.9 *Fluorescence of a PMMA film containing begonia red QD's after exposure in the microscope for 4 minutes under a mask, image on the left. The contrast was enhanced using Photoshop for printing purposes, see contrast enhanced image on the right.*

A film that was prepared with an approximate concentration 15:1 of green QD to begonia red QD had an initial fluorescence that was reddish and only enhancement of the red fluorescence could be observed after more than 20 minutes of exposure in the microscope, see Figure 5.10.

Figure 5.10 *Fluorescence enhancement of a PMMA film containing green 515 and begonia red QD's in a 15:1 mole ratio after exposure for more than 20 minutes in the microscope. Non-exposed area of the film, image on the left; exposed area, image on the right*

In a film where the concentration of green QD's was approximately 500 times larger than the concentration of begonia red QD's. The initial fluorescence was greenish. The film was placed under the microscope with an electron microscope grid for 25 minutes. Fluorescence images were acquired with the mask in place after 3 and 5 minutes, showing the changes in fluorescence in the exposed areas, see Figure 5.11. The initial fluorescence of the film is greenish and is increasing with time of exposure for the first 10 minutes.

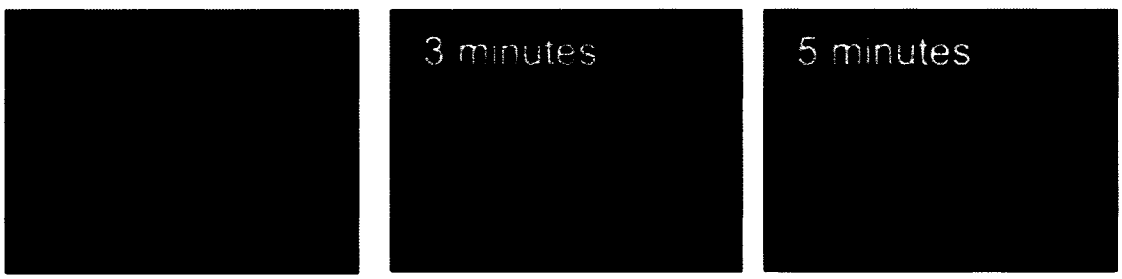

Figure 5.11 *Fluorescence images of a PMMA green 515 and begonia red QD film (molar ratio 500:1) with the mask in place, before exposure, left, after 3 minutes, center and after 5 minutes, right.*

After 25 minutes the exposed areas of the film, the centers of the grids, have a pale reddish fluorescence, see Figure 5.12. The mask has been removed for acquisition of the images in Figure 5.12. The unexposed areas retain a deep green fluorescence but are bordered by a region of lighter fluorescence.

Figure 5.12 *Fluorescence changes in a PMMA film containing green 515 and begonia red QD's. Mole ratio 500:1, after irradiation for 25 minutes (left) and 84 minutes (right) in the microscope.*

Figure 5.12 also shows a different area of the same film that was irradiated for 84 minutes where it can be observed that the center of the patterns have more reddish fluorescence than after 25 minutes. The fluorescence in the unexposed regions has been enhanced compared to the unexposed regions visible in Figure 5.11 image on the left. This could be explained by the fact that the electron microscope grid is only deposited on the surface and there may be a gap between the surface of the grid and the film. The light beam that is coming out of the microscope is probably not parallel, so some light is probably reaching under the grid. The differences in the width of the grid that can be observed in the different images could also be attributed to differences in the distance of the grid to the film. A greater gap between the grid and the film would permit more light to reach

regions of the film under the mask. The lighter region near the edges of the grid could then be a result of intermediate irradiation.

A digital color meter enables us to measure the intensity of red, green and blue in the images that were acquired with the microscope. Table 5.1 presents the values measured with a digital color meter (provided with Mac OS X) using the absolute values of red green and blue averaged over 10 different spots on the irradiated films of Figure 5.11 and 5.12. The films are divided in three regions for the purposes of color analysis: the center of the grid that is fully exposed, the region under the grid that receives little irradiation, and the border region of the grid.

Analysis shows that after more than 3 minutes of exposure, all regions show an increase in red, green and blue when compared to the initial colour levels. However, the fully exposed centers of the grid show an increase in red, green and blue up to 25 minutes of exposure and a decrease in all colours after 84 minutes of exposure. The levels of colour after 84 minutes of exposure are still greater than the initial colour levels of the film for all regions.

The lighter border, seen in Figure 5.12 after 25 and 84 minutes shows a greater increase in green than the fully exposed regions. This could be explained by an initial increase in green fluorescence followed by a subsequent decay. This decay in green colour is observed in the fully irradiated centers after 84 minutes compared to 25 minutes of exposure and no exposure.

The regions under the grid are not really unexposed because of the gap between the grid and the film surface, they have received a minimal amount of

irradiation but sufficient to increase the intensity of fluorescence. The analysis with the digital colour meter shows a greater increase in green than in red colour in the regions under the grid. After 24 minutes of irradiation the colour meter indicates that the region under the grid has the same colour intensity as the region that was exposed 3 minutes continuously. After 84 minutes of irradiation, the areas under the grid show a colour intensity similar to an exposure of 5 minutes.

Table 5.1 *Analysis of fluorescence enhancement of Figure 5.11 and 5.12 using a digital color meter.*

	RED	GREEN	BLUE
Figure 5.11			
Before Exposure	14	18	6
Exposed 3 min.	15	27	11
Exposed 5 min.	37	46	26
Figure 5.12 25 minutes			
Under grid Green colour	14	24	13
Border region lighter colour	48	53	35
Exposed center	48	47	34
Figure 5.12 84 minutes			
Under grid Green colour	24	47	35
Border region lighter colour	35	51	46
Exposed center	26	27	29

From this analysis with the digital color meter, it seems that irradiation initially increases the fluorescence of red and green QD's but that prolonged irradiation, more than 25 minutes, reduces their fluorescence. The intensity of green fluorescence increases faster than the red intensity in the first few minutes but the decrease following prolonged irradiation brings the red and green to the same level of intensity.

5.6 Discussion

Fluorescence enhancements have been observed in polymer films containing CdSe quantum dots after UV irradiation.

Enhancements of the fluorescence of the smaller quantum dots, amaranth green, green 505 and green 515 were observed after irradiation of PS, PMMA and PMSSQ films. Enhancements of the fluorescence of begonia red QD's incorporated in PS, PMMA and PMSSQ films was also observed. Films that contain two different sizes of quantum dots, green and red, show an initial increase in fluorescence, followed with prolonged exposure by a decrease in fluorescence intensity. Interesting fluorescent patterns can be produced by irradiation under a mask of CdSe QD's in polymer films.

Different mechanisms to explain the fluorescence enhancement observed either in solution, in films and in polymer films have been proposed by many researchers.[1-7] The initial decrease in fluorescence upon casting QD's in a

polymer film relative to the fluorescence intensity in solution is explained by a disordering of the surface ligands that induces traps by Hess et al.[2] Passivation of surface traps is explained by absorption of free ions in solution,[6] absorption of water upon irradiation,[1] electron transfer from the nanocrystal to oxygen in the presence of water,[4] surface reconstruction by photon-phonon coupling.[2,5] The following decrease in fluorescence observed at longer times of irradiation could be attributed to UV degradation of the QD's as reported by Bakalova et al. [6] After prolonged exposure the two opposing factors UV degradation and surface reconstruction would not be of the same magnitude as with small exposure times. The liberated Cd^{2+} and Se^{2-} ions that serve to passivate traps may not be able to counteract the UV degradation or if adsorption of oxygen is passivating traps, at longer exposure times there may not be enough oxygen present in the film to passivate the traps created by UV irradiation. The fact that the larger red QD's showed an initial decrease in fluorescence in PS and PMMA films after 1 minute of UV irradiation could be explained by differences in surfaces; larger dots having less surface defects than smaller dots, they would adsorb less oxygen or free ions that serve to passivate the traps than the smaller green QD's. Bakalova et al. report a size dependence on fluorescence enhancement, where smaller dots are more enhanced than the larger dots.[6] After more than one minute of irradiation, the larger red QD's fluorescence begins to increase until it starts to decrease again at longer irradiation times. More investigation into the mechanism is required to understand this pattern of fluorescence enhancement for the larger QD's.

The future of this project would rely on being able to quantify the changes in fluorescence by coupling a fluorimeter directly with the microscope. Fluorescence measurements have proven difficult with our present setup, the intensity required to detect a signal is too high. Fluorescence intensities have been reliable only for films that are much thicker than the ones presented here. An exhaustive study of the effect of the polymer matrix on the fluorescence enhancement would be crucial to understanding the effect of UV irradiation. The use of CdSe/ZnS core shell nanocrystals could also be useful in determining the nature of the fluorescence enhancement. It would be interesting to understand the role the polymer matrix plays in the photo-enhancement of QD fluorescence.

The stability of fluorescence of QD's incorporated in film needs to be addressed. Understanding and controlling the intensity of fluorescence of QD's incorporated in polymer films is crucial to the development of future applications.

5.7 References

(1) Cordero, S. R.; Carson, P. J.; Estabrook, R. A.; Strouse, G. F.; Buratto, S. K. *J. Phys. Chem. B* **2000**, *104*, 12137-12142.

(2) Hess, B. C.; Okhrimenko, I. G.; Davis, R. C.; Stevens, B. C.; Schulzke, Q. A.; Wright, K. C.; Bass, C. D.; Evans, C. D.; Summers, S. L. *Phys. Rev. Lett.* **2001**, *86*, 3132-3135.

(3) Kimura, J.; Uematsu, T.; Maenosono, S.; Yamaguchi, Y. *J. Phys. Chem. B* **2004**, *108*, 13258-13264.

(4) Muller, J.; Lupton, J. M.; Rogach, A. L.; Feldmann, J. *Appl. Phys. Lett.* **2004**, *85*, 381-383.

(5) Nazzal, A. Y.; Qu, L.; Peng, X.; Xiao, M. *Nano Lett.* **2003**, *3*, 819-822.

(6) Bakalova, R.; Zhelev, Z.; Jose, R.; Nagase, T.; Ohba, H.; Ishikawa, M.; Baba, Y. *J. Nanosci. Nanotech.* **2005**, *5*, 887-894.

(7) Jones, M.; Nedeljkovic, J.; Ellingson, R. J.; Nozik, A. J.; Rumbles, G. *J. Phys. Chem. B* **2003**, *107*, 11346-11352.

(8) Peng, Z. A.; Peng, X. *J. Am. Chem. Soc.* **2001**, *123*, 183-184.

(9) Yu, W. W.; Qu, L.; Guo, W.; Peng, X. *Chem. Mater.* **2003**, *15*, 2854-2860.

Chapter 6

Fluorescence Properties of Quantum Dots in Photonic Crystal Fibres

Table of contents

Chapter 6
Fluorescence Properties of Quantum Dots in Photonic Crystal Fibres

6.1 Introduction

Optical fibres rely on the difference in refractive index between silica and air to guide light along their lengths.[1] Light is guided by total internal reflection. New materials have emerged that have the same surface to volume ratio as the optical fibres but the material from which they are constructed is photonic in nature. Channels run the entire length of the fibres and constrain the light to the central core, see Figure 6.1. Photonic crystal fibres (PCF's) are well-known for their optical properties in light transmission applications.[1-3] There is potential for the development of PCF's for biological, biomedical or chemical sensing applications.[4-6]

Thin capillaries have been employed for gas chromatographic applications. Carbon nanotubes have also been employed as gas sensors.[7] Zeolites contain channels of molecular dimensions that have been used to direct chemical reactions and to develop sensors.[8] All these applications rely on the surface characteristics of the channels and their length to diameter aspect ratio.

Figure 6.1 *Contrast microscopy images of the PCF end without the acrylate coating (left) and of a segment of PCF with the acrylate coating (total diameter 220 μm) (center). Fluorescence microscopy image of the PCF with the acrylate coating, using the filter XF02-2 from Omega Optical (right).*

We have explored the use of PCF's as sensors. Dr Raquel E. Galian, a postdoctoral fellow in our group, filled the channels of PCF's by capillarity with Coumarin 6. The presence of the dye in the channels was observed by fluorescence microscopy. Addition of acidic solutions inside the channels by capillarity resulted in a shift of fluorescence due to the protonation of coumarin 6. The protonated form of the dye is shifted relative to the neutral form of coumarin 6. This shift in fluorescence of the neutral form upon protonation can be used to reflect changes in pH.[9] We also looked at the fluorescence properties of quantum dots inside the channels of PCF's. Addition of TEMPO or 4-amino-TEMPO leads to a local quenching of the fluorescence inside the channels followed by a recovery of fluorescence. The recovery is attributed to diffusion and to the non-linear quenching of quantum dots by the paramagnetic species TEMPO and 4-amino-

TEMPO. We observed a dependence of fluorescence on the binding interaction of the quencher with the QD as well as the size of the QD.

The work presented in this chapter is a collaboration with Dr. Raquel E. Galian who is a postdoctoral fellow in our group.

6.2 Experimental

Endlessly single mode photonic crystal fibres (PCF) ESM-12-01 manufactured by Blaze Photonics were purchased from Thorlabs. They consist of 54 microchannels of 3.7 μm in diameter with a pitch of 8.0 ± 0.2 μm (spacing between channels) and a core diameter of 12 ± 1 μm. The acrylic coating that covers the PCF was removed using a SCS-1 soft contact acrylate stripper. An optical fibre cleaver FITEL S-315 was used to cut specific lengths of PCF's (usually 20 mm) whose coating has been removed; for shorter lengths an AMP fibre optic sapphire scribe tool (504064-1) was required.[9]

Amaranth green (2.4 nm in diameter) and Aster red (6.7 nm in diameter) CdSe quantum dots were purchased from Evident technologies. TEMPO and 4-amino-TEMPO were purchased from Aldrich. Solutions were prepared in toluene (Omnisolv, EMD) or mesitylene (98%, Aldrich), see Scheme 6.1.

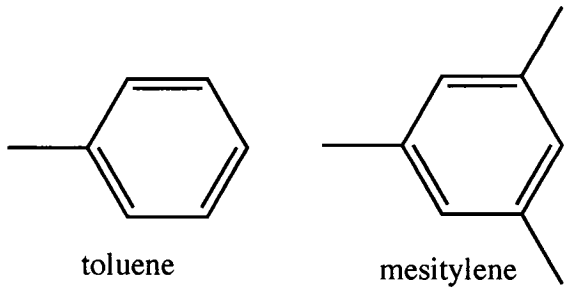

Scheme 6.1 *Toluene and mesitylene*

Fluorescence imaging was performed with a Leica DMLS microscope and a Leica cooled DFC300 FX camera using the XF02-2 filter cube from Omega Opticals, see Chapter 1 for more details.

Channels of the PCF's were filled by capillarity. A 1 µl drop of QD or quencher solution was placed at the tip of the fibre and most of the channels filled by capillarity. Some channels remained empty probably due to an imperfect contact between the fibre's end and the solution or due to blockage of the channels by debris during the cutting process.

6.3 Development of Sensors Using Photonic Crystal Fibres

6.3.1 Filling the Channels

Channels of photonic crystal fibres (PCF's) were filled by capillarity with quantum dots solutions in toluene or mesitylene. Fluorescence images were taken

with microscope of the fibre's tip and of the side view showing the channels that are filled with the fluorescent QD's, see Figure 6.2-6.3.

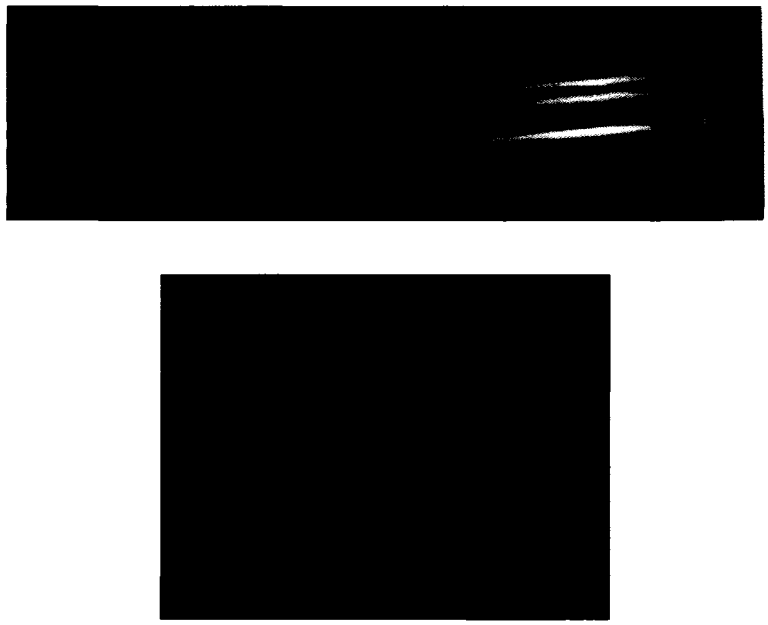

Figure 6.2 *PCF filled with an amaranth green QD solution. Fluorescence image, side view and end view.*

Fluorescence of the QD inside the channels can easily be viewed with fluorescence microscopy using the appropriate filter cube, XF02-2, once the acrylate coating is removed. The curvature of the fibre and the fact that the channels are at a variable distance from the objective prevents focusing on all channels at the same time but nevertheless a fluorescence image gives a clear view of the fluorescent solution inside the channels. The end view gives us an idea of how many channels were filled by capillarity; some may look empty only because the solution has moved further away from the end of the fibre. The channels were filled by dipping the end of the fibre in a few microliters of QD

solution followed by removing the excess before imaging. The brighter tip is probably due to the light transmission properties of the PCF's.

Figure 6.3 *PCF filled with an aster red QD solution. Fluorescence image, side view and end view.*

6.3.2 Quenching by TEMPO

A solution of TEMPO in toluene (≥ 0.5 M) was added at the fibre's tip of the channels previously filled with amaranth green QD's (3.7 x 10^{-6} M). The liquid filled the channels by capillarity and mixed with the QD solution already present. An initial decrease in fluorescence of the QD was observed followed by an almost total recovery. The fluorescence was monitored at the fibre's tip and not on the entire length of the fibre. Figure 6.4 shows the side view of a fibre filled with amaranth green QD and the decrease and recovery of fluorescence upon addition of a TEMPO solution in toluene.

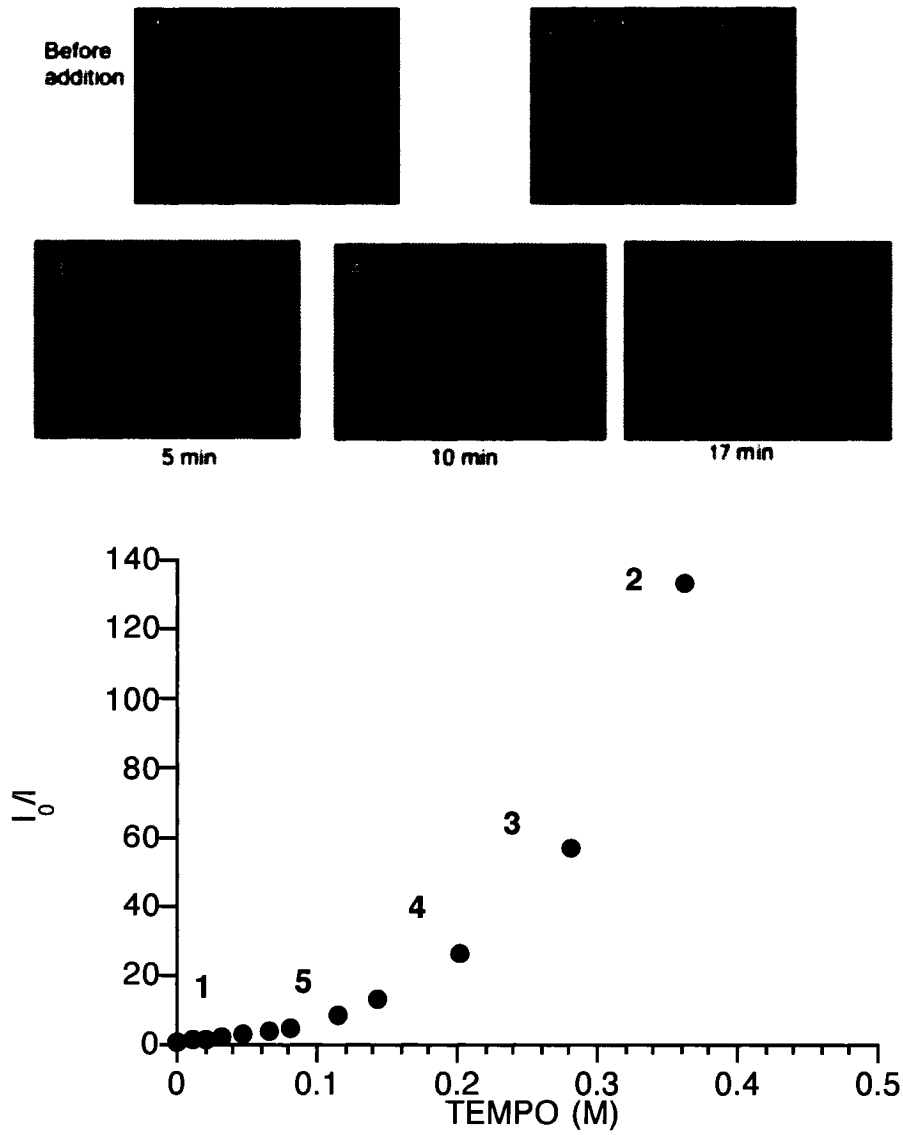

Figure 6.4 *Top: Amaranth green QD fluorescence quenched inside the channels of PCF's by addition of TEMPO. Recovery of fluorescence occurred over 17 minutes. Bottom: Stern-Volmer plot for the fluorescence quenching of amaranth green (4.1 μM, ●) QD's by TEMPO in toluene, numbers correspond approximately to concentrations of TEMPO for the time delays indicated for fluorescence in PCF's; 1 corresponds to fluorescence before addition of TEMPO.*

Before the addition of TEMPO, the green fluorescence of the amaranth green CdSe QD's can be observed in the channels of the fibre. Upon addition of the TEMPO solution at the fibre's tip, the fluorescence is totally quenched. Initially, the concentration of TEMPO is at its maximum at the fibre's tip. Upon diffusion the concentration of TEMPO at the tip is reduced and the fluorescence begins to recover. After 17 minutes, the fluorescence recovery reaches a maximum. Upon addition of TEMPO, the concentration of TEMPO is at a maximum near the fibre's tip; this can be related to a TEMPO concentration sufficient to quench the fluorescence enough that it cannot be viewed by fluorescence microscopy.

The upward curvature of the Stern-Volmer plot and the fit to a Perrin model gives a value of α equal to 13.7 M^{-1} for the amaranth green QD's, see Chapter 4. These α values can help understand the facile recovery of fluorescence for the green QD's. The high value of α explains the initial quenching upon addition of TEMPO and an inspection of the Stern-Volmer curve shows that at a concentration of 0.5 M TEMPO the value of I_0/I is so high that no fluorescence would be detectable. The curvature of the Stern-Volmer plots is so pronounced that any decrease in concentration of TEMPO leads to a big decrease in the value of I_0/I. The Stern-Volmer curve is also very pronounced at low concentrations of TEMPO leading to a more facile recovery of fluorescence as the concentrations of TEMPO are diminished.

Aster red QD's were diluted in mesitylene to obtain a 1.8×10^{-7} M solution that was used to fill the channels of a PCF. A solution of TEMPO in mesitylene was added to quench the fluorescence. Mesitylene was used because it has a

higher boiling point than toluene and was less volatile. This was useful in preventing evaporation of the solution inside the channels, however the fluorescence intensity was less than with toluene. The recovery of fluorescence for the larger aster red QD's was slower, it took about 60 minutes to observe recovery. Figure 6.5 shows a side view of the PCF filled with aster red QD before and after addition of TEMPO.

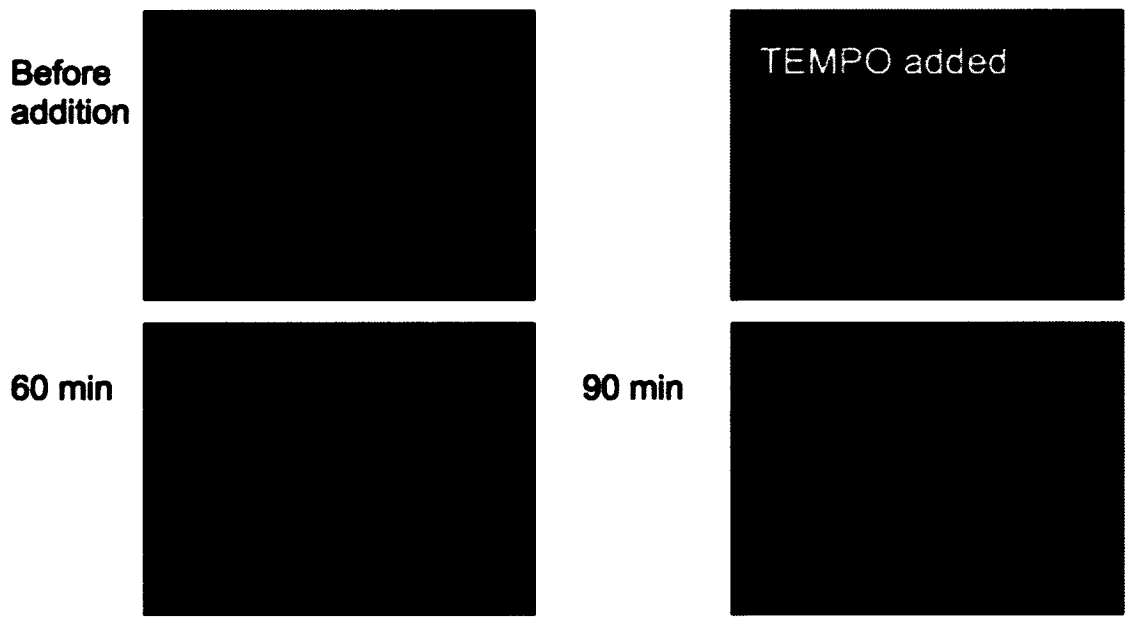

Figure 6.5 *Aster red QD fluorescence quenched inside the channels of PCF's by addition of TEMPO in mesitylene. Recovery of fluorescence occurred over more than 1 hour.*

The differences with the smaller green QD's can be explained by the solvent choice of mesitylene, which is more viscous than toluene and slows the diffusion of the QD and TEMPO as well as the fact that the fluorescence intensity was less than in toluene.

Upon diffusion, the concentration of TEMPO at the fibre's tip is decreased and returns to a level that permits fluorescence imaging. The curvature of the Stern-Volmer plot for the larger red QD's is not as pronounced as for the smaller green QD's as can be seen from the value of α, 1.6 M^{-1}, see Chapter 4. The initial concentration of TEMPO is sufficient to quench the fluorescence of the larger QD's but a change in concentration does not lead to a change as dramatic in the value of I_0/I as for the smaller QD's. This is one of the factors that can explain the slower recovery of fluorescence of the aster red QD's after quenching with TEMPO inside the channels of the PCF's

6.3.3 Quenching by 4-Amino-TEMPO

4-Amino-TEMPO (4AT) has been shown to bind to the amaranth green CdSe QD's by ESR and fluorescence quenching experiments. Stern-Volmer plots for the addition of 4AT to amaranth green QD in toluene solutions show a downward curving trend, see Figure 6.6. It is interesting to note that the concentrations required to quench the fluorescence of the QD's by 4AT is micromolar as opposed to molar for quenching by TEMPO.

Addition of a 3.7 x 10^{-6} M 4AT solution to PCF's filled with amaranth green QD's (3.7 x 10^{-6} M) leads to complete fluorescence quenching. In solution, as seen from Figure 6.6, such a concentration of 4AT would lead to a fluorescence quenching of more 80%, with less than 20% of fluorescence remaining. In the fibres, no fluorescence recovery is observed in the following hour. This strong quenching could be explained by the binding of the nitroxides with the QD's. Initially the concentration of 4AT is the highest just at the fibre's tip but unlike the

case for quenching by TEMPO where diffusion could lower the local concentration of the quencher, the concentration of quencher is not allowed to diffuse as much because the quencher molecules bind to QD's as soon as they enter the channels.

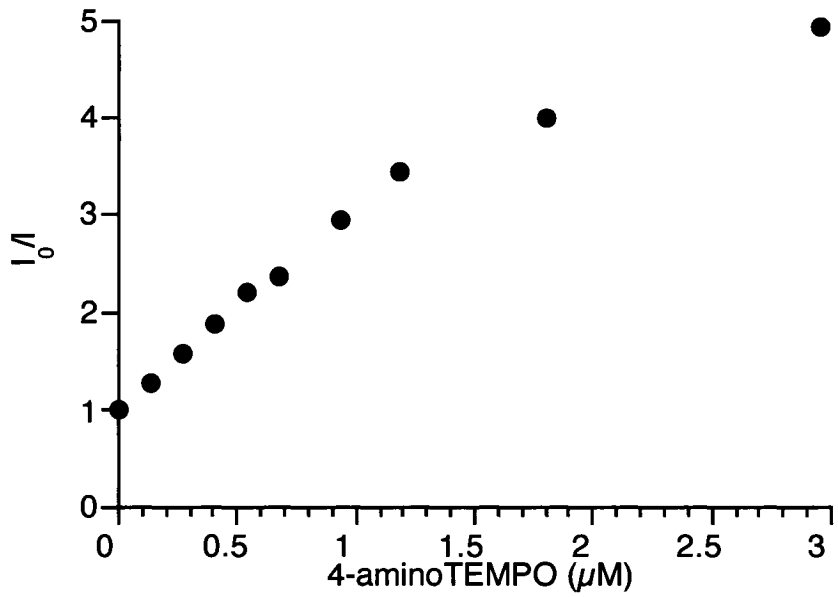

Figure 6.6 *Stem-Volmer plot for the fluorescence quenching of amaranth green QD's (1.2 μM) by 4-amino-TEMPO.*

From the previous discussion in Chapter 4, one or two 4AT molecules are enough to quench the fluorescence of the CdSe QD's, but more can actually bind to each QD. The binding constant was found to be (6.7 ± 3.4) x 10^6 M^{-1}. This new complex 4AT-QD may not diffuse as fast as the quencher and the QD's alone. The concentration gradient of quencher remains higher near the entry of the channels where we probe the fluorescence intensity.

6.4 Discussion

Photonic crystal fibres are recognized for their light guiding properties. We have used these fibres not for their optical properties but more for their topographical properties. They possess very long and narrow (a few μm in diameter) channels that we used as test tubes. In a conventional optrode (optical electrode) changes in optical properties of an analyte placed on the surface or end of an optical fibre or other surface are monitored.[10] Glass capillaries with a chemical sensitive interior coating have been used as sample chamber, optical sensor and light collecting optics all in one.[10]

The ultimate goal is to develop optosensors or optrodes with channels that can be addressed individually. We can develop sensors using quantum dots because they have a broad absorption and a fluorescence that is size-dependent and of good intensity. The sensors based on these QD's would have high sensitivity and selectivity.

We have shown that we can detect fluorophores inside the channels of PCF's and can monitor their interaction with different quenchers. QD's of different size have been incorporated into the channels of PCF's and their fluorescence was quenched by TEMPO and 4-amino-TEMPO. This was followed by a fluorescence recovery that can be attributed to the deviations from linearity observed in Stern-Volmer plots for fluorescence quenching in solution and to diffusion of the quencher and fluorophore inside the channels. We do not believe that the

fluorescence enhancement observed in films and reported in Chapter 6 is responsible for the fluorescence recovery observed with the PCF's. Recovery of fluorescence for the larger red QD's was slow and minimal and occurred over more than 90 minutes more than enough time to enhance dramatically the fluorescence of QD in films.

We can select different parameters such as the size, ligand coverage and diffusion characteristics of the QD's and by selecting the appropriate quencher can control the fluorescence recovery process. We would take advantage of the optical properties of the PCF's by using the PCF's light guiding mode to address analytes present in the PCF's channels and monitoring the optical change induced by the quencher molecules. Preliminary experiments have shown that acrylates can be polymerized inside the channels of the PCF's. This could lead to incorporation of the QD's for example on the inside walls of the channels. Evaporation of the solvent inside the channels, in order to deposit the QD's on the inside walls, has lead to uneven and discontinuous films.[9] Functionalization of the QD's such that they have a greater affinity for the PCF's channels could be useful. Future work will require looking at the design of photonic crystal fibres such that they possess the right geometry for incorporation of the analyte inside the air channels and that they still retain their light guiding properties at the wavelengths of interest.

6.5 References

(1) Russell, P. *Science* **2003**, *299*, 358-362.

(2) Knight, J. C. *Nature* **2003**, *424*, 847-851.

(3) Knight, J. C.; Birks, T. A.; Russell, P. S. J.; Atkin, D. M. *Opt. Lett.* **1996**, *21*, 1547-1549.

(4) Konorov, S. O.; Zheltikov, A. M.; Scalora, M. *Optics Express* **2005**, *13*, 3454-3459.

(5) Jensen, J.; Pedersern, L.; Joiby, P.; Nielsen, L.; Hansen, T.; Folkenberg, J.; Riishede, J.; Noordegraaf, D.; Nielsen, K.; Carlsen, A.; Bjarklev, A. *Optical Lett.* **2004**, *29*, 1974-1976.

(6) Ma, J.; Bock, W. J.; Wang, W.; Hao, W.; MacKinnon, S. M. *Proc. SPIE* **2005**, *5970*, 597006.

(7) Kong, J.; Franklin, N. R.; Zhou, C.; Chapline, M. G.; Peng, S.; Cho, K.; Dai, H. *Science* **2000**, *287*, 622-625.

(8) Scaiano, J. C.; García, H. *Acc. Chem. Res.* **1999**, *32*.

(9) Galian, R. E.; Laferrière, M.; Scaiano, J. C. *Mater. Chem.* **2006**, *16*, 1697-1701.

(10) Lippitsch, M. E.; Draxler, S.; Kieslinger, D.; Lehmann, H.; Weigl, B. H. *Appl. Optics* **1996**, *35*, 3426-3431.

Conclusion

Fluorescence microscopy was used to record latent images of acid formed in polymer films and photoresists upon exposure at 157 nm. The use of the dye coumarin 6, which undergoes a shift in fluorescence upon protonation, was used to map acid formation in these thin films. Disappearance of the neutral form of the dye in the exposed areas combined with appearance of the protonated form in the exposed areas of the film show that acid is generated upon exposure at 157 nm. Irradiation with less than 3 $mJcm^{-2}$ at 157 nm was sufficient to generate acid and protonate coumarin 6 in photoresists that contain a PAG. Irradiation of polymer films that did not contain a PAG also generated acid, as monitored by coumarin 6 protonation, but required a much higher dose of 157 nm irradiation.

Irradiation at 157 nm of fluorinated polymer films generates fluoride as monitored by C4TIPS, a fluoride sensor that is being developed in the group. Solution work has shown that 1,1,1,3,3,3-hexafluoro-2-propanol (HFP) traps electrons with a rate constant of 6.56×10^{10} $M^{-1}s^{-1}$. We propose that HF is formed by electron ejection from the non-fluorinated moieties of the polymer followed by deprotonation at the ionization site, trapping of the electron by fluorinated moieties and subsequent release of fluoride in the presence of protons.

AFM was used to map laser ablation of different polymer films after exposure to 157 nm irradiation. Laser induced periodic surface structures (LIPSS) were observed by AFM.

Laser flash photolysis using 157 nm as the excitation wavelength has proven difficult because of technical difficulties, high absorbance of water, oxygen and most organic materials, and birefringence of CaF_2. Fluorescence of pyrene in films and in solution was observed after laser excitation at 157 nm. Unfortunately, no transient decay spectra could be recorded. A kinetic decay trace at 610 nm for xanthone in perfluorononane was observed. The trace was obtained by subtraction of the solvent absorbance from the trace of xanthone and solvent.

Fluorescence of CdSe quantum dots can be quenched by TEMPO. Upward curving Stern-Volmer plots indicate that the quenching could be a combination of static and dynamic quenching or quenching of two distinct electronic states. The curves were a better fit to the Perrin model. The Perrin model defines a sphere of action for the fluorophore such that only quenchers present in that sphere will quench the fluorescence. For QD's, this model is better viewed as a "reverse" Perrin model, where the sphere of action is positioned around the quencher. The quenching of CdSe QD's by TEMPO is size dependent, smaller QD's being more efficiently quenched than larger QD's. The size dependence is so strong that it is reflected within each fluorescence peak; a small difference in emission wavelength, such as 15 nm, will show as a significant difference in Stern-Volmer plot curvature, especially for smaller QD's. The Perrin radii point to a short-range process such as the Dexter electron exchange, where the electron would be shuttled from the conduction band of the QD to the SOMO of TEMPO and back to the valence band of the QD.

4-Amino-TEMPO was shown to be a more efficient quencher of CdSe QD's than TEMPO. A similar size-dependence on quenching was also observed. ESR studies have shown that there is formation of a complex between 4AT and QD's. Stern-Volmer plots are downward curving, indicating the presence of two different sites for binding or sites with different accessibility. 4AT would bind to vacant sites on the QD surface and subsequently by displacement of TOPO ligands on the surface. Development of prefluorescent probes for sensing free radicals using the QD-4AT complex is promising. Photogeneration of radicals from AIBN in solution with the QD-4AT complex leads to an increase in fluorescence intensity to almost the initial QD fluorescence intensity before formation of the complex with 4AT.

Photoenhancement of the fluorescence of QD incorporated in films was observed upon UV irradiation. Initial passivation of trap sites by oxygen, water or ions could lead to an enhancement of fluorescence but prolonged irradiation would lead to degradation of the QD and decrease in fluorescence intensity.

Incorporation of QD's inside the hollow channels of photonic crystal fibres (PCF) was followed by fluorescence microscopy. Addition of quenchers, such as TEMPO and 4AT inside the channels leads to a decrease in fluorescence intensity followed by a recovery that can be attributed to the diffusion of the quencher and QD's inside the channels as well as the strong non-linearity observed in solution for the quenching of CdSe QD's by TEMPO and 4AT.

Appendix 1
Claims to Original Research

(1) Acid generation at 157 nm in thin films by photoacid generators (PAG's) is established, (collaboration with M. G. Ivan).

(2) Photodecomposition of fluorinated polymer films at 157 nm to yield hydrofluoric acid (HF) is established, (collaboration with M. G. Ivan and C. N. Sanramé). Solution work shows that 1,1,1,3,3,3-hexafluoro-2-propanol (HFP) traps electrons in methanol with a rate constant of 6.56×10^{10} $M^{-1}s^{-1}$. Ablation of polymer and creation of LIPSS upon irradiation with a mask at 157 nm is reported.

(3) Laser Flash photolysis at 157 nm was challenging, however a trace for the transient decay of xanthone in perfluorononane was obtained.

(4) Demonstration of a size-dependence for the quenching of CdSe quantum dots (QD) by TEMPO and 4-amino-TEMPO.

(5) Demonstration that 4-amino-TEMPO forms a complex with CdSe quantum dots. Demonstration of the use of the QD-4AT complex as a radical sensor by fluorescence spectroscopy. The fluorescence of the QD-4AT complex is restored to the fluorescence intensity prior to formation of the complex by photogenerated radicals of AIBN (collaboration with V. Maurel).

(6) Photoenhancement of CdSe quantum dot contained in thin polymer films fluorescence upon UV exposure at 157 nm. Demonstration of quenching and subsequent recovery of quantum dot fluorescence by TEMPO or 4AT

inside the air channels of photonic crystal fibres (collaboration with R. E. Galian).

(7) Work not included in this thesis. Isolation and characterization of the carbanion derived from photolysis of ketoprofen in dry, basic THF is reported.

Appendix 2
Future Directions

We have filled the air channels of photonic crystal fibres (PCF's) with quantum dots and have shown that we could monitor the fluorescence using fluorescence microscopy. We would like to be able to use the optical properties of the PCF's by performing laser flash photolysis (LFP) inside the channels. The monitoring beam would be directed by the PCF optical guiding properties and the laser or excitation beam would be pointed at the fibre, perpendicular to the long axis. Detection of the change in absorbance upon laser irradiation will then be monitored and amplified giving us the desired signal. The PCF is chosen such that it can guide the desired wavelength that we want to monitor, for example a PCF that can guide 620 nm is chosen to monitor the transient absorbance of xanthone. Eventually, the system could be tested with 157 nm excitation, bridging the two key topics of my thesis, LFP with 157 nm and work with nanoparticles and PCF's. This project is currently under preparation.

The project on enhancement of fluorescence in quantum dot films would require linking a spectrometer to the microscope such that more quantitative measurements of fluorescence could be recorded.

Fluorescence quenching of quantum dots by molecules that contain a nitroxide moiety linked to the amino moiety but at variable distances is already underway in Professor Scaiano's laboratory. This will further elucidate the role of the free radical moiety on fluorescence quenching of CdSe quantum dots.

Appendix 3
List of Publications

(1) Scaiano, J. C.; Laferrière, M.; Ivan, M. G. *Macromolecules* **2003**, *36*, 6692-6694.

(2) Laferrière, M.; Sanramé, C. N.; Scaiano, J. C. *Org. Lett.* **2004**, *6*, 873-875.

(3) Laferrière, M.; Galian, R. E.; Maurel, V.; Scaiano, J. C., *Chem. Commun.* **2006**, 257-259.

(4) Scaiano, J. C.; Laferrière, M; Galian, R. E.; Maurel, V.; Billone, P. *phys. stat. sol. (a)* **2006**, *6*, 1337-1343.

(5) Galian, R. E.; Laferrière, M.; Scaiano, J. C. J. *Mater. Chem.* **2006**, *16*, 1697-1701.

(6) Ivan, M. G.; Laferrière, M.; Sanramé, C. N.; Scaiano, J. C. *Chem. Mater.* **2006**, *18*, 2635-2641.

(7) Maurel, V.; Laferrière, M.; Billone, P.; Godin, R.; Scaiano, J. C. *J. Phys. Chem. B* **2006**, *110*, 16353-16358.